Doctoral Dissertation

André Vagner Gaathaug

Experimental Study of Deflagration to Detonation Transition in Hydrogen-Air Mixtures

Telemark University College
Faculty of Technology

Experimental Study of Deflagration to Detonation Transition in Hydrogen-Air Mixtures

André Vagner Gaathaug

Thesis submitted to the Telemark University College
for the degree of philosophiae doctor (PhD)

Dedicated to the my wife Mariann, and my sons William and Casper

Preface

This work has been carried out at Telemark University College (HiT), Faculty of Technology. The financial support of the Norwegian Research Council through RENERGI and ENERGIX is gratefully acknowledged. The work has been a part of the the IEA HIA task 19 and task 31. The author would also like to acknowledge the financial support from Statoil ASA.

I want to thank my professor Dag Bjerketvedt for most inspirational supervision and always keeping me busy with inspiring tasks. He has given me lots of feedback, excellent guidance and freedom to develop my own career in science.

I owe all my academic education to Dr. Knut Vaagsaether, since he always helps me, guides me and inspires me. He pushed me from the first day of my BSc all the way through to my PhD. Thank you very much.

I would also like to commemorate Talleiv Skredtveit. He taught me practical workshop engineering and welding, and was very helpful in the development and maintenance of my experimental rig and much more.

Further thanks to Øyvind Johansen, Jan Gunnar Lode, Eivind Fjelddalen, Joachim Lundberg and Per Morten Hansen for technical support. Thanks to Lars Skau Ekornrød and Larus Bjarnason for help during the experimental testing. I would also like to thank Per Otto Ålråk for assistance and equipment.

A special thanks to my family for supporting me and encouraging me to a career in technology ans science.

Summary

Gas explosions in a square channel have been investigated with a main focus on the deflagration to detonation transition (DDT). The gas mixtures were hydrogen and air at different concentrations. This work have been motivated by issues of process safety and hydrogen infrastructure development. There is a need to understand the deflagration to detonation transition from a safety perspective. Recent accident have shown possibilities of DDT in premixed fuel and air. At present there are no software tools capable of predicting DDT in real scenarios, and there is a need to produce accurate experimental data for validation, but also a better understanding of the physics related to DDT.

The experiments presented in this thesis were performed in a square channel with transparent side walls and one obstacle. The obstacle was placed $1\,m$ from the closed ignition end, and the first results chapter presents the experimental study of flame propagation from ignition up to the obstacle. The ignition source was both a single spark and a distributed ignition, were the latter was assumed to produce a 2 dimensional flame front. The main conclusion of this study was that the 2D assumption was only valid up to the point of tulip flame formation.

The study of DDT was divided in two parts, one in homogeneous gas mixtures, the other regarding inhomogeneous gas mixtures. The homogeneous gas mixture experiments showed that transverse waves were important for the DDT, but also that these waves originated from far behind the leading tip of the deflagration. This conclusion was also found in a numerical study using the in-house FLIC code developed by Dr. Vaagsaether.

The study of inhomogeneous gas mixtures were done to investigate if inhomogeneities increased the likeliness of DDT. The conclusion was that it was not the case in this particular setup and method. However, other interesting results were found regarding detonation propagation in layers of reactants bound by a wall and a layer of air. The propagation mechanism of detonations in a reactive layer was also studied using the FLIC code, where it was observed a expansion effect and a merging of triple points at the top wall. This was qualitatively similar as the experimental results.

Contents

List of Figures

List of Tables

Chapter 1

Introduction

1.1 Background

The transition from turbulent subsonic deflagration to supersonic detonation in accidental gas explosions is a devastating phenomenon which is not fully understood [24]. The understanding of the deflagration to detonation transition (DDT) is of major interest since it is associated with the highest pressure loads in accidental gas explosions.

In the oil and process industry there is a focus on explosion safety in gases. Large amounts of combustible gases are handled and processed in the plants and a constant focus on explosion safety is vital.

Nuclear energy production also focus on explosion safety, since a loss of reactor cooling could lead to production of hydrogen inside the reactor. This issue has been a concern and a motivation for gas explosion research for many years.

In the development of renewable energy resources it could be possible to store energy as liquid or compressed hydrogen. This will require a good understanding of gas explosions, since safety standards, codes and regulations must be made accordingly to accepted risk criteria.

Hydrogen powered vehicles are a possible option to reduce green house gas emissions, but must address the safety issues of gas explosions. It will require a development of hydrogen storage and use on board road vehicles. It will also be a focus on secondary transport systems such as ferries, tunnels and garages.

Many hydrogen powered forklifts that have been put into operations the latest years, and the release of hydrogen indoors and possible gas explosion are currently under investigation by many researchers.

This thesis is the documentation of an experimental study of gas explosions in hydrogen and air mixtures, with a focus on DDT. The work consists of a series of lab scale experiments which are complemented with numerical simulations. This work will contribute to the DDT knowledge base and provide experimental results of deflagration to detonation transition.

History is full of intentional and accidental explosions, many of which is presented by Krehl [25]. And the importance of understanding detonations and including them as likely accident scenarios is pointed out in a very important paper by Johnson [26]. The Buncefield Explosion Mechanism Joint Industry Project [27], also showed the importance of understanding flame

acceleration and DDT. The following four accidents are presented chronologically and all of them a relevant as they involve various degrees of detonation.

1.1.1 Port Hudson

The 1970 Port Hudson (Missouri, USA) explosion followed a leak from a liquid propane pipeline. The propane flowed into a valley for more than 20 minutes before ignition. No fatalities followed the explosion but $40000\,m^2$ of surroundings were severely damaged. Burgess and Zabetakis [28] at The US Bureau of Mines investigated the accident. It was concluded that a detonation was initiated, most likely at the confined volume of a warehouse where there must have been a jet coming out of the building. The detonation propagated through large parts of the unconfined propane-air cloud. An estimate suggests an energy equivalent of 50 tons of TNT.

1.1.2 N1 ammonia plant

The 1985 accident at the N1 ammonia plant in Porsgrunn were investigated by Bjerketvedt and Mjaavatten [29]. A series of events including a pump running dry, a faulty gasket and failed check valves lead to a $30\,bar$ leakage of H_2 in 20-30 s. Up to 20 kg was released and more than 7 kg was assumed to combust in the explosion. This is an equivalent of about 200 kg TNT. The hydrogen was most likely ignited by a hot bearing on the dry running pump, and a deflagration jet propagated from inside the motor cover and could have initiated a detonation in the combustible mixture. The following explosion killed two people, one severely injured and caused irreparably damage to the ammonia plant. Damage indicators suggests overpressure more than $10\,bar$ which is consistent with a detonation, at least in parts of the combustible mixture.

1.1.3 Buncefield fire

The Buncefield fire of 2005 at the Buncefield (UK) fuel storage tank facility started with an explosion estimated to be 100 times larger (scaled by energy) than the Port Hudson explosion according to Bradley et al. [30]. 300 tonnes of winter grade gasoline was released and formed a large vapor cloud in the tank facility and around neighboring buildings. An emergency pump house was a likely ignition location. The conclusions of Bradley et al. [30] are not absolute, but give strong indications of detonations at Buncefield. The paper by Johnson [31] concludes that detonation was very likely to have occurred due to the accidental indicators and modeling results. Like Port Hudson there was a building where the DDT could occur, but also a possible flame acceleration mechanism along hedges and undergrowth of alongside pathways. It is also pointed out that inhomogeneities of the vapor-cloud could trigger DDT more easily than homogeneous conditions.

1.1.4 Fukushima Nuclear Power Plant

The Fukishima Daichi Nuclear power plant explosions of 2011 followed the tsunami which rendered all cooling systems out of operations. In such events it is known that a lack of cooling will lead to production of gaseous hydrogen inside the reactor core. This had to be vented to

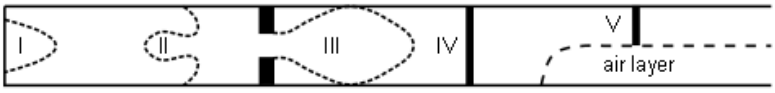

Figure 1.1: A sketch of the experimental setup. I Ignition and initial flame instability. II Tulip flame formation. III Jet through obstacle and DDT. IV Detonation propagation. V Detonation propagation in a layer of reactants.

Figure 1.2: A picture of the experimental setup in the laboratory.

prevent high over pressure inside the reactor. The vented hydrogen mixed with air and was ignited. This happened at several of the plants a the Fukushima site [32]. It is still too early to enter the site to conduct a full accidental investigation, but press videos were analyzed by Tsuruda [32] and at least one of the explosions were a "typical gas explosion". The IAEA report on Mitigation of Hydrogen Hazards in Nuclear Power Plants [33] clearly states that DDT and detonations are extremely destructive. At this point it is not possible to determine if the hydrogen-air mixture at any of the plants at the Fukushima site detonated, but it serves as a very recent reminder of the importance of fundamental knowledge on DDT and detonations.

1.2 Aim of thesis

The aim of this study is to understand the deflagration to detonation transition in channel and pipes, with a focus on jet ignition. The role of mixture inhomogeneities are also investigated to understand the influence on DDT. The work is a part of the IEA Hydrogen Implementing Agreement Task 19 and Task 31, and the knowledge can be used to prevent accidents and save lives. The method of investigation are experimental studies and the work is mainly motivated by the industrial safety and infrastructure applications of hydrogen. Vaagsaether [12] and Knudsen [34] investigated similar problems and this work is a continuation of their work. DDT can occur in mixtures of fuel and oxidizer where the deflagration has been accelerated enough. There have been reported many studies of DDT, and the formation of induction time gradients and hot spots

are important factors in the DDT. These gradients and hot spots are often created by turbulent mixing and/or shock compression. The experimental investigations in this work will also be used as validation data for CFD codes

The experimental setup is sketched in Figure 1.1 and a picture is shown in Figure 1.2. It has a square cross section of 10-by-10 cm^2 and is 3 m long. A single baffle type obstacle is located 1 m from the closed end. This setup is made to represent simple pipe equipment in process plant or hydrogen infrastructure installment. When the hydrogen-air mixture inside the channel ignited, the resulting flame pushed the unburned reactants in front itself and through the obstacle opening. The flow through the obstacle generated a jet, and this jet enhanced the combustion rate and was a potential source for a DDT event. A jet initiated DDT is relevant for several accidents.

In risk assessments there is a need to quantify the relevant hazards, and computational fluid dynamics (CFD) are very good tools for this task. The CFD codes should however be validated against experimental results and this project will produce data for this. The lab scale experiments will provide data to validate the capabilities of CFD codes to predict DDT.

In Figure 1.1 the numbers refer to different stages of combustion from ignition to complete combustion of all reactants. **I** is the expanding deflagration after ignition, while **II** is the change of shape and tulip flame formation in the channel. **III** is the combustion in the jet through the obstacle and **IV** is a detonation wave propagating in the channel. A lot of focus is put on the transition from **II** to **IV**. While **V** is the propagation of a detonation in a layer of reactants on top of a inert layer of air. By following the combustion wave from ignition to completion, the aims of this work are summarized as follows.

I and II Investigate the propagation of hydrogen-air deflagrations as it propagates from ignition up to the obstacle. This investigation shall document the shape, velocity and pressure of a flame propagating in a channel with one obstacle. Also the effect of ignition source shall be investigated.

III Investigate the onset of detonation in a jet behind a single obstacle in a channel. Identify where the detonation onsets, whether it is at the tip of the turbulent flame jet or at the walls.

III and IV Possibly identify the event that lead up to onset of detonation behind the single obstacle.

III and V Investigated the influence of inhomogeneous gas mixtures on DDT.

I to IV Produce experimental results as a basis for validation of numerical methods.

1.3 Structure of thesis

Figure 1.1 illustrate the propagation of the combustion wave from ignition to all reactants are burned. The literature study and results chapter will follow the same order.

- A literature review of work related to the phenomenas observed in the experiments.

- A description of the experimental setup. The experimental method is described as well as a short explanation of processing of experimental results and other calculations.
- The experimental results are divided into sections following the path of the combustion wave. A discussion and conclusion follows at the end of this chapter.
  - The experimental study of flame propagation in the first meter is presented as a minor revision of the paper in the appendix A.1.
  - A chapter about the main study of DDT in homogeneous gas mixtures.
  - A chapter about DDT and detonations in inhomogeneous gas mixtures.
  - The numerical study of DDT in the setup is presented as a short summary of paper in the appendix A.2.
- A summarized conclusion of the thesis.

Chapter 2

Relevant literature on hydrogen gas explosions

This chapter gives a selected review on some phenomena related to the flame propagation, detonations and deflagration to detonation transition (DDT) observed in the series of experiments presented in this work. The review is based on selected papers which gives a background for the discussions to follow in the later chapters. Details of the experimental geometry and setup will be given in the next chapter, but a brief description is given here as the order of the reviewed topics follow the same order as the different stages of the propagating combustion wave (i.e. deflagration and detonation).

Figure 2.1 shows the order of the combustion wave propagation. It follows as:

I Ignition and expanding deflagration with flame instabilities.

II Change of shape to tulip flame in the channel.

III Combustion in the jet through the obstacle.

- With possibility of deflagration to detonation transition (DDT).

IV Detonation propagation in the channel.

V Detonations in inhomogeneous mixtures, i.e. stratified layers of reactants.

The focus of this work are hydrogen-air mixtures, but the different phenomena described in this review are also related to other reactants.

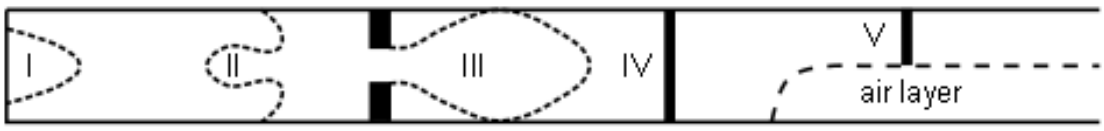

Figure 2.1: A sketch of the geometry with the different stages of combustion wave propagation from ignition and tulip flame to DDT and detonations in layers.

2.1 Ignition and initial flame propagation with flame instability

The field of flame instability is extensive and considered outside the scope of this study. It is however necessary to give a brief overview of the different instability mechanisms as a short explanation and essential work. Figure 2.2 shows the initial flame propagation of a deflagration ignited close to the closed back wall of a square channel.

2.1.1 Ignition and initial flame propagation

The ignition phenomenon of a reactive gas mixture is an extensive study in it self and will not be presented here. The phenomenon of the initial stages of a propagating hydrogen-air flame is shown in Figure 2.2. The flame expands spherically from the spark gap, and quench at the walls. After this initial spherical expansions it propagates as an elongated half sphere. The propagating flame is subject to different flame instabilities. A brief description of some flame instabilities are given next.

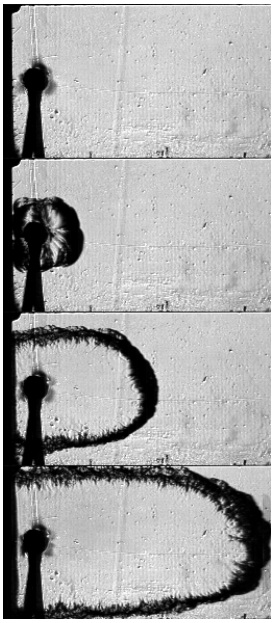

Figure 2.2: 4 frames showing the initial flame propagation on a hydrogen-air deflagration.

2.1.2 Thermal diffusive instability

This is also called the nonequidiffusion instability [3]. The ratio of thermal diffusivity ($\alpha = \frac{k}{c_p \rho}$) to mass diffusivity ($D$) is called the Levis number, $Le = \frac{\alpha}{D} = \frac{k}{c_p \rho D}$, where k is the thermal conductivity $[W\,m^{-1}\,K^{-1}]$, c_p is the specific heat $[J\,kg^{-1}\,K^{-1}]$, ρ is the density $[kg\,m^{-3}]$ and D is the diffusion coefficient $[m^2\,s^{-1}]$.

If we consider a 1D flame front where the Lewis number $Le > 1$, then heat is transported (by diffusion) away from the reaction zone faster than reactants are transported (by diffusion) into the reaction zone. This reduces the flame temperature and the burning velocity as $S_L = f(T, ...)$. If $Le < 1$, the temperature is increased and increases the burning velocity. Law [1] writes that for a curved flame front, the Karlovitz number and the Lewis number influence the flame temperature T_b relative to the $T_{Le=1}$ together as:

$$\begin{aligned} T_b > T_{Le=1}\ for\ \left[Ka^0 > 0, Le < 1\right]\ or\ \left[Ka^0 < 0, Le > 1\right] \\ T_b < T_{Le=1}\ for\ \left[Ka^0 > 0, Le > 1\right]\ or\ \left[Ka^0 < 0, Le < 1\right] \end{aligned} \tag{2.1}$$

The $Ka^0 = [(k/c_p)_{unburned}/(f^0)^2](\rho_{unburned}\,\kappa)$, where f^0 is the unstretched burning flux $[kg\,m^{-2}\,s^{-1}]$ and κ is the stretch rate $\kappa = \frac{1}{A}\frac{dA}{dt}$. As an example; an outward propagating spherical flame has positive stretch rate, while an inwards propagating flame has negative stretch rate.

For a slightly perturbed flame, non unity Lewis numbers will affect the burning rate at the flame front. A schematic given by Law [1] is shown i Figure 2.3

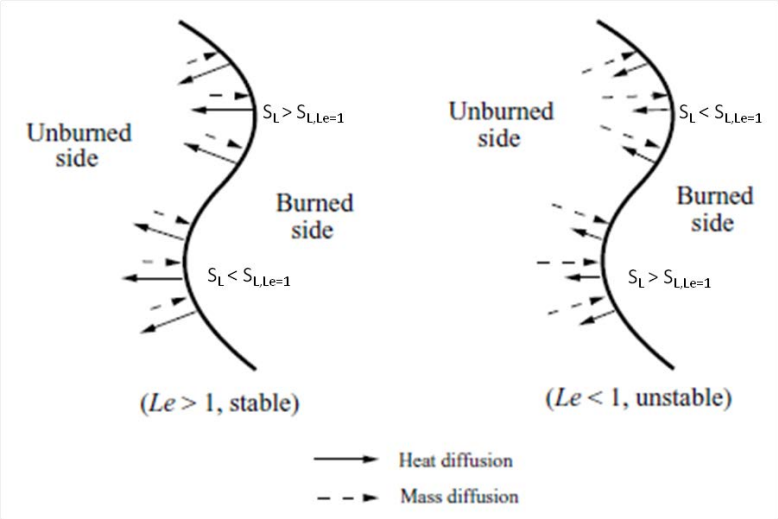

Figure 2.3: Law (2006) has given a schematic of the thermal-diffusive instability [1].

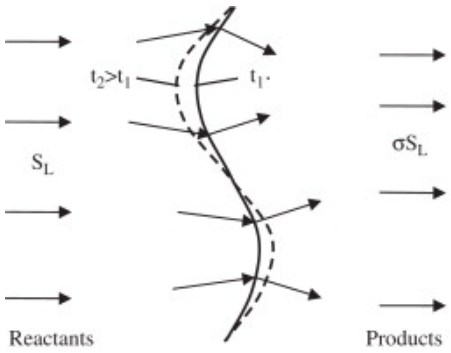

Figure 2.4: The Landau-Darreius instability, where it is shown how the streamline diverge and converge behind the flame front [2].

2.1.3 Landau-Darreius instability

The paper "On the Theory of Slow Combustion" by Landau (1944) [35], presents an analysis of the propagation and stability of flames. It is assumed that the flame is infinitely thin, basically a density discontinuity. The flow is considered to be incompressible and viscosity is neglected. If it is given that $\rho_b < \rho_u$, then small perturbations are always unstable. A sketch of the Landau-Darreius instability is given by Ciccarelli and Dorofeev [2], and shown in Figure 2.4. It is seen that the streamlines converge (increase flow velocity) behind the convex parts of the flame and diverge (decrease flow velocity) behind the concave parts. The linear stability analysis [35] shows that the flame is unstable for all wavelengths.

The thermal diffusive instability and the Landau-Darreius instability can counteract each other as the thermal diffusive instability can dampen the Landau-Darreius instability. Cellular growth on laminar flames are shown in Figure 2.5, from experiments by Law (2006) [3], exper-

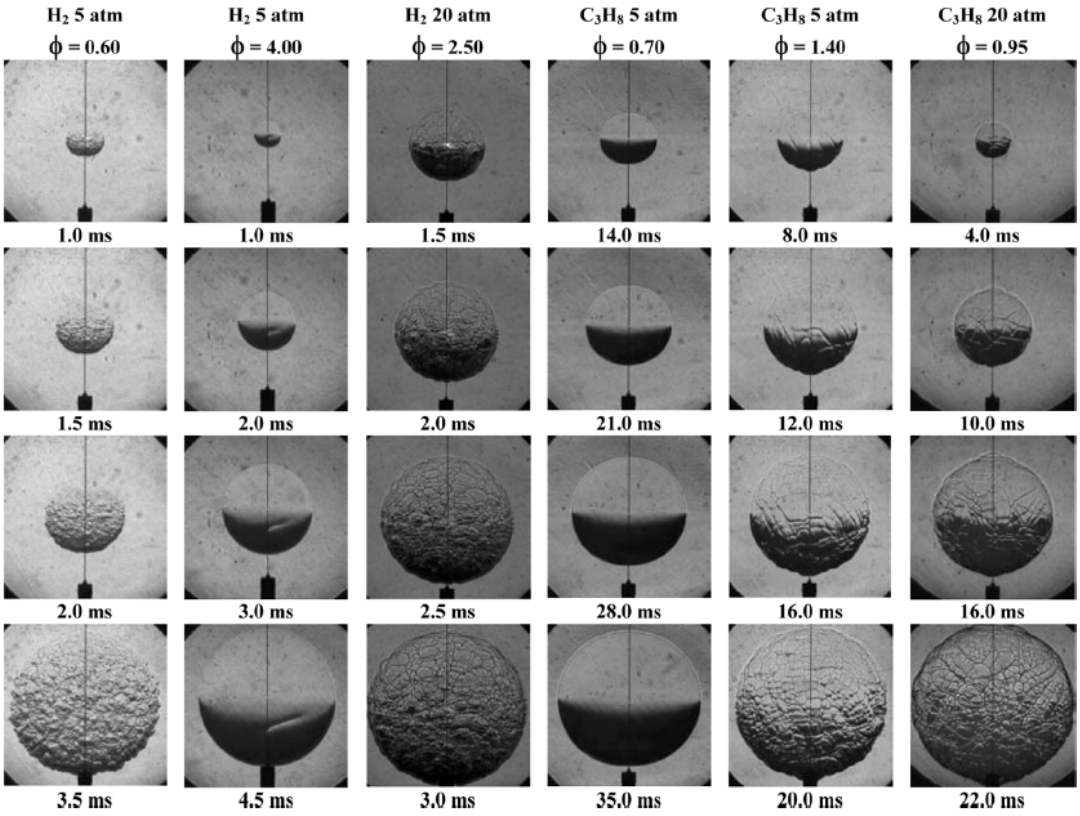

Figure 2.5: Shadowgraph images of spherically expanding flames, with and without cellular growth. The elevated pressures lead to the onset of Landau-Darreius instability due to decreased flame thickness. Experiments by Law (2006) [3].

iments at 1 atm were done by Rai [4] and shown in Figure 2.6. It is seen that the cellular growth depends on the Lewis number, but also the pressure. As increased pressure reduces the flame thickness, the flame front is more prone to Landau-Darreius instability.

2.1.4 Rayleigh-Taylor instability

This fluid instability regards the acceleration of two fluid with different density separated by a discontinuity. The overall direction of the discontinuity is normal to the acceleration. Rayleigh (1895) [36] worked on the issue of fluids accelerated by gravity, and Taylor [37] work the same problem in 1949. Their work showed that if the force of acceleration acts from the side of the heavier fluid the interface will be stable. If the force acts from the side of the lighter fluid towards the heavier fluid, the amplitude of the initial interface pertubation will grow in time. For premixed combustion applications, the Rayleigh-Taylor instability could be observed when hot reactants are accelerated into the denser, cold reactants.

A more detailed mathematical description and derivation of the Rayleigh-Taylor instability

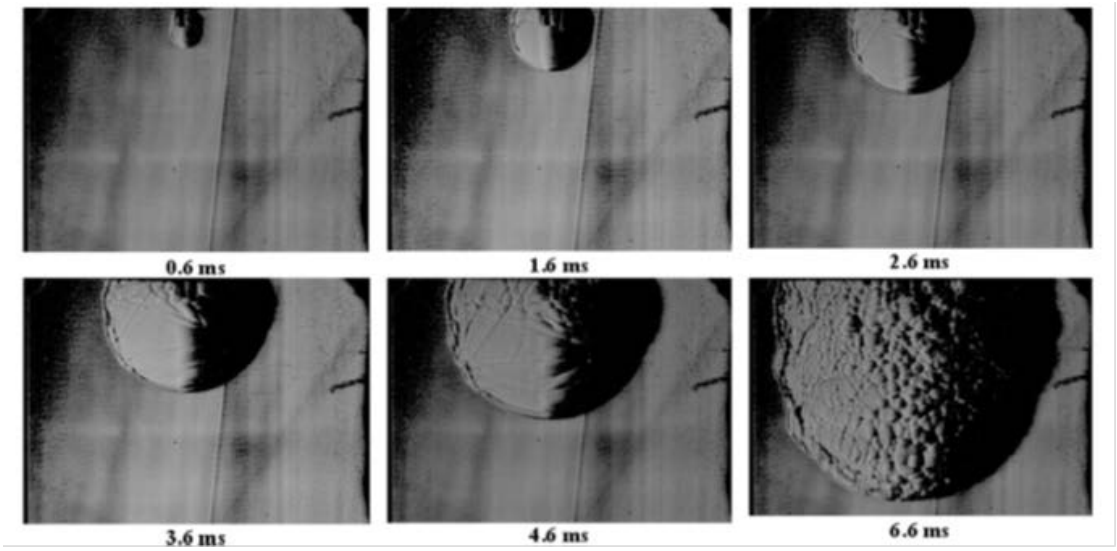

Figure 2.6: Shadowgraph images of hydrogen-air flame at 1 atm. Experiments by Rai (2009) [4].

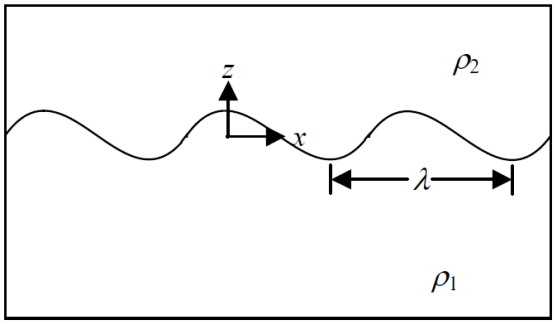

Figure 2.7: Sketch of Rayleigh-Taylor problem [5].

is given in the lecture notes by J. Oakley [5]. A sketch of the problem is given in Figure 2.7. It is given that the interface is stable when the pressure gradient has the same sign as the difference in density. As an example, consider the case in Figure 2.7 where positive direction is up the then pressure gradient is negative. The interface will be stable according to Rayleigh-Taylor theory when $\Delta\rho = \rho_2 - \rho_1$ is negative, as the case when fluid 1 is water and fluid 2 is oil. When considering the case with hot light products (ρ_2) and cold dense reactants (ρ_1),then $\Delta\rho < 0$. The interface will be stable according to Rayleigh-Taylor when $\Delta P < 0$, i.e pressure in the products are lower than the pressure in the reactants. The stability if any interface according to Rayleigh-Taylor theory also require the pressure gradient to be in the same direction all the time.

2.1.5 Richtmyer-Meshkov instability

The sudden acceleration of a fluid by a shock wave, require another type of Rayleigh-Taylor explanation. This was given theoretically by Richtmyer (1954) [38] and experimentally by

Meshkov (1969) [39]. The interface is unstable regardless of density difference and pressure gradient when it is accelerated by sudden shock compression. The work by Richtmyer is a comprehensive report and also investigates the effect of compressibility at the fluid surfaces. This fluid instability is important when pressure waves are present at the flame (deflagration) fronts. The Richmyer-Meshkov instabilities are also seen in the inner structure of detonation fronts [12].

2.1.6 Kelvin Helmholtz instability

The studies by Helmholtz (1868) [40] and Lord Kelvin (1871) [41], investigated the instability of two fluids with different density separated by a discontinuity and flowing parallel with different velocity. A simple example of this instability is the flow of air (wind) over water (the sea). Small ripples on the surface will in turn grow and develop into waves. This instability is relevant for shear flow of two fluids with same phase as well, and in combustion studies it is relevant when reactants and products flow parallel. The Kelvin-Helmholtz instability generate a swirling flow at the interface and could lead to enhanced mixing between reactants and products. Numerical work by Vaagsaether [12] (among others) showed Kelvin-Helmholtz instabilities in the detonation front.

2.2 Tulip flame

The propagation of premixed flames (deflagrations) in channels and pipes could be subject to the instabilities mentioned above. After ignition the flame propagate slowly as a laminar flame. Even though it is not overall laminar anymore, due to instabilities, it does not have to be turbulent. As flames propagate in pipes and channels it is often observed changes in the shape of the flame front. One type of shape change is called the tulip flame, and is given a short review in this section.

The early work of Mallard and Le Chatelier [42] reported "jerky movements" of flames related to the tulip shape. Ellis and Robinson [43] also reported a “cusp-shaped” flame in their experiments. Markstein [6] investigated in 1957 how a shock wave interacted with an inverted curved flame front. The short duration of the shock wave acceleration made Markstein suggest that a modified concept of the Rayleigh-Taylor instability was needed to explain the development of the flame front. Images from one of the Markstein experiments are shown in Figure 2.8. The figure shows how the shape of the flame front changes as the shock wave pass over it.

Richtmyer studied in 1954 the Taylor instability in shock acceleration of compressible fluids [38], and described mathematically how a density interface would response to shock acceleration. The report was originally classified, but unclassified in 1959 and answered some of Marksteins modifications to the Rayleigh-Taylor instability.

The name "tulip flame" was introduced by Salamandra et al. [44] in 1958 in their study on detonations. The experimental setup was circular and square cross sectional chambers. They used schlieren and streak photography and captured the initial slow deflagration. At first, the flame was ”meniscus-like”, but later the flame slowed down and changed shape to a tulip-like shape, hence the name.

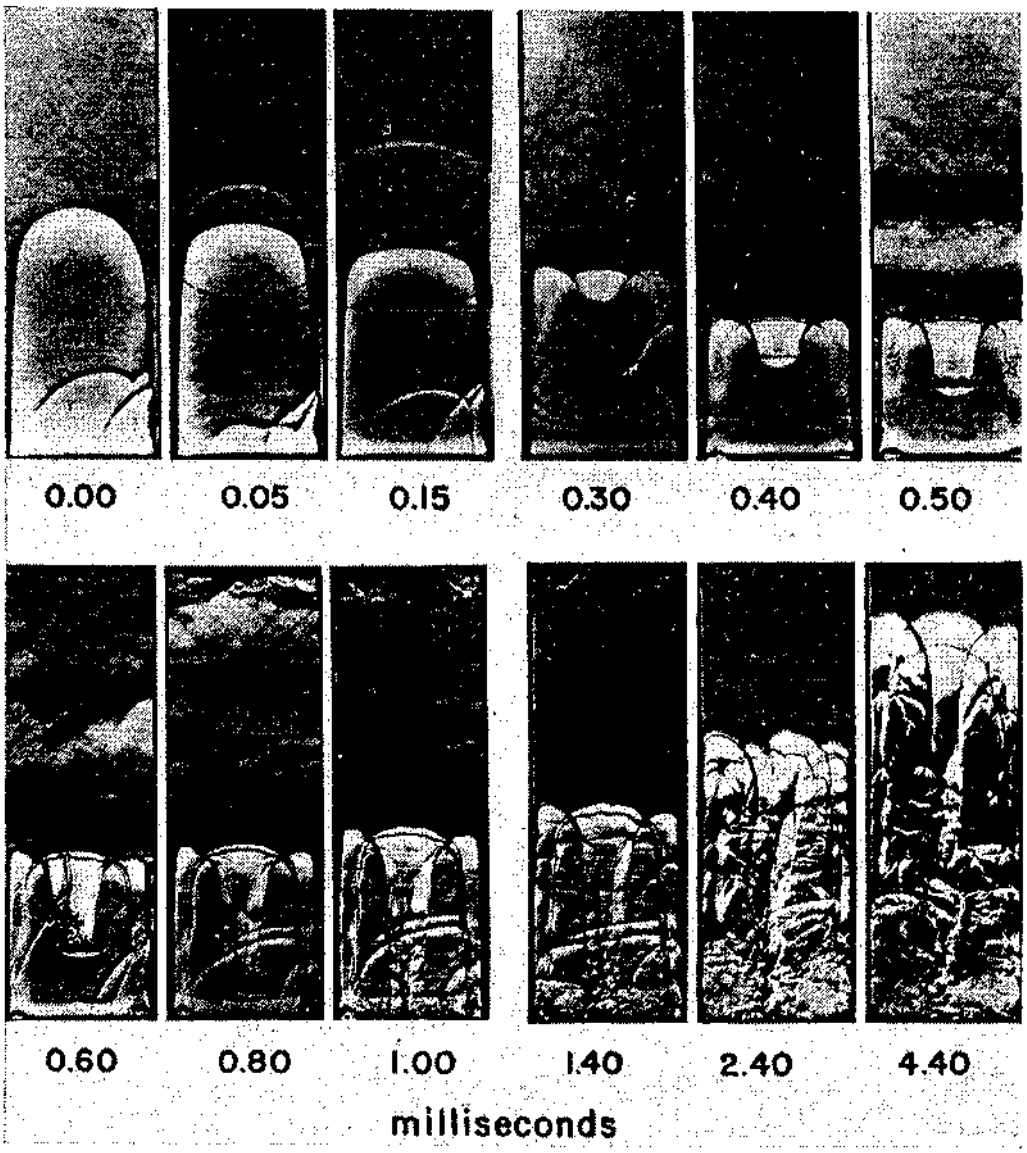

Figure 2.8: This figure shows the Markstein experiments with butan-air mixture, where a shock wave interacts with the flame front [6].

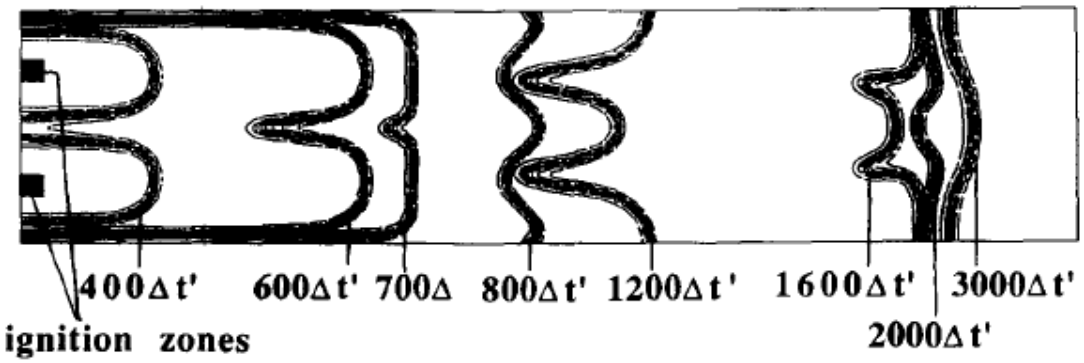

Figure 2.9: Development of the double tulip flame. Initially ignited a two locations. The time instance are given below the figure, from Gonzalez et al. (1992) [7]

Gonzalez et al. [7] studied the tulip flame numerically in 1992. They showed that the flame slowed down before it began to fold into a tulip flame. Also seen in the study was the formation of a double tulip flame. Gonzalez et al. also investigated the effect of the Landau-Darrieus instability (which is always present), and stated it to be different than the tulip flame formation but it would amplify the effect once the flame has turned into a slightly convex (towards the reactants) shape.

Among many, Clanet and Searby [45] studied experimentally the flame propagation in a pipe, ignited at the back wall, and divided flame propagation into four stages, each one followed the other. The times of which followed as $t_0 < t_{sphere} < t_{wall} < t_{tulip}$. The first stage begins at time of ignition (t_0) when the flame expands hemispherical. The second stage describes the flame as it is hemispherical (t_{sphere}) and expands towards the walls (t_{wall}) and becomes finger shaped. All this time the area of the flame increases. The third stage starts when the finger shaped flame starts to quench at the walls and area decreases again and the flame starts to invert and turn into a tulip shaped flame (t_{tulip}). During this stage the flame speed decreases as well as the flame area. The fourth stage is the propagation of the tulip flame from this stage and onwards.

The time t_{sphere} is given by Equation 2.2

$$t_{sphere} = \frac{D}{2S_L}.(0.1 \pm 0.02) \tag{2.2}$$

D is the diameter of the pipe. The time at which the flame reaches the walls is given by Equation 2.3

$$t_{wall} = \frac{D}{2S_L}.(0.26 \pm 0.02) \tag{2.3}$$

The inversion or formation of the tulip flame starts at t_{tulip}, given by Equation 2.4.

$$t_{tulip} = \frac{D}{2S_L}.(0.33 \pm 0.02) \tag{2.4}$$

Dunn-Rankin and Sawyer [8] investigated tulip flames in closed tubes. They recognized that the tulip formation was initiated when the flame quenched at the walls. They saw that there was a kink in the pressure records prior to the formation of the tulip flame as the total area of the flame front was reduced, see Figure 2.10. This is opposed to the work by Clanet and Searby who showed that the formation of the tulip flame occurred later than the quench at the wall, see Equation 2.3 and 2.4. Dunn-Rankin and Sawyer produced tulip flames for different kinds of ignition configurations.

Kratzel et al. [46] investigated the transition of a curved flame into a tulip shape for hydrogen/air mixtures. The tulip flame formation started after the flame quenched at the walls. They pointed out the baroclinic effect on the formation of an inverted flame front, due to pressure waves generated by the flame which were reflected at a closed end. The vorticity (the curl of the velocity) equation describes the movement of vorticity of a fluid. Kratzel et al. [46] described the formation of the tulip flame based on a source term in the vorticity equation. This source term is the baroclinic term (often referred to as the baroclinic effect) and is the cross product of the density and the pressure gradients divided by the squared density, Equation 2.5.

$$S_{baroclinic} = \frac{1}{\rho^2} \cdot \bigtriangledown \rho \times \bigtriangledown p \tag{2.5}$$

If the density and pressure gradient were parallel, there would be no vorticity generation. But any curved flame front will produce vorticity as it interacts with a pressure wave. The production of vorticity on a hemispherical flame front will result in a rotational flow given by Equation 2.5.

Dunn-Rankin [47] point out that the Landau-Darrieus instability is important for the growth and maintenance of the inverted flame front for relatively short closed tubes. In the cases of flame propagation in short tubes Dunn-Rankin recognize a recirculating flow as the cause of tulip flame generation. Acording to Dunn-Rankin, the formation of an inverted flame front or tulip flame does not arise from one single phenomenon. It is dependent on the system under study. No definitive mechanism of the tulip flame formation has yet been proposed.

Metzener and Matalon [48] also state that the vortices generated behind the flame advects the flame into the tulip shape, which is very consistent with the baroclinic explanation. The study of Kaltayev et al. [49] also recognize the vorticity of the flow as major contributor to the tulip flame development.

Recent studies of flame propagation in a closed channel are done by Xiao et al. [50, 51], where they observed the "distorted tulip" flame. The numerical simulations with the Ulster LES model showed that the flame acceleration due to turbulence was very small, hence other flow and wrinkling mechanisms accelerated the flame. The tulip flame formation coincided with the reflected acoustic waves in the channel. The "distorted tulip" flame coincided with the second reflection of the waves in the channel, and the vortices generated by the pressure waves and flame front and consistent with the baroclinic effect. This is also in agreement with the baroclinic explanation as the reflected pressure waves interacts with the already curved flame front.

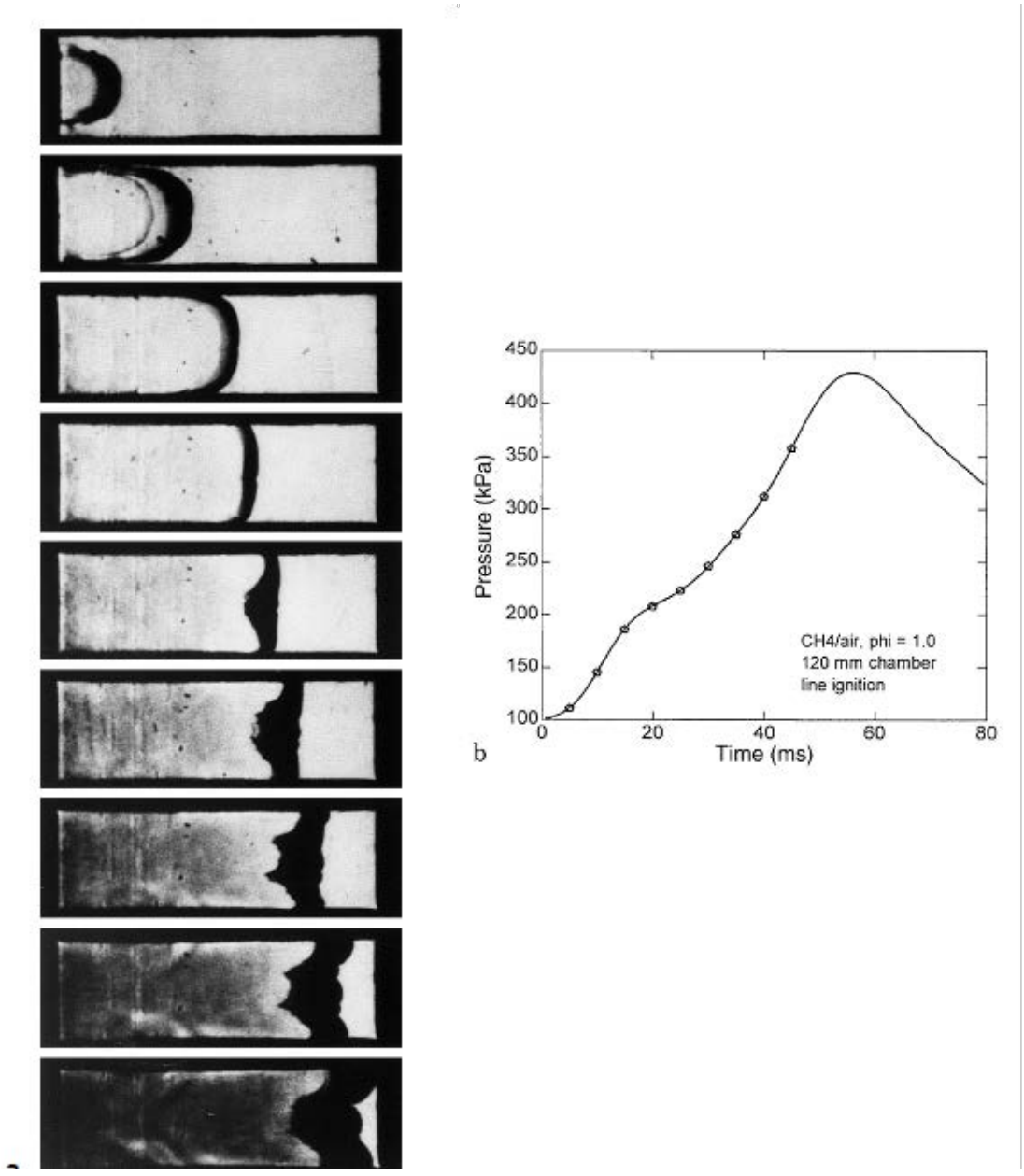

Figure 2.10: Development of the double tulip flame and pressure records. From Dunn-Rankin and Sawyer [8]

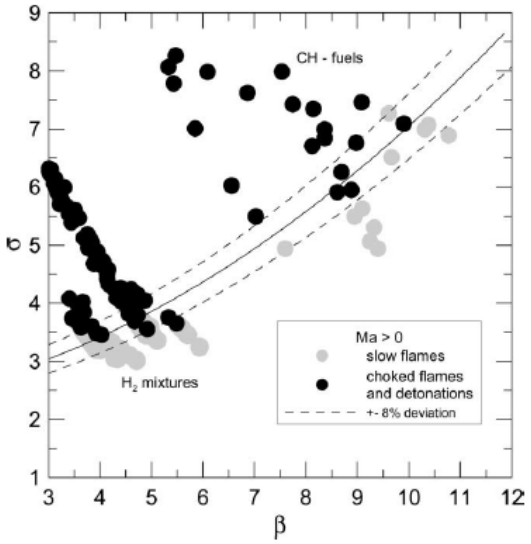

Figure 2.11: The limit between fast and slow flames given in the σ and β plane [9] for $Ma > 0$

2.3 Flame acceleration and turbulent combustion

Important elements of flame acceleration (FA) have been studied by Dorofeev et al. [9, 52]. A potential for flame acceleration was estimated based on the expansion ration ($\sigma = \frac{\rho_u}{\rho_b}$), the Zeldovich number $\beta = E_a(T_b - T_u)/(RT_b^2)$ and the Markstein number, see Figure 2.11 and Figure 2.12. This potential could be estimated independent of geometry. The flame acceleration was considered as two regimes, one with slow flames and one with fast flames. The fast flame regime include choked deflagrations and detonations. Dorofeev also states that fast flames are a prerequisite for DDT [13].

Even though the potential for flame acceleration has been suggested to be independent of geometry it is by no means a statement to marginalize or suppress the influence of instabilities and geometry generated turbulence. Turbulence will influence flame fronts at many different length scales. The smallest length scales will influence the reaction zone, while larger length scales will wrinkle and stretch the flame front. This influence is illustrated by Chomiak [10], in Figure 2.13. The figure shows an analogy between a flame front and an ink spot. The case a) shows the evolution of the ink spot if it is subject to turbulence at a length scale larger than itself. This will stretches the ink spot. The same will happen to a flame front if the turbulent length scale is larger than the flame thickness. The stretched flame will have increased surface area and hence increased overall reaction rate. The case b), where the ink spot is larger than the turbulent length scale, the whole shape and structure becomes wrinkled and internally distorted. If the flame thickness is larger than the smallest turbulent length scale then the inner structure of the flame will be wrinkled and distorted. This will also lead to an increased mixing within the reaction zone and hence locally increase the reaction rate.

The influence of turbulence on flame front is often summarized in a Borghi diagram. Figure 2.14 shows a Borghi diagram according to Warnatz et al. [11]. As discussed there are two

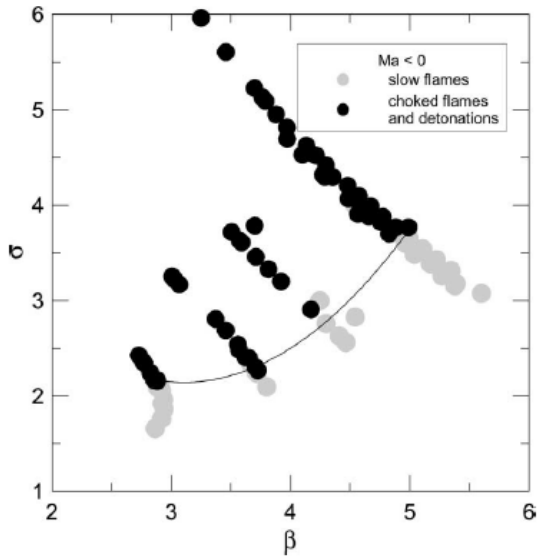

Figure 2.12: The limit between fast and slow flames given in the σ and β plane [9] for $Ma < 0$

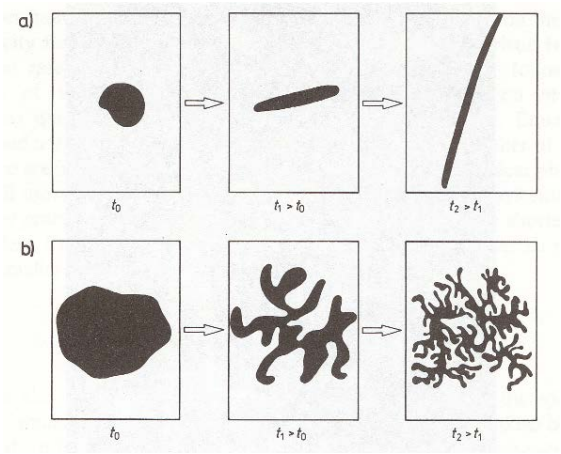

Figure 2.13: Illustration of how turbulence could influence a flame front. Here an analogy to an ink spot. If the ink spot (flame front) is smaller than the turbulent length scale it stretches it a). If turbulence is smaller than the ink spot (flame front) it breaks it into many smaller structures b). [10]

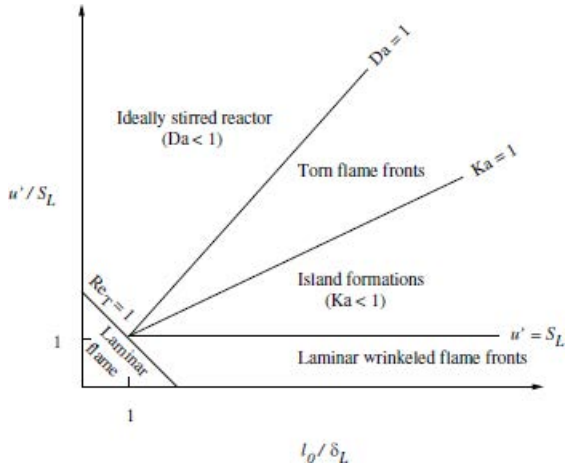

Figure 2.14: The Borghi diagram according to Warnatz et al. [11]

important length scales: The flame thickness $\delta_L\,[m]$ and the turbulent length scale $l[m]$. The flame thickness could be given by the laminar burning velocity and a reaction time scale as $\delta_L = \tau_L S_L$. The turbulence is not given by one turbulent length scale, but rather a spectrum of length scales. The large scale is often referred to as the integral length scale l_0 and the smallest scale as the Kolmogorov scale l_K with the corresponding time scales $\tau_0\,[s]$ and $\tau_K\,[s]$. Also needed in the study of the Borghi diagram is the rms value of the turbulent fluctuations $u'\,[m/s]$. The vertical axis of the Borghi diagram is given by the ratio of turbulent intensity to laminar burning velocity and the horizontal axis is given by the ratio of integral length scale to flame thickness. The Borghi diagram has five different regimes which are explained as follows:

- Laminar flame: Where $Re_T = \frac{u' l_0}{S_L \delta_L} < 1$
- Laminar wrinkled flame fronts: Where $S_L > u'$ and $l_0 > l_K > \delta_L$
- Island formation: Where $u' > S_L$ and $l_0 > l_K > \delta_L$ as the turbulent Karlovitz number is less than unity and $Ka = \frac{u'}{S_L}\frac{\delta_L}{l_K}$. The turbulence will stretch the flame analog to Figure 2.13 a).
- Torn flame fronts: Where $l_0 > \delta_L > l_K$, as $Da = \frac{l_0}{\delta_L}\frac{S_L}{u'} > 1$. The turbulence will stretch the flame analog to Figure 2.13 a) and b) at the same time.
- Ideally stirred reactor: Where $Da < 1$ and $l_0 < \delta_L$. All turbulent length scales influence the inner structure of the flame front as Figure 2.13 b).

The Borghi diagram illustrates turbulent combustion and relations to turbulent length scales. Recent studies by Oran et al. have addressed the issue on turbulent length scales [53]. It is pointed out that shock and sudden compressions will influence flame fronts on a multitude of length scales. Vorticity could be generated due to Richtmyer-Meshkov instabilities by repeated interactions between density and pressure gradients. The Kolmogorov theory would not be

applicable when turbulence is created on all length scales, possible also below the Kolmogorov scale.

2.4 Deflagration to detonation transition - DDT

The main focus of this review is experimental investigation of DDT. The section is divided into three parts where the first part reviews the work on DDT in smooth tubes, the second part is on tubes and channels with obstacles, while the last part is a review on jet initiation of DDT. These three modes of DDT have been chosen because they are relevant for the experimental study of this thesis. Although the geometrical setup of this study does not directly represent any of the three parts of the review, it is still important to compare it to experiments with some similar phenomenon.

Thomas [54] has given a comprehensive discussion on various forms of DDT, and differentiates the terminology between the macroscopic DDT and the microscopic DDT. The large scale macroscopic DDT includes the process from accelerating deflagration up to a propagating detonation. The small scale microscopic DDT governs the actual onset of detonation at the point where the combustion process changes from diffusion controlled to shock heating controlled. In this work, the term DDT are used in the larger definition and include both acceleration and onset of detonation. Thomas also gives a discussion on the understanding of the weak DDT, where it is not onset by a strong reflected shock wave but rather point out the importance of non isotropic and non equilibrium turbulence to accelerate a deflagration and create small hot spots which in turn generate transverse waves and add up to strong pressure waves capable of forming the required shock/reaction complex known as the detonation.

2.4.1 DDT in smooth pipes and channel

The transition from deflagration to detonation in smooth channels governs the investigation where there are no flow obstacles and the flow is confined in either circular pipe or square/rectangular channel. This is chosen as a part of the review because most of the channel in the experimental study of this thesis is smooth.

Early work was done by Urtiew and Oppenheim [55], and important developments of photography techniques was important for their work. Laser illumination and ultra fast camera captured the shock fronts, flames and the DDT. They showed that DDT occurred at either the turbulent flame front, behind a leading shock wave or at the contact surface as two shock waves merged together. It is shown that not one single macroscopic phenomenon is responsible for DDT, but there are rather several ways to DDT. Oppenheim A.K. named the term "An explosion within the explosion", which is often used to describe the phenomenas leading up to onset of detonation. The explosion within the explosion is a process where reactant burn very fast relative to the rest of the combustion process. Sometime it is referred to as a constant volume combustion, hot spot or local explosion. The explosion within the explosion could cause locally high pressure and pressure waves propagating in the system. These local explosions are known to be strong enough to cause DDT by shock compression and heating. Meyer et al. [56] showed that an explosion within the explosion occurred far behind the leading edge of the flame front. A

sequence of two local explosions lead to DDT. The first explosion decayed to a shock wave as it became isolated by combustion products. The second explosion lead to the onset of detonation. They also showed that the pure gas dynamic compression heating caused by the shock waves propagating ahead of the deflagration was not alone enough to ignite the reactants behind the shock.

The tube diameter criteria for onset of detonation was established by Peraldi et al. (1986) [57] to be equal to the detonation cell size. Lindstedt and Michels [58] found the critical diameter to be $D > \lambda/\pi$. In these studies there were orifice plates or Shchelkin spirals to accelerate the flow and flame speed. A discussion on these studies and other aspects of detonation onset criteria is given by Ciccarelli and Dorofeev [2]. The tube diameter criteria is mostly relevant for safety applications and the more conservative criteria of Lindstedt and Michels should be considered.

The study of DDT in smooth channels downstream a perforated plate by Chao [59] showed that there was a critical deflagration velocity of about half the CJ detonation velocity (corresponding to the CJ deflagration velocity) prior to the onset of detonation. Detonations were initiated and propagated up to and reflected off a perforated plate and the down stream expansion of the hot products and rapid mixing pushed a deflagration forward. Local explosions lead to the onset of detonations and retonation waves propagated back into the products. For other mixtures, the deflagration propagated further than the turbulence generated by the perforated plate, thus by a self turbulizing effect. DDT was also observed without any retonation waves. The transverse waves "rode" the deflagration reaction zone, and these waves coupled with the chemical reaction zone and gradually increased the reaction rate and transit to a detonation. This behavior was not observed for mixtures with regular cell patterns.

2.4.2 DDT in obstructed channels

DDT in obstructed channels is given as a brief review as the experimental setup in this thesis has one obstacle. DDT in obstructed channels might be the most widely studied geometry in the DDT litterature.

A lot of work has been done to investigate deflagrations and DDT in obstructed channels. Detailed studiescan be found in Lee et al. [60, 61] and Teodorczyk et al. [62–64]. A summary of the work by Shchelkin are given by Frolov [65]. The Shchelkin spiral is a well know method to accelerate a deflagration up to detonation. Teodorczyk et al. studied the quasi-detonation phenomena which were associated with detonation velocities as low as half the detonation CJ velocity. The photographic study showed that, in an obstructed channel, a detonation could fail as it diffracts around an obstacle. While reflections at one of the next obstacle causes a re-initiation of a detonation. Chan [66] showed that shock waves reflecting at obstacles initiated detonations, but pointed out that local explosions was not a sufficient criterion for detonation onset. The DDT in obstructed channels have been studied numerically and include the works of Gamezo et al. [67] which simulated similar experiments as Teodorczyk. Vaagsaether [12] also investigated this geometry for stoichiometric hydrogen-air mixtures and his explanation of the DDT process is given in Figure 2.15, where the deflagration has been accelerated enough to produce a shock wave in front of the deflagration. The flame is marked f and the shock wave is i. Mach stem is m and the reflection of i at the obstacle is ri. The Mach stem and reflection causes ignition at the bottom of the obstacle (f2) and a shock wave b propagates from

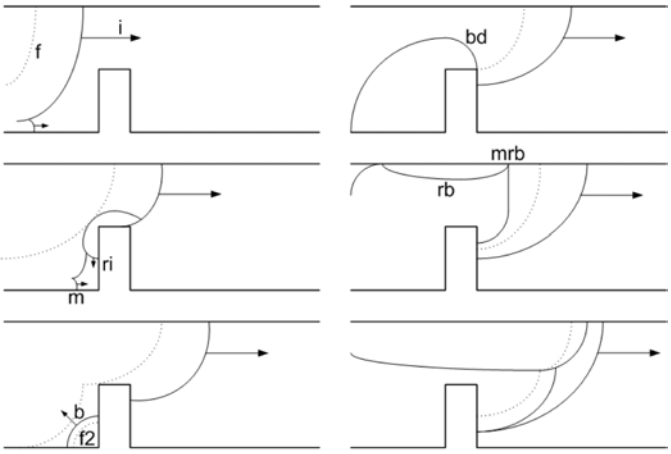

Figure 2.15: Explaination of DDT in obstructed channels given by Vaagsaether [12].

this local explosion. The diffraction of b around the obstacle is bd and the reflection at the top wall is rb. The top wall Mach stem is mrb. And when rb and mrb catches up with f it leads to DDT. Vaagsaether also computed the speed of the reaction wave (deflagration and detonation) which is shown in Figure 2.16. The reaction wave propagates with speeds between $800m/s$ and $2100m/s$ relative to the lab frame. The CJ detonation velocity for stoichiometric hydrogen-air is calculated using Cantera software with shock and detonation toolbox [68] $1976m/s$.

In the study of scale effects on detonation onset by Dorofeev et al. [13] they compared large scale and lab scale experiments [61, 62, 69–72] and found a critical cell size correlation. The comparison of large amounts of experimental results lead to the correlation of $L \approx 7\lambda$. The length scale L is given by the average of lengths in a room, but for a channel with obstacles it is given by a series of compartments. the special case where the obstacle spacing S equals the channel height H is given in Figure 2.17. The length scale criterion was shown to be a necessary, but not sufficient criterion for the onset of detonation in an obstructed channel. Flame acceleration and generation of gradients in reactivity must also be present. Dorofeev at al. calculated the detonation cell sizes according to the works of Gavrikov et al. [73]

2.4.3 DDT in turbulent jets

Jet initiation of detonations regards the process where a deflagration propagates from a pipe or through an orifice into an unconfined volume of combustible gas. The flame acceleration is mainly driven by the flow through the pipe opening or orifice. Detonation initiation usually occur in the mixing of reactants and hot products. This DDT phenomenon is relevant for the experimental study of this thesis as a jet is formed when the flame propagate up to and through the obstacle opening (in the experimental setup of this thesis). It is not directly comparable to the turbulent jet initiation experiments as the jet in this work is confined by the channel walls.

Knystautas et al. (1979) [14] observed a jet initiation of detonation in a small scale experiment. They investigated DDT in a turbulent jet as a flame propagated from one small chamber

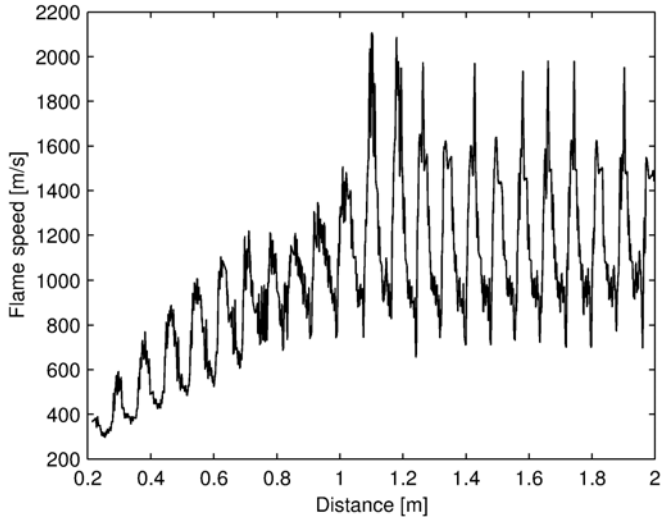

Figure 2.16: Vaagsaether's simulation of the reaction wave velocity. [12].

through a circular or rectangular opening into a large detonation chamber, see Figure 2.18. They varied the size and shape of the opening and concluded that three criteria had to be met for DDT to happen. First they had to have sufficiently large scale energetic turbulent eddies, then secondly enough small scale turbulence to promote the mixing. The third criterion is the generation of gradients of induction time inside a turbulent eddy where the DDT could happen. The size of this eddy should be in the order of the cell size of the detonation

Thomas and Jones (2000) [74] later argued that the time scale is too short to have induction time gradients generated by conduction between products and fresh reactants. They stated that the high shear stress in the flame front caused mixing at the length of the flame thickness. This caused increased energy release in the flame front which in turn leads to auto-ignition of unburned gas and a development of a hot spot transition.

Large scale experiments with DDT in jets were conducted at Raufoss Norway in 1979 [75]. Propane air mixtures were ignited in a $4m$ long $0.5m$ diameter pipe which opened into a $10m$ long $1.26m$ diameter pipe. This work followed the lab scale experiments by Knystautas et al. The Raufoss experiments showed that transition to detonation was achieved in the ignition pipe (when obstacles were installed to generate turbulence and shock reflections), but it did not propagate into the larger pipe. This is in good agreement with the simple critical tube criterion of $d_c \approx 13\lambda$ [76, 77].

Some years later at Raufoss investigations of jet initiation of DDT was studied by Moen et al. [15]. The experimental setup of Moen et al. consisted of a steel tube (with one end closed) with a plastic bag attached to the open end. The tube and bag was filled with acetylene/air and ignited at the closed end. The open end of the tube was completely open, central blocked or open with orifice plate. They observed DDT as a deflagration propagated through the opening into the plastic bag. In some experiments DDT was observed at the ground or near the plastic boundary, see Figure 2.19.

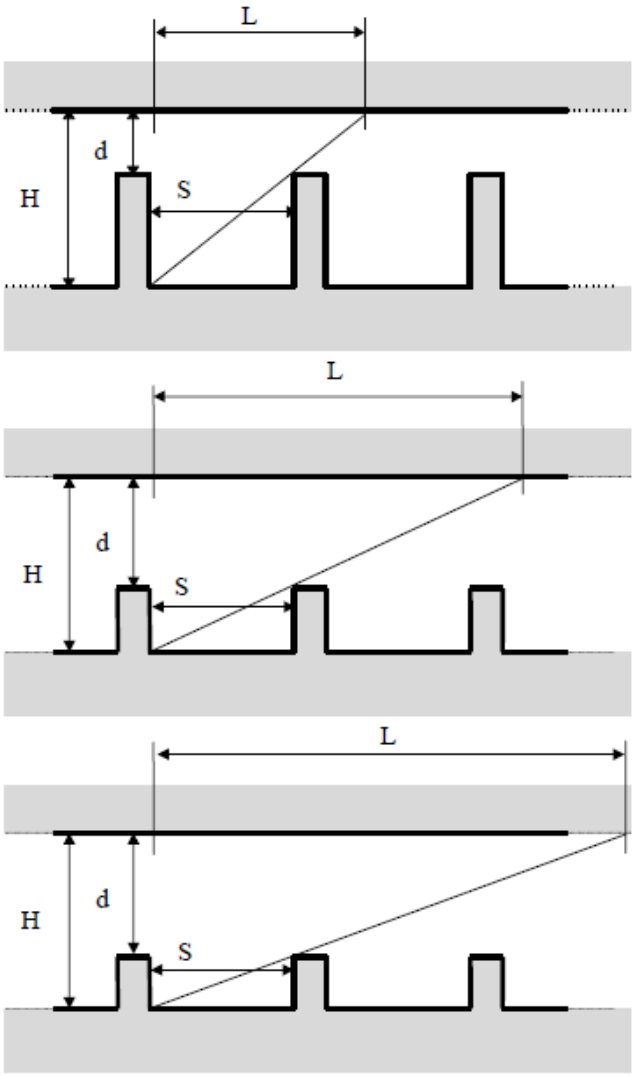

Figure 2.17: Explaination of the length scale by Dorofeev et al. [13].

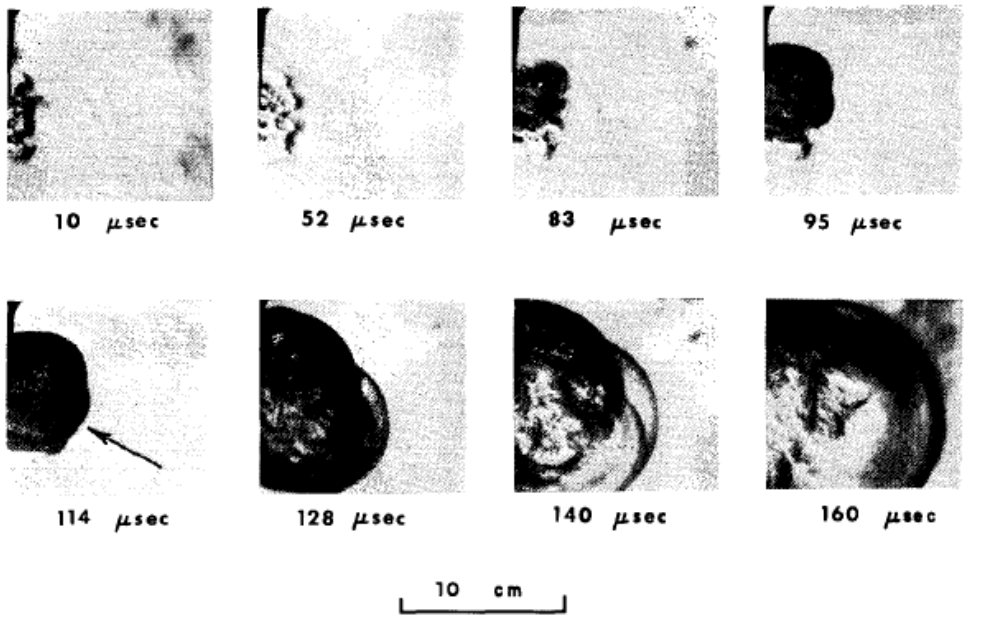

Figure 2.18: Schlieren photos of a deflagration to detonation transition in a turbulent jet. The detonation onset is marked with an arrow in frame number 5. Experiments by Knystautas et al. [14].

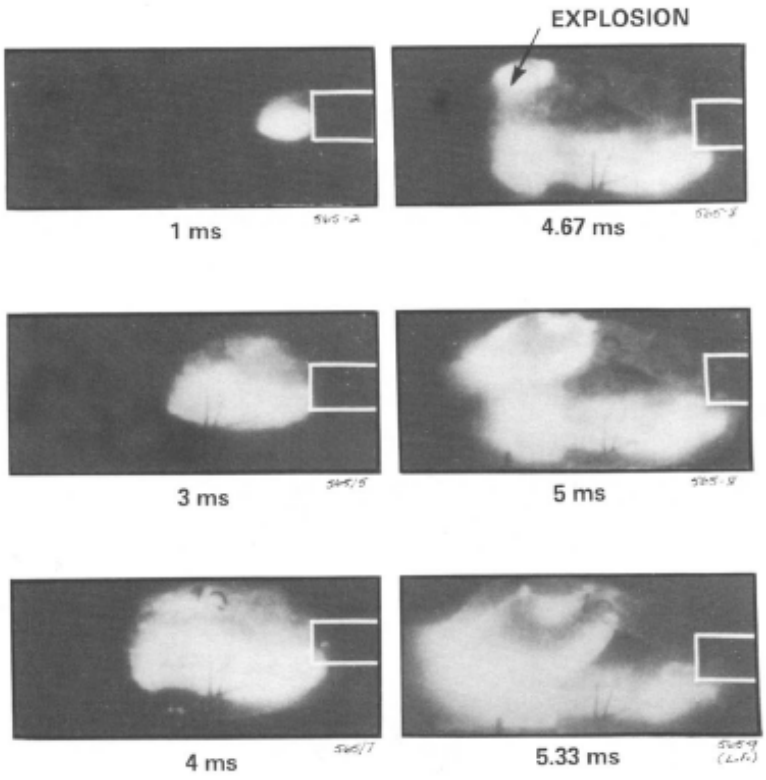

Figure 2.19: Experimental results from the large scale experiments at Raufoss were DDT was observed at the plastic bag boundary. Experiments by Moen et al. [15].

Large scale experiments were also done at Defence Research Establishment Suffield in Canada the year after the Raufoss experiments by Mackay et al. [78]. They investigated acetylene-air mixtures and observed different DDT phenomenas. The entrainment of hot products into a vortex of reactants caused local explosions that lead to DDT. Large flow vortices and small scale turbulent mixing were assumed to be important. They also reported other modes of DDT, as transition downstream a central blockage, the interaction of two flame fronts and an important interaction between flame front and either the plastic bag or the ground. They also reported the flame speed in the experiments and found that the flame reached a speed about the speed of sound in the products before DDT.

Compared to the critical tube diameter for a planar detonation to develop into a spherical detonation, the critical tube diameter for a deflagration to develop into a detonation is smaller. Üngüt and Shuff [79] showed that for propane air mixtures the critical diameter was as low as $d_{c,def} = 5.2\lambda$ compared to the $d_{c,det} = 13\lambda$ for detonations.

2.5 Detonations

This section reviews detonations from the simplest one dimensional theories to a short description of the three dimensional description of a real detonation. The review also includes a short summary of some selected experimental studies of detonations.

The first observations of detonations were done by Mallard and Le Chatelier in 1881 [42] and Berthelot and Vielle in 1882 [80]. Berthelot and Vielle measured the detonation velocity in hydrogen, ethylene and acetylene in oxygene diluted by nitrogen. The work by Mallard and Le Chatelier utilized a drum camera, and they observed the deflagration to detonation transition. Already at this time, the shock heating and compression to ignition was assumed responsible for the detonation propagation, so for over 130 years, we have distinguished deflagrations from detonations. The development of camera technology proved to be important for the study of deflagrations and detonations, and still it is the most important diagnostic tool for explosion study.

The development of a theoretical understanding and description of detonation were based upon the work by William J. M. Rankine in 1870 [81] and Pierre H. Hugoniot in 1887 and 1889 [82, 83]. Their work described the changes of pressure, density, temperature and velocity across a shock wave by considering the conservation equations for a stationary wave.

As the solution for the non reacting shock wave was established before the works of Mallard, Le Chatelier, Berthelot and Vielle, they continued the work for reacting waves. The minimum detonation velocity was investigated by Chapman [84] and he argued that since there was observed a unique detonation velocity it should be the minimum velocity. Jouguet [85] investigated the entropy variation along the Hugoniot curve and found that there was a minimum at the same point as Chapman. The Chapman-Jouguet (CJ) point is found where the Rayleigh line equals the Hugoniot curve and the slope of tangents are also equal, see [86]. More details on CJ history, theory and mathematics can be found in [1, 86–88]. The work of Mikhel'son actually preceded both Chapman and Jouget, but according to Lee [86] it was not known outside Russia until much later.

A further development of the CJ-theory for detonations was done almost simultaneously by

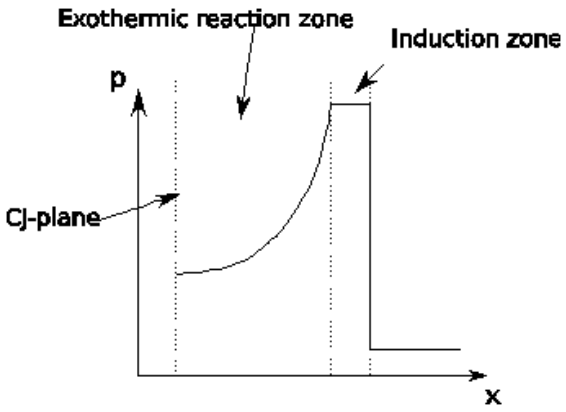

Figure 2.20: Illustration of the ZND structure of a detonation [12].

Zeldovich [89], von Neumann [89] and Döring [90] in the early 40's. It is know as the one dimensional ZND theory, and takes into account the chemical reaction time and length related to a shock wave that propagate in front of the reaction. As the CJ theory is only concerned with the up and down stream equilibrium states, the ZND theory includes the chemical reactions of the reactants. The theory states that a leading shock wave is followed by an induction zone and third a reaction zone where the exothermic reactions occur before the equilibrium (CJ) state follows last.

Lee [86] summarizes the procedure to compute the ZND structure as first the detonation velocity is determined by the CJ theory for a given γ (ratio of specific heats) and energy q_c. The state behind the shock is given by the Rankine-Hugoniot relations for a shock wave. Then the conservation equation of mass, momentum and energy with one step chemical kinetics are integrated between the shock and the CJ state. An illustration of the ZND structure is given in Figure 2.20.

Real detonations are three dimensional and non steady with transverse waves propagating normal to the detonation leading front shock. The leading shock and the transverse waves merge in points called the triple points. Lee [91] also point out that there is currently no theory that can describe the real three dimensional detonation with details of the reaction zone. This is still a matter of scientific importance, but a lot of effort has been put into experimentally describing and quantifying the detonation.

Detailed studies of the instabilities of detonations are given in Lee [86], Fickett and Davis [87] and Ng and Zang [92]. For a one dimensional transient study of detonations with two step chemical kinetics, the instability of detonations is controlled by many parameters as studied by Ng. et al. [16]. The reaction energy, the ratio of specific heats and the initial shock strength were kept constant while the activation energy (E_a) varied. For sub critical values the oscillations of the detonation were dampened, while above critical the oscillations increased. An example from Ng's work is given in Figure 2.21

Experimental investigations of detonation often include the study of detonation cell sizes. A well know technique called smoke foil technique has been used to record the trajectory of triple points, and the characteristic size of the cellular pattern has been called the detonation cell size

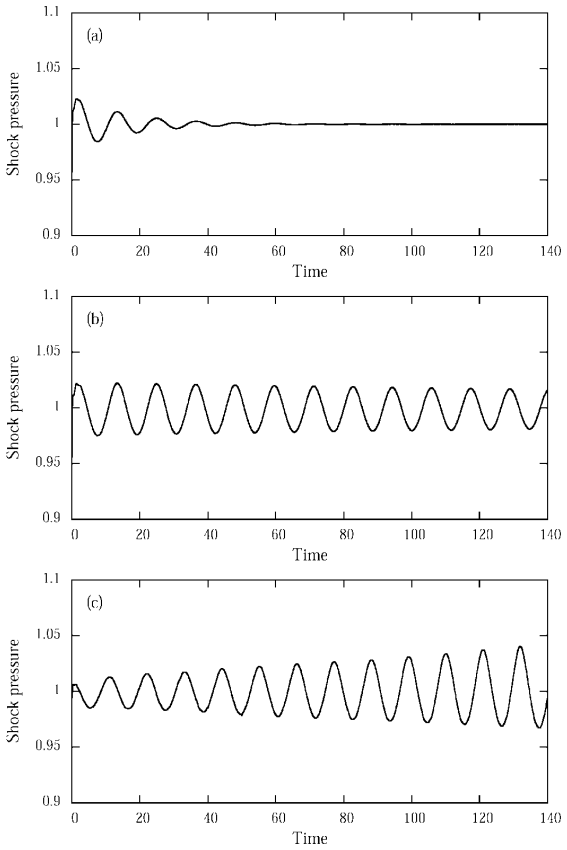

Figure 2.21: Leading shock pressure history for non dimensional activation energies (E_a) close to the stability limit: (a)$E_a = 24.00$; (b)$E_a = 25.24$; (c) $E_a = 25.28$. [16]. Other parameters were kept constant.

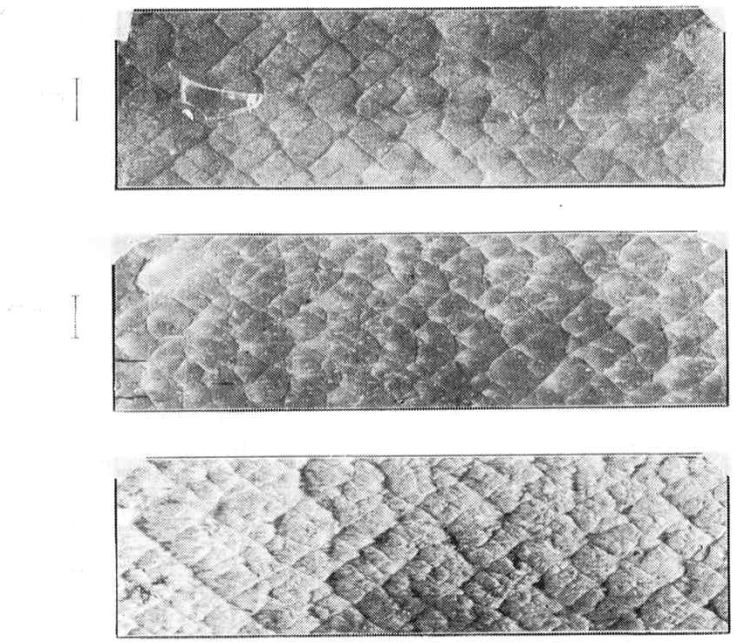

Figure 2.22: From the work of Moen et al. [17]. Smoke foil records showing the detonation cell sizes. On top $2C_2H_2 + 5O_2/75\%Ar$ at 100 Torr. Middle: $2C_2H_2 + 5O_2$ at 10 Torr. Bottom: $2C_2H_6 + 7O_2$ at 75 Torr

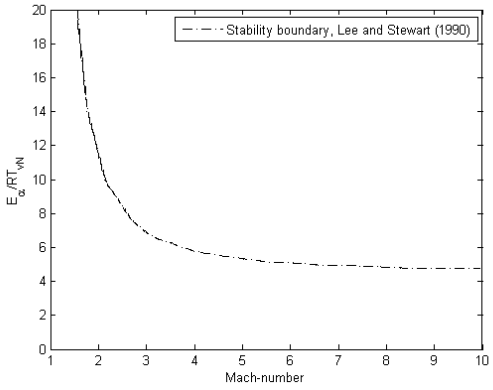

Figure 2.23: The Lee and Stewart boundary between regular and irregular detonation cells [18].

λ. Strehlow [93] reviewed the early work in 1963 and summarized much work on the complex detonation front.

It has been shown that the regularity of the cellular patter (see Figure 2.22) influences the detonation propagation. In the 1980's investigations of detonations it was discovered discrepancies between the lab experiments with acetylene oxygen diluted with argon and the larger scale outdoor experiments with acetylene air [17]. The fuel-air experiments detonated relatively much easier than the fuel-oxygen and especially the argon diluted mixtures. The velocity deficit experiments by Murray [94] showed failure of detonation propagation as the velocity decreased due to higher cell size to tube diameter ratio. Murray investigated argon diluted acetylene oxygen mixtures. Moen at al. [17] investigated acetylene air mixtures and did not observe velocity deficit or detonation failure as predicted by Murray. This was clearly correlated with the regularity of the detonation cells. The regularity of cell sizes were later studied by Shepherd et al. [95] and a specter of cell sizes were observed, but also a change in regularity as the gas properties were changed.

Irregularity of detonation cells have been shown to correlate with the activation energy E_a [16] (among others). The works of Lee and Stewart (1990) [18] showed a criterion for detonation cell regularity based on the activation energy and the von Neumann temperature and the CJ-Mach number:

$$\theta = \frac{E_a}{RT_{vN}} \tag{2.6}$$

This result is plotted in Figure 2.23 accordingly to Austin et al. [96]. Above the line are detonations with irregular cellular patterns while below are detonations with more regular cellular patterns.

For detonations with regular cell pattern the transverse waves are less dominating compared to the irregular. The induction zone and the induction time is mainly given by the leading shock compression. For detonations with irregular cell pattern there are sudden appearing transverse waves that coalesce with the others and yet other appearing again. On a smoke foil this can be seen as suddenly appearing triple points. This is due to the sensitivity to small perturbations

associated with high activation energy (among other parameters). A small change in temperature could suddenly make one volume react, but also cause pockets of unreacted reactants relatively far behind the mean reaction front, this was reported by Oran et al. in 1982 [97] related to the experimental work by Edwards. As the detonations with irregular cell pattern are very sensitive to small perturbations, the addition of other external perturbations only add to the already present disturbances [86].

Numerical investigations of detonation fronts include the works of Guirguis et al. [98] where they used a two step combustion mechanism and investigated the effect of changing the induction time dependence on the temperature. They found that a strong dependence on temperature gave more regular cellular patterns. Gamezo investigated the effect of perturbations on detonations with regular and irregular cell pattern [99], and showed how the irregularity of the cellular pattern grow as the $\frac{E_a}{RT_{vN}}$ increase. Ettner et al. [100] investigated reactive flow using a 9 species combustion mode, and showed it could simulate both deflagrations and detonations. They used a reaction mapping method which makes a "look up" table of the reaction variables and pick the solution from the table.

Recent work by Radulescu et al. [101] propose the χ-factor as a measure of a reactive mixtures propensity to generate structured or unstructured cells on soot foils. It is also a measure of the hot spot ignition or local explosions. The χ-factor is given by Equation 2.7:

$$\chi = \frac{t_i}{t_r}\frac{E_a}{RT_{vN}}\frac{Q}{RT_{vN}} \tag{2.7}$$

Where t_i and t_r are the induction and reaction times. The $\frac{E_a}{RT_{vN}}$ is the non dimensional activation energy and $\frac{Q}{RT_{vN}}$ is the non dimensional heat release. T_{vN} is the von Neumann spike temperature.

A thorough review on detonation history, theory and instability is given by Shepherd [24].

2.6 Detonations in inhomogeneous mixtures

This section regards the influence of stratified layers of reactants bound by compressible non reacting fluids. This specific setup is relevant for accidental leakage of light or dense fuel which mix with air and form a layer of combustible mixture in confined geometries. For hydrogen safety applications it is relevant as hydrogen/air mixtures are light and could generate a cloud of combustible gas along the ceiling of buildings or other confined geometries.

Sommers [19] and Dabora [22] investigated the influence of compressible boundaries on the propagation of detonations. The investigation by Sommers used hydrogen and oxygen mixtures as fuel, and air, helium and argon as the inert. A sketch of a detonation propagating in a layer bounded by a compressible fluid layer (inhomogeneous gas mixture) is given in Figure 2.24. The sketch illustrates how the expansion behind the detonation front also expands into the inert section, this poses an increased expansion and it is the main cause of the detonation failing.

Dabora [22] used a two dimensional shock tube analogy and predicted the angle between the detonation front and the oblique shock front. It was shown to be a function of the ratio of densities between the reactants and the bounding inerts. It was also shown that a velocity deficit (due to increased expanssion) of $8-10\%$ could lead to detonation failure. The experimental

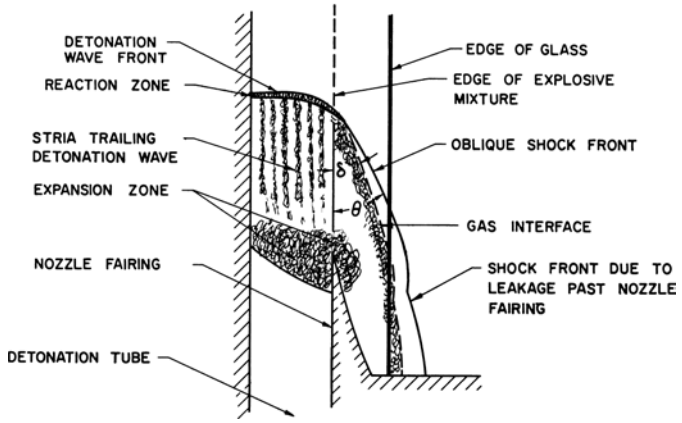

Figure 2.24: A sketch illustrating the phenomenon of a detonation propagating in a layer bound by a commpressible fluid layer. From the work of Sommers [19].

investigations by Dabora included hydrogen/oxygen known to have moderately irregular detonation cell pattern and methane/oxygen known to be unstable [101]. The influence of detonation stability was not considered by Dabora or Sommers.

Williams [102] has given a model relating the expansion and the reaction length to a quenching criteria.

More recent work of hydrogen detonations in stratified layers can be found in [103–105]. It is shown that a necessary criterion for a detonation to propagate in a stratified layer was if the reactant layer thickness (h) was $h > 3\lambda$. The study by Kuznetsov [104] showed that DDT was observed in the stratified layer when the thickness of the reactant layer was more than $h > 14\lambda$.

Recent work by Böck et al. [106] investigated flame acceleration and DDT in a channel with vertical hydrogen concentrations. They showed that the flame accelerated faster when it burned in these gradients. DDT was also observed as reflected shock waves interacted with the deflagration front.

Chapter 3

Experimental setup and method

This chapter provides a background of the experimental setup and method. The main focus is experimental studies of DDT and detonations, while the setup of the experiments with flame propagation in the first meter before the obstacle is also given.

3.1 Experimental Setup

The experimental geometry and gas mixtures are presented in this section. The measurement instruments are also given.

3.1.1 Geometry

The experimental setup is sketched in Figure 3.1. The setup consisted of a 3000 mm (DDT study) or 1500 mm (first meter study) long channel with a square $100 \cdot 100\,mm^2$ cross section. One end was closed and the other end was open to the atmosphere. The top and bottom walls were made of smooth painted steel, while the side walls were transparent polycarbonate.

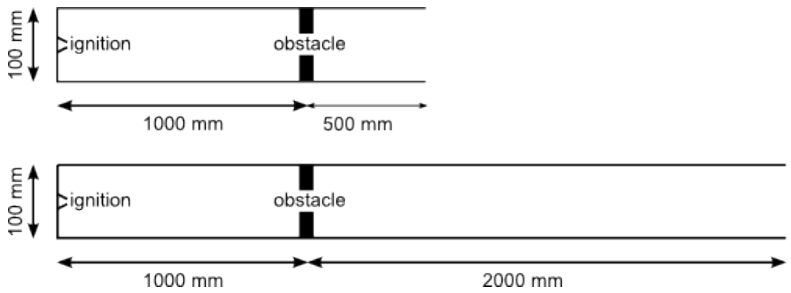

Figure 3.1: Sketch of the experimental setup showing dimensions, obstacle and ignition. On top is the setup for the study of the first meter, while bottom is the setup for the study of DDT.

One adjustable baffle type obstacle (Figure 3.1) was located 1000 mm from the closed end. It was made of 4 mm thick steel. The blockage ratio ($BR = A_{obstacle}/A_{total}$) of the obstacle is the ratio of obstructed to total area. The blockage ratio varied from $BR = 0.5$ to $BR = 0.9$ in the

Figure 3.2: Picture of the adjustable baffle type obstacle

DDT experiments and were set by adjusting the baffles up and down. In the experiments with flame propagation in the first meter before the obstacle the blockage ratio was $BR = 0.9$. The obstacle opening was always centered between the top and bottom wall, see Figure 3.2.

3.1.2 Reactants - Hydrogen and air

The gas mixtures (reactants) used were hydrogen and air at 1 atm. Industrial grade compressed hydrogen was used in the experiments. The air was supplied from and oil-free gas compressor. Both gas sources was set to $0.5\,bar$ overpressure. Their concentrations were set with two rotameters which were calibrated using drum-type gas meters. The reactants were mixed in a T-pipe junction before it was flushed through the channel for 10 min. This corresponded to a total gas volume at least ten times the volume of the channel. The hydrogen concentrations varied from 15% to 40% by volume, where 30% was the stoichiometric concentration.

3.1.3 Homogeneous and inhomogeneous

The homogeneous gas mixtures were made by flushing the channel with reactants for $10\,min$ before shutting off the gas flow and ignite immediately after. This method was assumed to give a homogeneous concentration of reactants in the whole channel. The inhomogeneous gas mixtures were made to give a layer of pure air at the bottom of the channel behind the obstacle, see Figure 3.3.

The air layer for the inhomogeneous experiments was created by letting air flow back into the channel (after filling) as a gravity current, for between 7 and 10 seconds. Details for the gravity current, layer thickness, and flow velocity are provided in [107]. The length (from the open end) of the air layer was controlled by elapsed time, and the thickness was about half the channel height.

Figure 3.3: Sketch of the experimental setup showing the differrence between homogeneous and inhomogeneous mixtures

3.1.4 Ignition

After filling of reactants and air the gas mixture was ignited by a $10\,kV$ spark between two electrodes. The current was supplied from the grid (through a transformer) resulting in an ignition delay according to the frequency of the grid ($50Hz$). As a result of this delay there might be a $\pm 10ms$ uncertainty in the pressure measurements and high speed frames relative to the trigger signal referring to the measurement time $t = 0s$. The uncertainty of the timing could be more if the mixture does not ignite at the first spark. Time instances should be regarded relative to each other and not relative to the time $t = 0s$.

The spark electrodes were located at the closed end of the channel, see Figure 3.1. The distributed ignition (line ignition) for the experiments in the first meter of the channel was made by making 5 spark gaps along a central rod. The distributed ignition was made to approximate a two dimensional flame propagation in the channel.

3.1.5 Pressure transducers and logging

Kistler 7001 and Kistler 603b piezoelectric pressure transducers measured the explosion pressures in the channel. The Kistler 7001 transducer has a natural frequency of $f \approx 70kHz$, while the 603b transducer is more favorable on detonation measurements as its natural frequency is $f \approx 300kHz$. The diameter of the 7001 transducer is $9.5mm$ while the faster 603b has a diameter of $5.5mm$

The position of the transducers varied in the experiments, but are specified in the results chapters. The pressure records are presented together with the location of the transducer behind the obstacle, see section 3.2.1.

A Kistler 5011 charge amplifier was used to amplify the signal from the transducers and the output voltage signal was recorded on a digital oscilloscope recording at different frequencies. In all relevant experiments the recording frequency was equal or larger than 2 MHz. All pressure results were exported in ASCII format. The analysis and plotting of data was done in MATLAB.

3.1.6 High speed film

Photron APX-RS (black and white) and Photron SA-1 (color) high speed cameras were used to record the flame propagation in the experiments. The resolution and frame rate varied in the experiments. Some films gave an overview, while other looked into the details. In the results section the frame rate is given in the experimental details. Spacial dimensions are given in millimeters (mm), usually ranging between $200\,mm$ to $1500\,mm$.

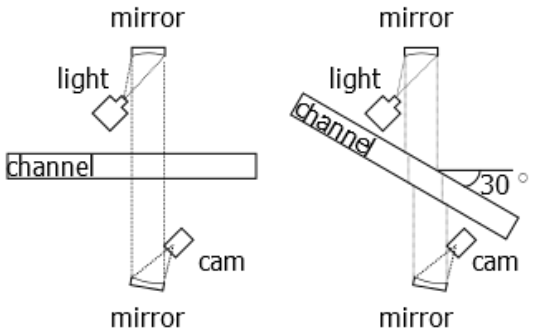

Figure 3.4: Sketch of the perpendicular and angular schlieren setup.

3.1.7 Schlieren photography

Some DDT experiments related to this thesis were performed by Larus Bjarnason [21] and the author. These experiments used a z-type schlieren method [108] to visualize the details of the propagating deflagration and detonation front in the square channel. The experimental investigation of flame propagation in the first meter of the channel also used schlieren visualization, both perpendicular and angular schlieren, see Figure 3.4. More information on this technique can be found in appendix E.1.

3.2 Experimental results processing

The main results from this method are pressure records and high speed films. A short description of the data processing are given below.

3.2.1 Pressure signal

The voltage signal from the amplifier were stored on the digital oscilloscope and exported as ASCII text. The .txt files were read in MATLAB and displayed as a pressure signal in either bar or MPa. The Matlab algorithm imported the charge amplification and the sensor position so that the pressure results could be offset on the vertical axis equal to the position of the transducer. This will show both the pressure level and the wave velocity in the same plot as the pair of axis will be both time-pressure and time-distance. One example of the pressure plot is given in Figure 3.5. On the left is an example of the pressure plot with offset along the vertical axis, equal to the position behind the obstacle. The position-time (x-t) data of the flame propagation is also shown, with dashed line representing the deflagration and the solid line representing the detonation. On the right shows a plot of the velocity along the channel length. The x shows the first order derivative, while the dashed line and solid line shows the polynomial derivated x-t data. Also shown are the CJ detonation velocity and half the CJ detonation velocity. In some plots there are vertical gray lines. These line show the same time instance as the frames from the corresponding high speed film.

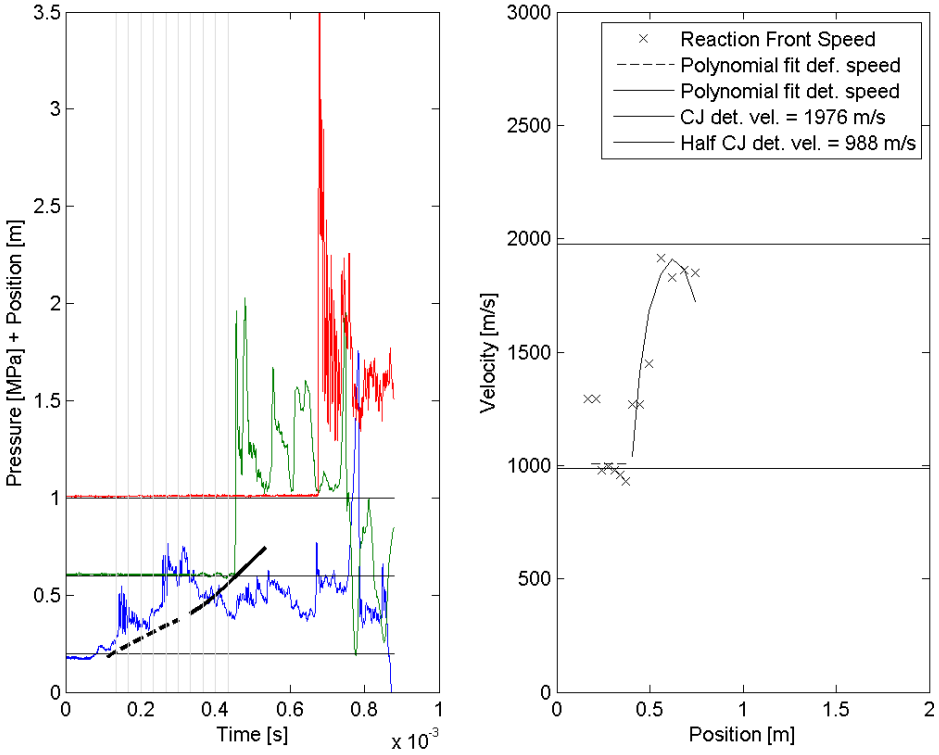

Figure 3.5: On the left is an example of the pressure plot with offset along the vertical axis. On the right is the velocity data.

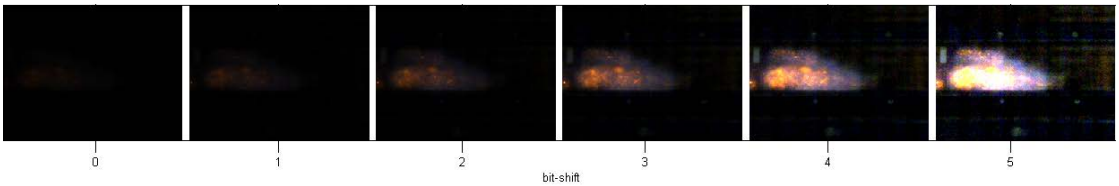

Figure 3.6: An example of the bit-shift function. All frames are equal 16 bit images, only the bit-shift is changed.

3.2.2 Image processing

The first high speed films were stored as 8-bit images (.avi), while the latter ones were stored as 16-bit images (.raww). The 16-bit images contained more information, especially in the underexposed parts of the film. By using bit-shift on the images, more details were seen in the darker parts of the film frames. An example of the bit-shift is shown in Figure 3.6. It shows the same high speed frame but with different bit-shift.

The self-illuminated images from the high speed films showed the flame propagation. It was important to capture both the relatively slow and low light deflagration and the fast strong light detonation in the same film to have a common reference. The length of the channel section investigated varied through the experiments.

Schlieren photography was utilized for investigations of the flame propagation in the first section of the experimental setup. It was a standard Z-type schlieren setup with concave mirrors of $220\,mm$ diameter. Only a few experiments with DDT investigations utilized schlieren visualization.

Time and flame position data was extracted from all high speed films manually, and always at the leading tip of the deflagration or detonation. A difference between deflagration and detonation was also made, based on the illumination on the high speed film frames. A detonation emits more light than a deflagration. The set of time and position data made up a full x-t information of all experiments. These data were quite smooth, but the first order derivative ($v = \frac{\Delta x}{\Delta t}$) was quite noisy. To smooth the velocity data, a polynomial fit was made to the x-t data. A smooth velocity curve was found by deriving the x-t polynomial.

3.2.3 Thermodynamic and kinetic properties

The thermodynamic properties of the reactants and products were calculated using the Cantera software [109] in MATLAB including the Shock and Detonation toolbox [68]. The detonation cell size data were extracted from the Detonation Database [20], and consisted of the [110–113], all these date were measured at between $293\,K$ and $300\,K$, and around atmospheric pressure. The data was curve fitted to give a relationship between the hydrogen concentration and the detonation cell size. The following correlation between the data is given by eq 3.1 and plotted agaist the experimental data in Figure 3.7.

$$ln(\lambda) = 51.194(\frac{\phi}{1+\phi})^2 - 56.202(\frac{\phi}{1+\phi}) + 17.919 \tag{3.1}$$

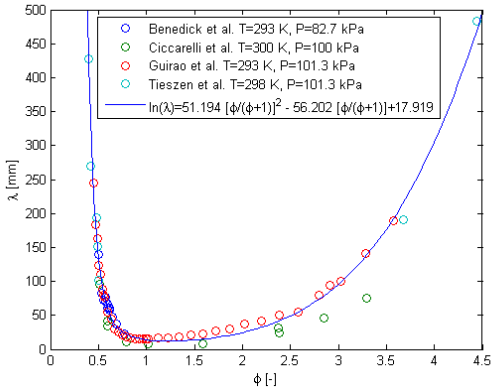

Figure 3.7: Correlation of the experimental cell size data from the detonation database [20].

Chapter 4

Flame propagation in the first meter before the obstacle

The aim of this part was to investigate the propagation of hydrogen-air deflagrations as it propagates from ignition up to the obstacle. This investigation shall document the shape, velocity and pressure of a flame propagating in a channel with one obstacle. Also the effect of ignition source shall be investigated to investigate if a 2D assumption could be justified by using a line ignition source. This chapter is presented as the paper "Experiments with Flame Propagation in a channel with a Single Obstacle and Premixed Stoichiometric H_2-Air" in the journal "Combustion Science and Technology" [114].

An example of results from the experiments is shown in Figure 4.1. The self illuminate streak photo on the left hand side show the flame propagation in the center of the channel while the pressure records recorded at P2 are shown at the right hand side. There are quite good relations between the pressure peaks and the instances when the flame speed is almost zero. These relations are investigated in this chapter. Flame inversion is a term used in this chapter to describe the change from a finger shaped flame to a tulip shaped flame. This term is also used in the famous paper by Clanet and Searby [45].

4.1 Results and discussion

The gas mixtures were ignited with either a point ignition or a distributed ignition source. The point-ignited flame expanded spherically while the distributed-ignited flame expanded as a parabolic cylinder. The flames propagated toward the obstacle while sending pressure waves ahead of the flame. These waves were reflected at the obstacle and they interacted with the flame. Self illuminated pictures (Figure 4.2) from the high-speed video along the whole length of the channel showed the shape of the flame front.

Figure 4.3 shows the pressure records and two traces of the flame position. One trace shows the flame position at the center of the channel and the other shows the flame position close to the wall. Figure 4.2 shows the corresponding self illuminated flame front pictures of the same experiment. At time A the flame is spherical. Between times B and C the flame invert

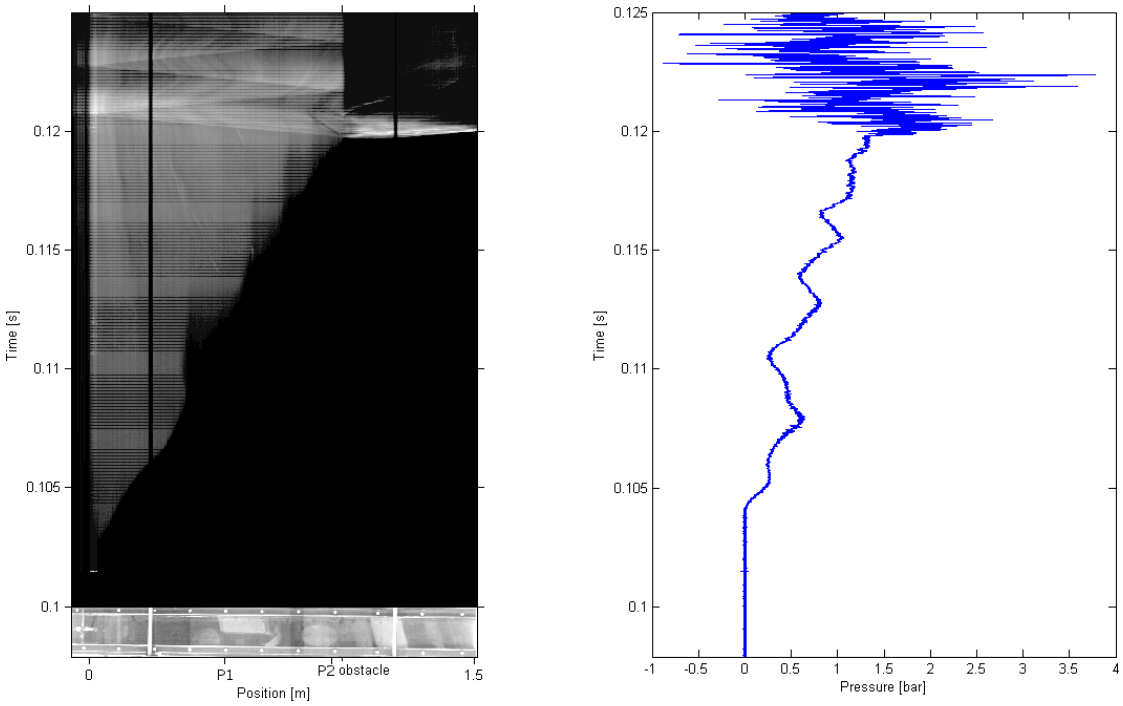

Figure 4.1: Self illuminate quasi streak results of the flame propagation (from left to right) with the corresponding pressure results. The experimental channel is shown at the bottom of the streak photo. Pressure records are recorded at P2.

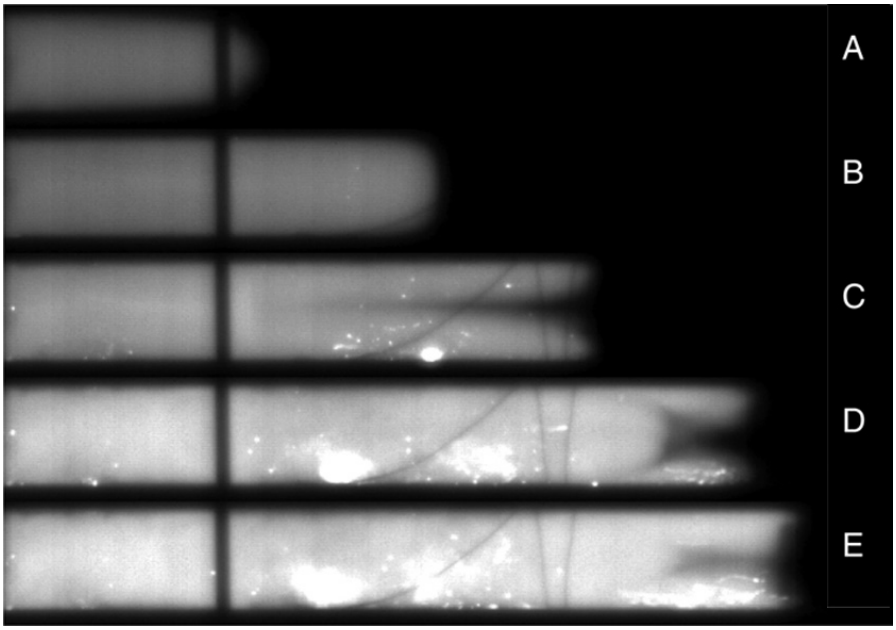

Figure 4.2: Self illuminated pictures of the flame front. The times correspond to the letters (A to D) in Figure 4.3. This result is for point ignition, and the dimensions of the setup can be seen in Chapter 3. The corresponding time vector is $[11.4, 13.6, 17.0, 19.9, 21.1]ms$

and the pressure record P2 shows a local minimum. The change of shape is also visible in the flame position plot as the edge position of the flame is further ahead than the center position of the flame. Between times C and D the pressure records show a new local minimum and the corresponding flame front picture shows the formation of a second inverted shape. This second inverted shape is illustrated in the flame position plot as an increase in the distance between the center and edge position. Frame E of Figure 4.2 shows the start of a third inversion of shape as the flame approaches the obstacle; these secondary inversions are discussed later.

4.1.1 Flame propagation dependence on ignition source

The type of ignition source influenced the initial flame propagation. After the point where it started to invert, less influence were observed. The average flame speed from ignition end to the obstacle was not strongly influenced by the ignition source (will be shown later). The time of arrival at the obstacle differed by the order of 1 ms. For both ignition types the local flame speed (i.e., relative to the tube), varied from 0 to 120 m/s during one experiment. The flame position can be seen in the x-t plot in Figure 4.3.

Schlieren photos of the flame front with distributed and point ignition are shown in Figure 4.4. A, C, E, G, and I show a point ignited flame, and B, D, F, H, and J show a distributed ignited flame. Pictures A and B show the flame at the ignition end. Picture A shows a visible cellular pattern indication that the flame has not quenched at the transparent wall yet. Picture B shows no cells indicating that it has quenched at the transparent wall, as the density is nearly

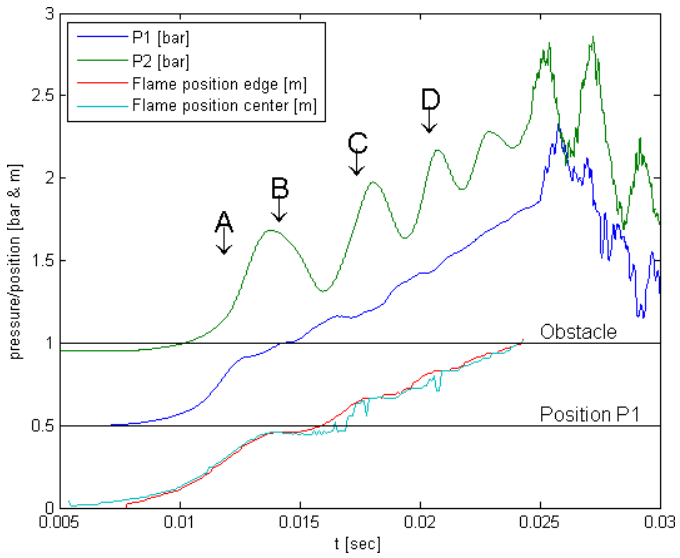

Figure 4.3: The pressure records from one experiment with 30% H_2 in air. P1 is 0.5 m from the closed end, P2 is 0.96 m from the closed end. Flame position (center and edge) is also plotted. Point ignition.

invariant in the direction normal to the plane of the image. The relatively thin black zone in front of the flame in Figure 4.4 picture B is due to the curvature in the direction normal to the plane of the image. The experiment with point ignition did not quench at the wall until 5.8 ms after ignition, while the distributed ignition quenched at the transparent wall approximately 0.8 ms after ignition. At this time there is clearly a difference between the two types of ignition sources, and it is reasonable to assume that at this stage the distributed ignition could justify a two dimensional flame propagation.

Pictures C (point ignition) and D (distributed ignition) shows the flame 330–510mm from the ignition end. At this point the flame changed shape to the inverted flame front. The point-ignited flame started to invert approximately 30mm further from the ignition end than the distributed ignited flame. After the flame inverted there was a large area of bent light (e.g., density gradients) at the front of the flame. This indicated that the flame was not invariant in the direction normal to the plane of the image.

Pictures C and D of Figure 4.4 shows that after the inversion of the flame front, it can no longer be assumed as two-dimensional due to the same invariance. In the next two pictures of Figure 4.4 (520–700mm from the ignition end), Frame E (point ignition) and F (distributed ignition) show that there is a small difference between the shape and both flames should be considered three- dimensional.

The pressure records were also influenced by the type of ignition source. Figure 4.5 shows the difference between point and distributed ignition. The point ignition gives slightly higher pressure at the first pressure peaks than the distributed ignition. However when the flame reached the obstacle the pressure were more or less equal. The time of arrival at the obstacle differs by approximately 1 ms. As the distributed ignition gives a larger flame area in the beginning it also

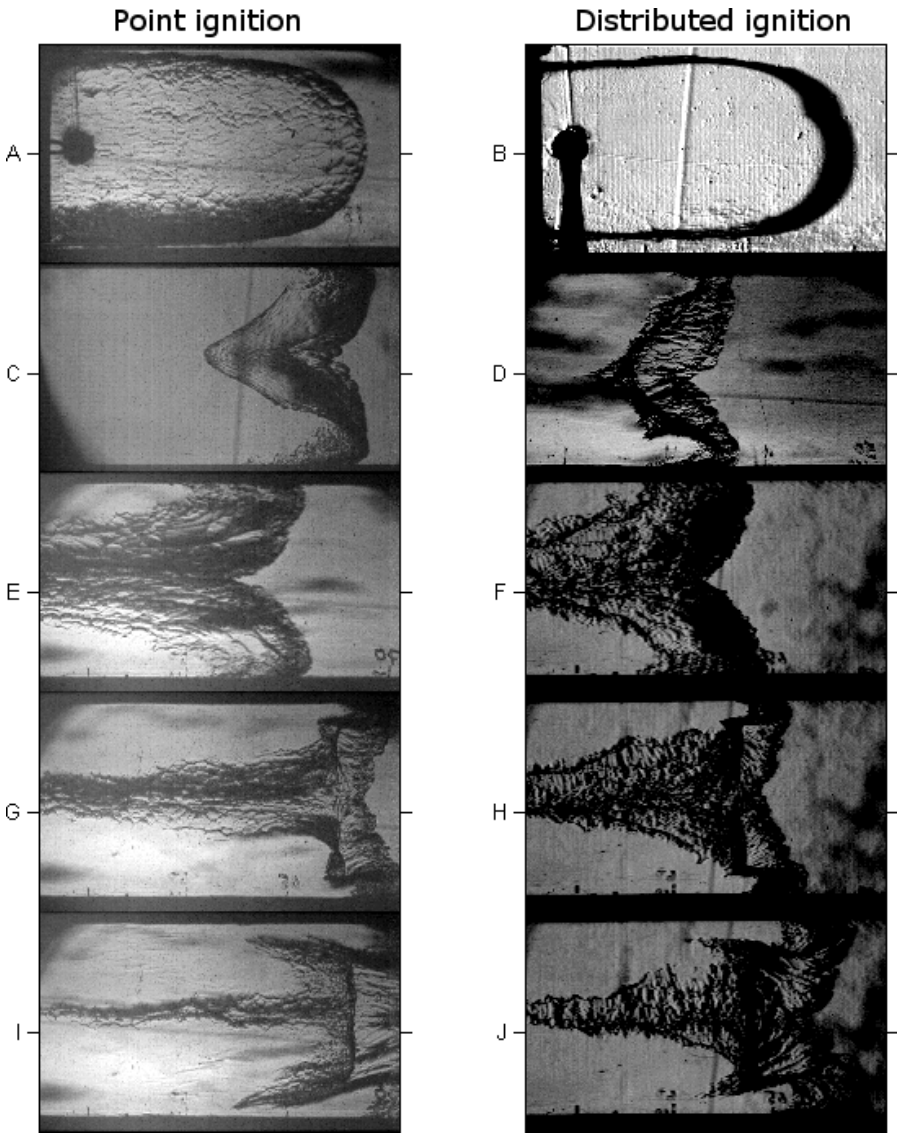

Figure 4.4: Shows the shape of the flame at three different positions in the channel and two different ignition sources. A and B show the ignition end, where A is point ignition and B is distributed ignition. C and D show 330–510mm from the ignition end where the flame inverts. C is point ignition and D is distributed ignition. E to J shows 520–700mm from the ignition end. E, G, and I are point ignition and F, H, and J, are distributed ignition. All pictures are of and 30% vol H_2 flames, but not from the same experiment.

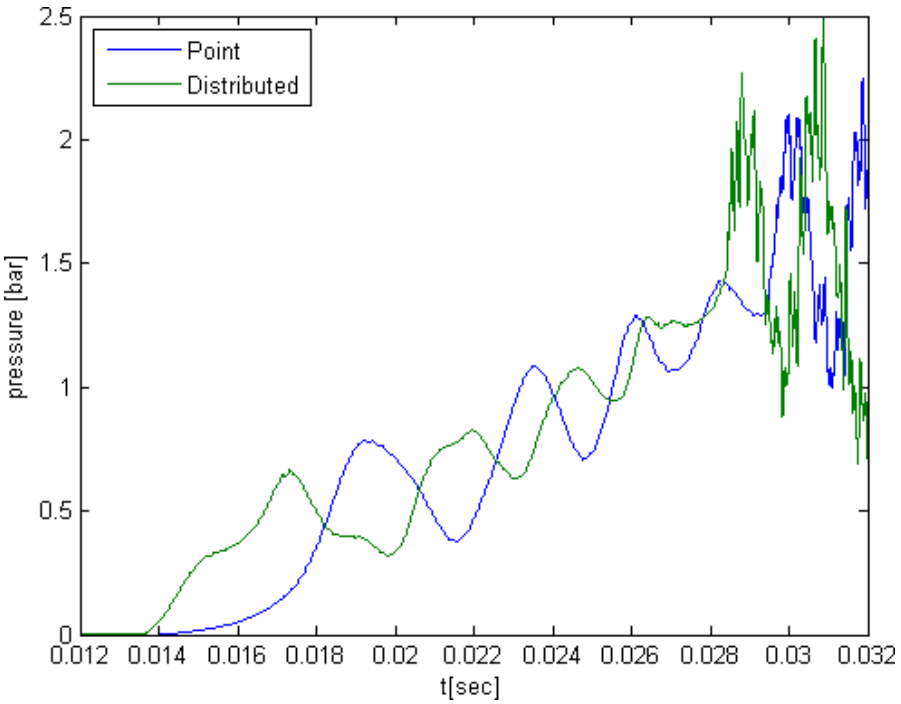

Figure 4.5: Comparison of pressure from distributed and point ignition at P2.

quenches at the walls faster, this could explain why the first pressure peak comes earlier than for the point-ignited flame. The distributed ignition pressure records show a plateau before the first peak (local maximum), this was most likely caused by the decreased flame area when the five spherical flames from the distributed ignition joined together. The later peak of the point-ignited flame could also explain why it propagates approximately 30mm further than the distributed ignited flame before it changes shape.

4.1.2 First inversion

High-speed film shows that the flame front inverted in the experiments. The flame started to invert at 390mm and 360mm for point and distributed ignition, respectively. The inversion was seen after the first pressure peak, but it is also in good agreement with the model of Clanet and Searby [45]. Calculating the time and position at which the flame touches the walls using the hydraulic diameter and laminar burning velocities from Bradley et al. [115] gives a position between 340 and 590 mm. This position corresponds well with the position where the first inversion of the flame occured in our experiments. A propagating flame is illustrated with angled schlieren images in Figure 4.6, and perpendicular schlieren images in Figure 4.7. The figures are from two different experiments but with the same setup, mixture, and procedure. Frame 78 of Figure 4.6 shows four visible sections of the flame. These sections plus one more behind them originate from the five sparks of the distributed ignitor. Frame 90 of Figure 4.6 shows how a square section in the middle of the flame was pushed backward relative to the front, with

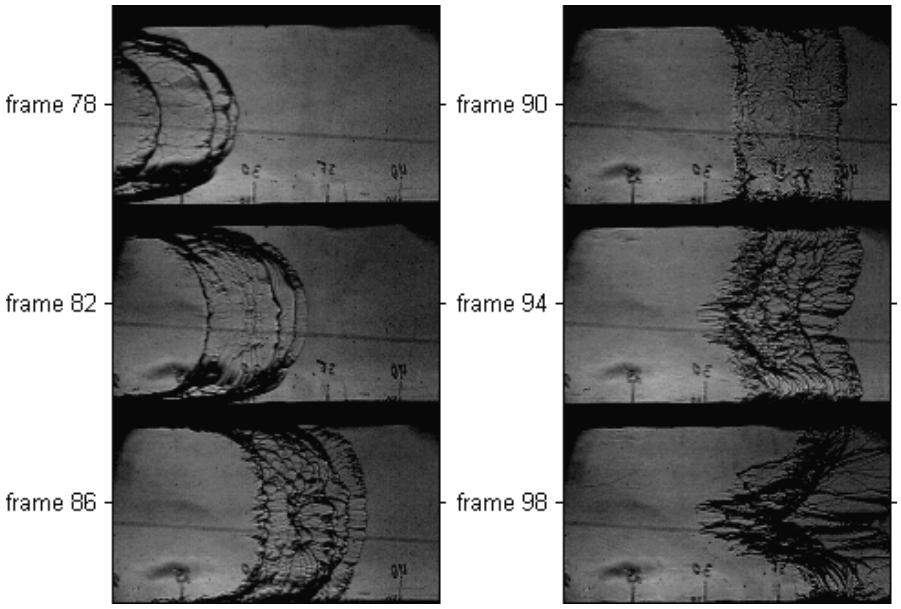

Figure 4.6: Angular schlieren of the flame inversion. Distributed ignition. Recorded at $5000 fps$

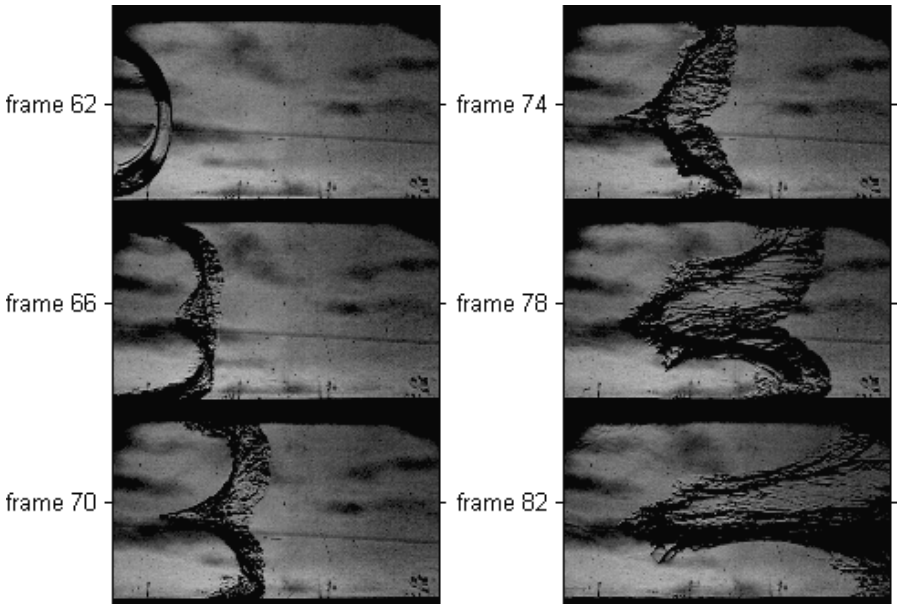

Figure 4.7: Perpendicular schlieren of the flame inversion. Distributed ignition. Recorded at $5000 fps$

the flame anchored to the walls. Figure 4.7 shows that the center part (bottom of the funnel shape) of the inverted flame was almost stationary (i.e., the flame speed was practically zero), while it propagated forward along the walls. As the flame inverted, it grew along all four walls, and it was clearly visible that the flame propagated in the direction normal to the transparent wall. Flame motion and flow in this direction cannot justify a two-dimensional flame shape, as it was variant in three directions. The flame also became highly corrugated as the curvature of the flame changed, see frame 86 (Figure 4.6). This corrugated flame front support the necessity of three-dimensional simulations. After the flame inverted, it did not change shape back to the original shape, and this could be caused by an anchoring effect to the wall as the flow velocity is reduced in the boundary layer. Larger scale flow convergence in front of the funnel-shaped flame also contribute to keeping the funnel shape of the flame, as pointed out by Dunn-Rankin [47].

4.1.3 Subsequent flame inversions

As seen in Figures 4.3 and 4.2, the flame inverts or changes shape several times, see frame D in Figure 4.2. A second inversion occured after local maximum pressure at time C in Figure 4.3. The first and second inversions start right before the flame speed is reduced to zero. Both instances coincide with the time of local pressure maximum of the pressure records (P2). These inversions of the already curved flame front could be explained by the vorticity generated as the pressure gradient interacts with the flame front, as described by the baroclinic term in Eq. (2). This could also show a link between the flame inversion and local pressure maximum. We have also observed similar subsequent inversions for circular geometries. Figure 4.4 shows schlieren photo of the second inversion of the flame in picture G, H, I, and J. Pictures G and I are point ignited while H and J are distributedly ignited. These pictures are taken from the same position as pictures E and F. The curved part of the flame front curl toward the top and bottom walls, and a new funnel seems to be created. These pictures are only a two-dimensional projection of what is believed to be a three-dimensional phenomena. The actual three dimensional structure can not be characterized until we have good angular schlieren pictures of the flame at this stage. The third time the flame speed is reduced is right before the flame passes through the obstacle, see Figure 4.3. It coincides with the third local maximum of the pressure records. This third inversion starts in picture E of Figure 4.2. All of theses changes occur after a local maximum is recorded at P2, but as pointed out by [47], these phenomena are dependent on the system under study.

One comment to the subsequent flame inversions is that it is remarkable similar to the results of Xiao et. al [50, 51], where it is called a distorted tulip flame. A description of the vortex generation for normal and distorted tulip flame is also given, which is similar to the baroclinic explanation.

4.1.4 Flame propagation through the obstacle

The overall research objective of this thesis is to investigate DDT in the square channel and the flame propagation through the obstacle should be investigated to possibly determine the actual process of flame propagation through the obstacle. The experiments showed that as the flame burned toward the obstacle, it was funnel shaped (inverted). After the flame propagated through

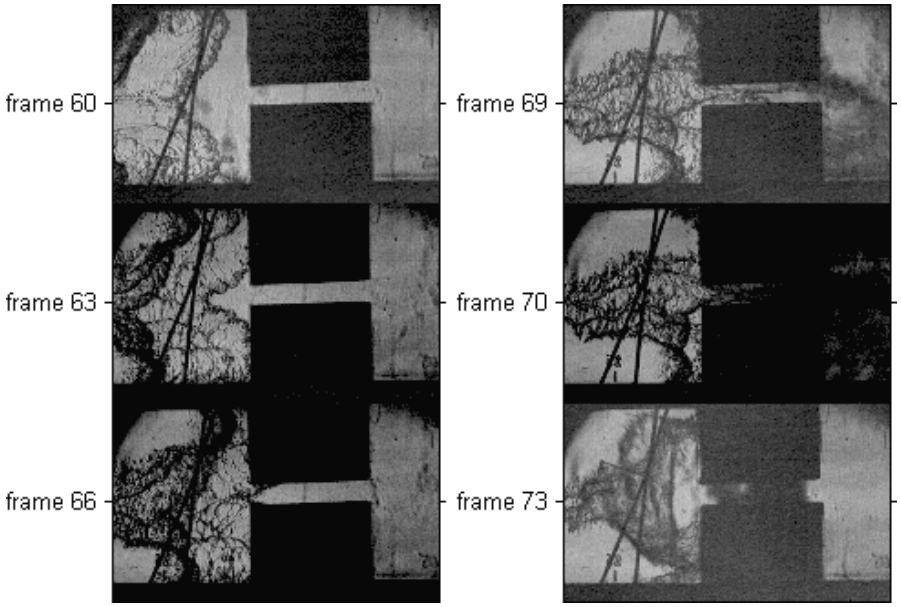

Figure 4.8: Angular schlieren of the flame propagating through the obstacle. Recorded at $5000 fps$

the obstacle it reacted much faster and left behind a pocket of unreacted mixture in front of the obstacle. The flame propagated through the obstacle opening along the side walls and from the top and bottom, and left behind this unreacted pocket. This is shown in Figure 4.8 and sketched in Figure 4.9. Frame 69 shows how the flame propagates through the rectangular slit of the obstacle, while frame 70 shows the explosion behind the obstacle. Frame 73 shows the combustion of the reactant pocket. This phenomenon was only visible when using the angled schlieren setup. The perpendicular setup only shows how the flame propagates through the obstacle opening from the top and bottom, while the angled setup shows how the flame propagates through the obstacle opening along the side walls.

The sequence of the high-pressure peaks related to the flame propagation through the obstacle opening was also investigated. Upon closer investigation it was clear that the peak consisted of two different peaks (see Figure 4.5). This was also clearly visible when viewed in conjunction with the high speed film. The first peak was related to when the flame propagates through to obstacle opening. The second peak was related to when a shock wave from the explosion outside propagated back into the first section and the combustion of the pocket of reactants left in front of the obstacle. The process is visualized in Figure 4.8, frame 73. This figure shows angular schlieren photo which clearly gives additional information compared to the perpendicular schlieren. As seen in the sequence of photos, the propagation through the obstacle opening is considered highly three-dimensional.

The experimental setup gives only one flow configuration, and other blockage ratios or lengths of the first section give different results.

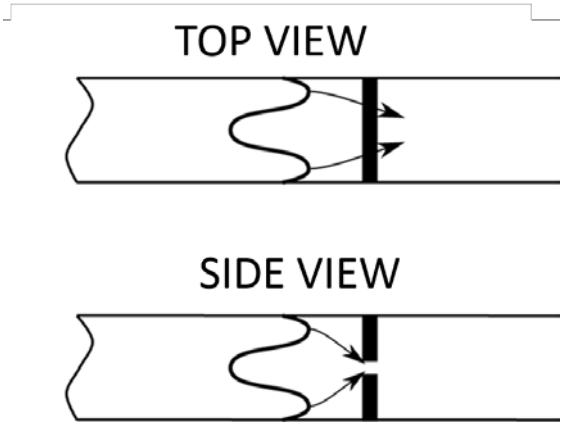

Figure 4.9: Sketch of the flame propagating through the obstacle.

Chapter 5

DDT in homogeneous hydrogen air

This chapter focuses on the combustion wave propagation behind the obstacle, including the deflagration to detonation transition in homogeneous mixtures of hydrogen and air. Point ignition was used in all experimental studies of DDT, and positions are given relative to the obstacle. After ignition (number I Figure 5.1) the flame propagated up to the obstacle (II Figure 5.1) and displaces reactants in front of the deflagration. A jet of reactants was formed through the obstacle opening (III Figure 5.1). When the flame reached the jet the overall reaction rate increased and the flame speed increased. DDT occurred in some of the experiments after the obstacle, and then the detonation propagated through the rest of the channel (IV Figure 5.1).

5.1 Experimental results

This section describes the experimental results with pressure plots, position-time (x-t) diagrams and velocities as described in Chapter 3. Selected experiments are presented in Table 5.1. Some experiments are not included in this chapter, because they could not be investigated on the same level as the other experiments. Reasons for exclusions were; no pressure records or no high speed film. The results will be presented based on the blockage ratio. The experiments are organized as projects and test number as seen in Table 5.1. For example P114_T4 refers to the experiments with $BR = 0.75$ and with $30\,\%\,H_2$ in air which had a $395\,mm$ run up distance behind the obstacle.

5.1.1 Blockage ratio BR = 0.2 and BR = 0.5

These experiments were conducted with the lowest blockage ratios. $BR = 0.2$ was studied with hydrogen concentrations of $35\,\%$. The experiments P112_T3 to P112_T9 with $BR = 0.5$ were

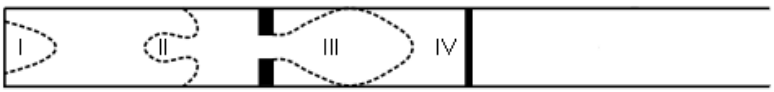

Figure 5.1: Sketch of the combustion wave propagation in the homogeneous mixtures

Table 5.1: The experimental matrix

Year	Project	Test	BR	$\%H_2$	ϕ	ITD [s]	λ [mm]	X_{DDT} [mm]	CJ_{vel} [m/s]
10	111	3	0.2	35	1.28	0	12.21		2048
10	112	3	0.5	30	1.02	0	13.37		1976
10	112	4	0.5	30	1.02	0	13.37		1976
10	112	5	0.5	30	1.02	0	13.37		1976
10	112	6	0.5	30	1.02	0	13.37		1976
10	112	7	0.5	30	1.02	0	13.37		1976
10	112	8	0.5	30	1.02	0	13.37		1976
10	112	9	0.5	30	1.02	0	13.37		1976
10	113	4	0.75	30	1.02	0	13.37	440	1976
10	113	5	0.75	25	0.79	0	21.65		1858
10	113	6	0.75	28	0.93	0	15.37		1935
10	113	7	0.75	30	1.02	0	13.37	619	1976
10	113	8	0.75	35	1.28	0	12.21	351	2048
10	114	1	0.75	28	0.93	0	15.37		1935
10	114	2	0.75	30	1.02	0	13.37	452	1976
10	114	3	0.75	30	1.02	0	13.37	390	1976
10	114	4	0.75	30	1.02	0	13.37	395	1976
10	114	5	0.75	30	1.02	0	13.37	496	1976
10	114	6	0.75	35	1.28	0	12.21	455	2048
10	115	5	0.84	30	1.02	0	13.37	457	1976
10	115	7	0.84	27	0.88	0	16.91		1911
10	115	8	0.84	35	1.28	0	12.21	333	2048
10	116	1	0.9	30	1.02	0	13.37	405	1976
10	116	2	0.9	27	0.88	0	16.91		1911
10	116	3	0.9	28	0.93	0	15.37	465	1935
10	116	4	0.9	35	1.28	0	12.21	336	2048
10	116	5	0.9	35	1.28	NaN	12.21	168	2048
10	117	1	0.5	35	1.28	0	12.21		2048
11	117	2	0.6	35	1.28	0	12.21		2048
11	117	3	0.6	30	1.02	0	13.37		1976
11	117	4	0.6	40	1.59	0	14.98		2096
11	117	5	0.6	40	1.59	0	14.98		2096
11	120	1	0.84	30	1.02	0	13.37	533	1976
11	120	6	0.84	28	0.93	0	15.37	451	1935
11	120	7	0.84	27	0.88	0	16.91		1911
11	120	9	0.84	30	1.02	0	13.37	426	1976

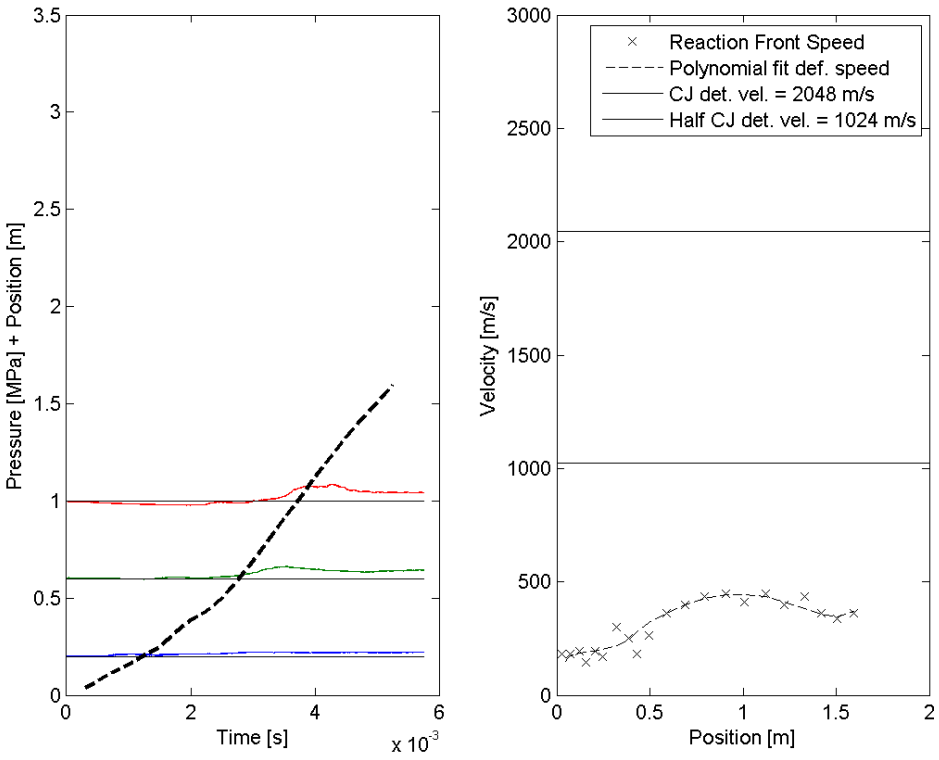

Figure 5.2: $BR = 0.2$ and $35\,\%\,H_2$ in air. (P111_T3). Slow flame, and no local explosions.

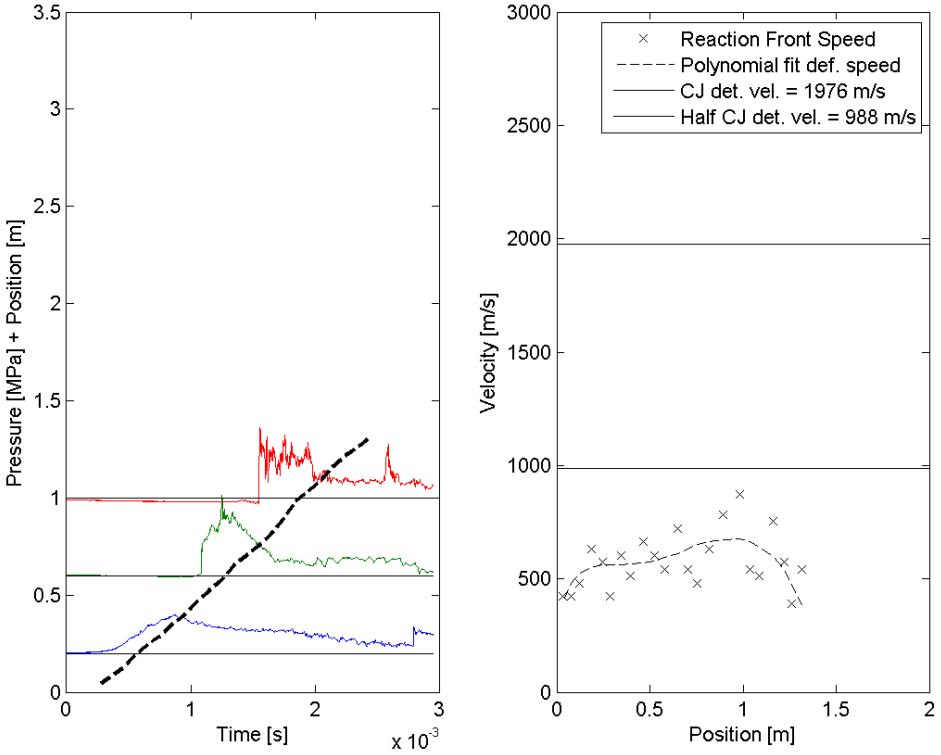

Figure 5.3: $BR = 0.5$ and $30\,\%H_2$ in air. (P112_T7). Fast flame and propagating shock wave in the channel. No clear evidence of local explosions.

done with stoichiometric concentration of 30 $\%H_2$ in air, and one experiments P117_T1 was done with 35 % hydrogen.

These experiments did not detonate. The flame speeds observed were lower than half the CJ detonation velocity. The $BR = 0.2$ experiment (see Figure 5.2) showed maximum flame speed of about $500 m/s$. Low overpressure were recorded as it peaked at $0.08 MPa$. No pressure oscillations were recorded at the first transducer behind the obstacle. This shows that there were no transverse waves behind the flame front. The $BR = 0.5$ (see Figure 5.3) showed pressures of about $0.4 MPa$, and no oscillations. The maximum curvefitted flame speeds were between 600 and $700 m/s$. This was below half the CJ detonation velocity. It is also seen from the x-t and pressure plots that the flame propagate behind the pressure wave.

5.1.2 Blockage ratio BR = 0.6

These experiments were studied for concentrations of 30 %, 35 % and 40 $\%H_2$ in air. DDT was not observed for this blockage ratio ($BR = 0.6$). The maximum flame speeds varied between 400 and $900 m/s$. The richest mixture gave the fastest flames and the highest pressure. The experimental results of P117_T5 (40 $\%H_2$ in air) are given in Figure 5.4. Relatively strong pressure spikes were recorded on the transducers at $0.6 m$ ($1 MPa$) and $1 m$ ($0.6 MPa$) behind the obstacle. The maximum flame speed were about $900 m/s$ which were below half the CJ detonation velocity. The pressure and position plot shows that the shock wave and reaction front propagated close together up to $1 m$ (third transducer) behind the obstacle. The distance between the shock and the reaction front increased at $1.6 m$ (4th transducer) behind the obstacle. This separation of shock and deflagration was observed at shorter distance behind the obstacle for the 35 %. The 30 % hydrogen in air experiment of P117_T3 showed no coupling of shock and deflagration.

5.1.3 Blockage ratio BR = 0.75

The 0.75 blockage ratio was investigated for concentrations ranging from 25 to 35 $\%H_2$ in air. There were no transition to detonation when the hydrogen concentrations were 28 $\%H_2$ in air or lower. The 30 % experiments detonated between $390 mm$ and $690 mm$ behind the obstacle. This showed that there were large variations in the distance behind the obstacle at which detonation was initiated.

The experiments where transition to detonation was observed, also showed that the max speed of the deflagration was about half the CJ detonation velocity or higher. The near limit concentrations of 28 $\%H_2$ in air (see Figure 5.5) also showed just as high flame speeds as the experiments with DDT. It is also seen that the deflagration and leading shock wave is coupled with the reaction front at $0.6 m$ behind the obstacle. The 25 $\%H_2$ in air (see Figure 5.6) showed a clear deceleration of the flame speed and a decoupling of shock and reaction.

The experiments were no transition to detonation was observed still gave relatively high pressures. The experimental results plotted in Figure 5.5 and Figure 5.6 shows 0.3 and $0.4 MPa$ over pressure on the first transducer and oscillations. $2 MPa$ over pressure was recorded on the second transducer in the 28 $\%H_2$ experiment (Figure 5.5), which is higher than the CJ detonation pressure ($1.54 MPa$).

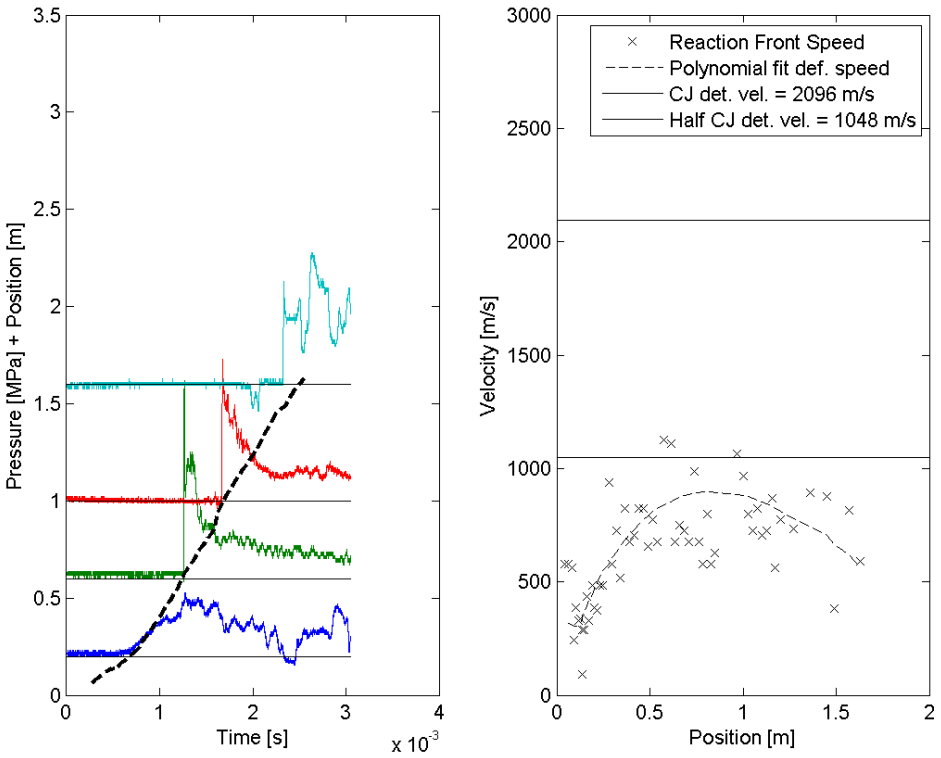

Figure 5.4: This shows an experiment with $BR = 0.6$ and $40\,\%\,H_2$ in air. (P117_T5). Fast flame and strong shocks. Oscillations were recorded behind the flame front, and flame speeds close to half the CJ detonation velocity. At $1.6\,m$ there is a decoupling of flame front and shock wave.

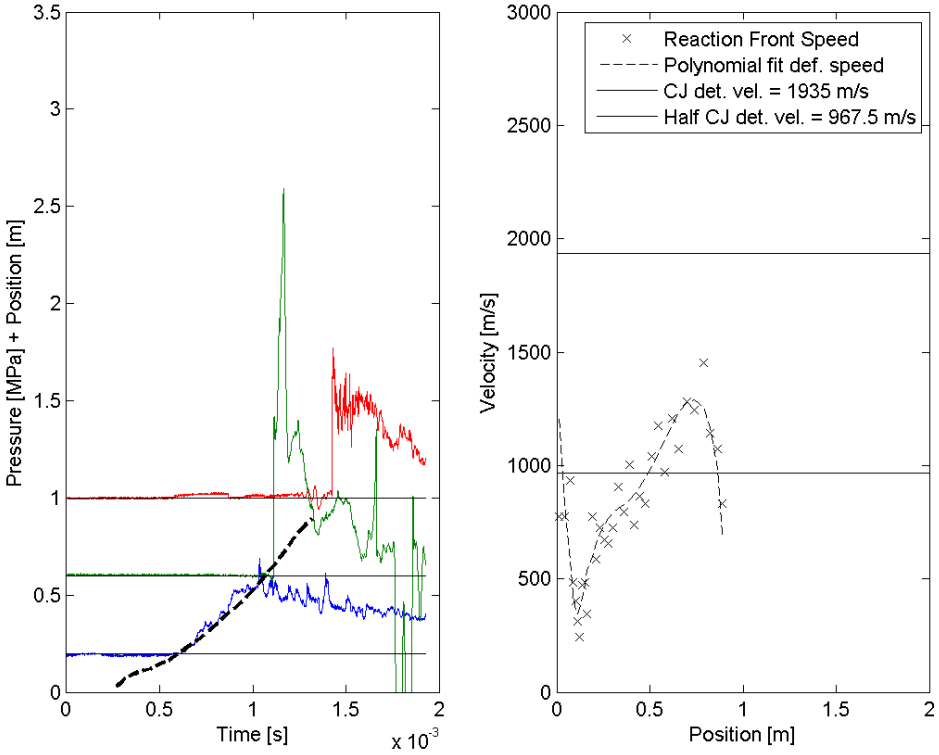

Figure 5.5: $BR = 0.75$ and $28\,\%\,H_2$ in air. (P113_T6). Fast flame and high pressure pulse. This experiments shows that there were pressure oscillations behind the flame front. These results did not show a sustained CJ detonation.

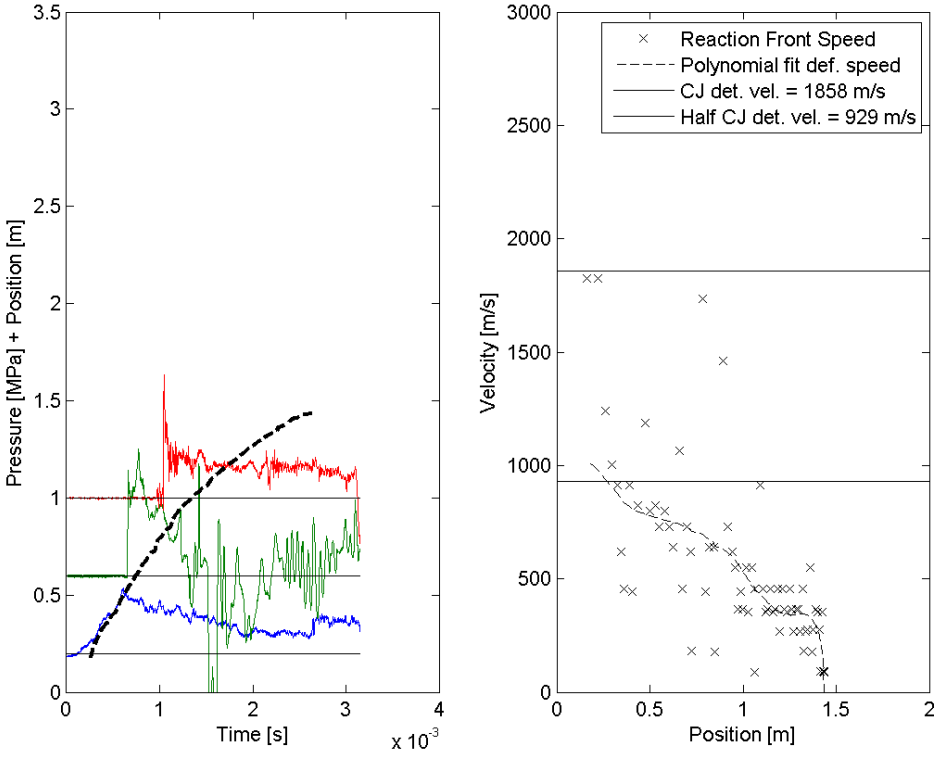

Figure 5.6: $BR = 0.75$ and $25\,\%H_2$ in air. (P113_T5). Fast flame and shock waves up to $0.6\,m$ behind obstacle, but later a decoupling of deflagration and shock wave.

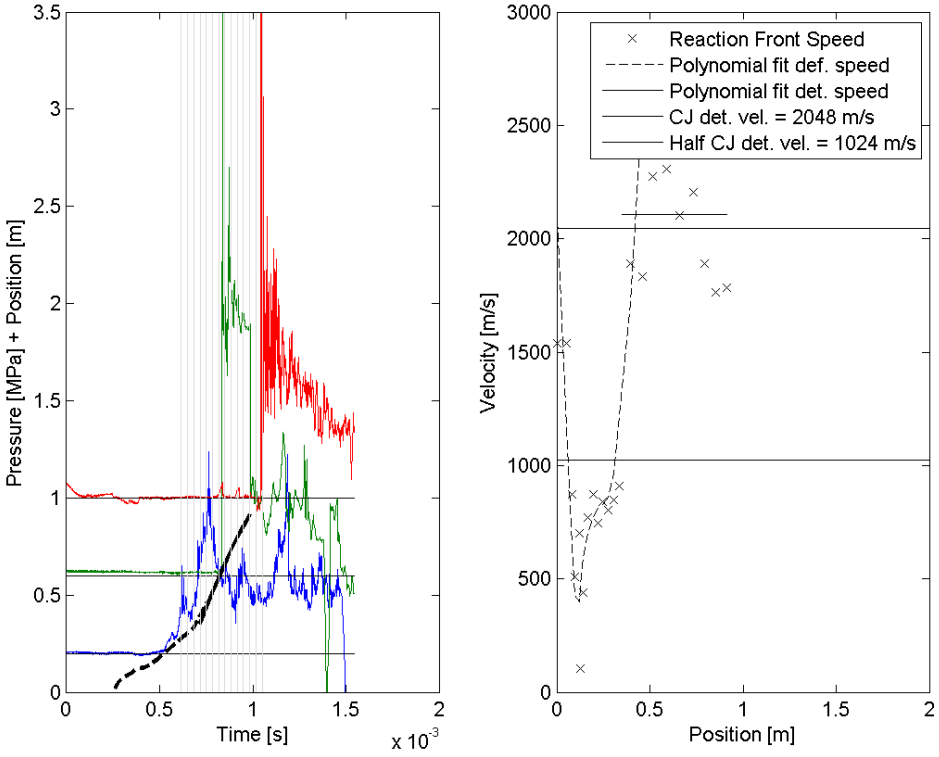

Figure 5.7: This shows an experiment with $BR = 0.75$ and $35\,\%H_2$ in air. (P113_T8). The vertical lines are related to the frames of Figure 5.8. Fast flame and DDT and a detonation which fails to propagate further.

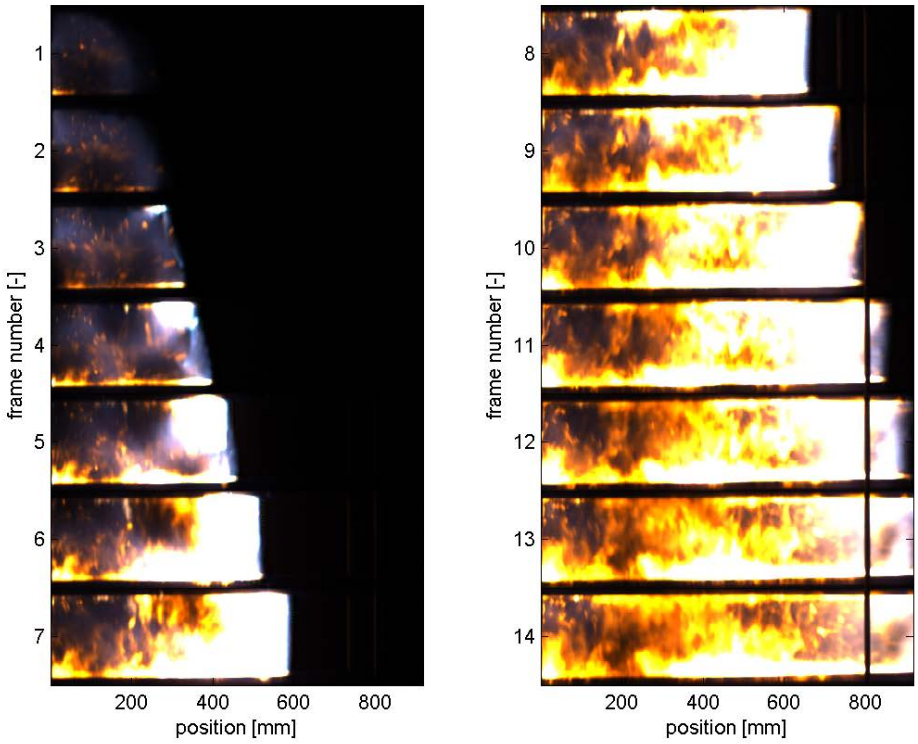

Figure 5.8: High speed frames from an experiment with $BR = 0.75$ and $35\,\%H_2$ in air. DDT is seen at the top wall of frame 3, but it fails to propagate as a detonation from frame 9 and onwards. (P113_T8). The frames are related to the vertical lines of Figure 5.7. Recorded at $30000 fps$, giving time between frames of $3.33 \cdot 10^{-5} s$

Also observed from the experiments is that P113_T4 and P113_T8 and possibly P113_T7 undergoes a transition to detonation only to fail to propagate as a detonation afterwards. It is seen that the speed of the detonation decreases as it fails. The pressure signal (see Figure 5.7) does not show any clear indication of a failed detonation. This is because there were no pressure transducer beyond the point of detonation failure. High speed film frames of the experiment with failing detonation are seen in Figure 5.8, and the vertical lines $(1-14)$ of the pressure plot correspond to the frame numbers of the high speed frames $(1-14)$. The plane detonation front in frame 6,7 and 8 starts to fail at frame 9 and onwards. It is also seen in the reaction front speed, as it does not fit a constant velocity, but rather a reducing trend.

5.1.4 Blockage ratio BR = 0.84

The 0.84 blockage ratio was investigated for concentrations ranging from 27 to $35\,\%H_2$ in air and the experiments are summarized in Table 5.2. The experiments with $28\,\%H_2$ and richer did

undergo transition to detonation, while the 27 % H_2 did not. DDT was observed between 333 and 533 *mm* behind the obstacle.

Table 5.2: $BR = 0.84$ experiments

Year	Project	Test	BR	$\%H_2$	ϕ	ITD [s]	λ [mm]	X_{det} [mm]	CJ_{vel} [m/s]
10	115	5	0.84	30	1.02	0	13.37	457	1976
10	115	7	0.84	27	0.88	0	16.91		1911
10	115	8	0.84	35	1.28	0	12.21	333	2048
11	120	1	0.84	30	1.02	0	13.37	533	1976
11	120	6	0.84	28	0.93	0	15.37	451	1935
11	120	7	0.84	27	0.88	0	16.91		1911

The pressure records from the two experiments are shown in Figures 5.9 (27 % H_2) and 5.10 (28 % H_2). 0.4 *MPa* over pressure were recorded on the first transducer in both experiments. The 28 % H_2 experiment did undergo transition to detonation at 430 *mm* while a coupled shock and deflagration is seen at 600 *mm* for the 27 % H_2. The velocities suggest that this complex decouples, but there are insufficient x-t data to conclude. The maximum flame speed were close to the half CJ detonation velocity for the 27 % H_2 experiment and slightly above for the 28 % H_2 experiment. Oscillations were recorded on the first transducer for both experiments, but stronger oscillations were recorded for the P120_T6 (28 % H_2) experiment (with DDT). More than 5 *MPa* were recorded on the second transducer of the 28 % H_2 experiment, on the third and fourth transducer this was reduced to 2.6 *MPa*. This is higher than the CJ detonation pressure.

Figure 5.10 and Figure 5.11 are from the same experiment, and the vertical lines of Figure 5.10 correspond to the frame number of Figure 5.11. On the pressure plot there are oscillations recorded on the first transducer. The first peak is seen between frame 2 and 3, and the frames show that there is as a curved brighter section of the deflagration with a center close to 200 *mm*. Frame 8 to 10 show the DDT and the propagating detonation. In frame 10 there is a bright spot as the detonation reaches the bottom wall. The second pressure transducer is located at this position and one triple point might have hit the transducer. This could explain the pressure spike.

5.1.5 Blockage ratio BR = 0.9

Table 5.3: $BR = 0.90$ experiments

Year	Project	Test	BR	$\%H_2$	ϕ	ITD [s]	λ [mm]	X_{det} [mm]	CJ_{vel} [m/s]
10	116	1	0.9	30	1.02	0	13.37	405	1976
10	116	2	0.9	27	0.88	0	16.91		1911
10	116	3	0.9	28	0.93	0	15.37	465	1935
10	116	4	0.9	35	1.28	0	12.21	336	2048
10	116	5	0.9	35	1.28	NaN	12.21	168	2048

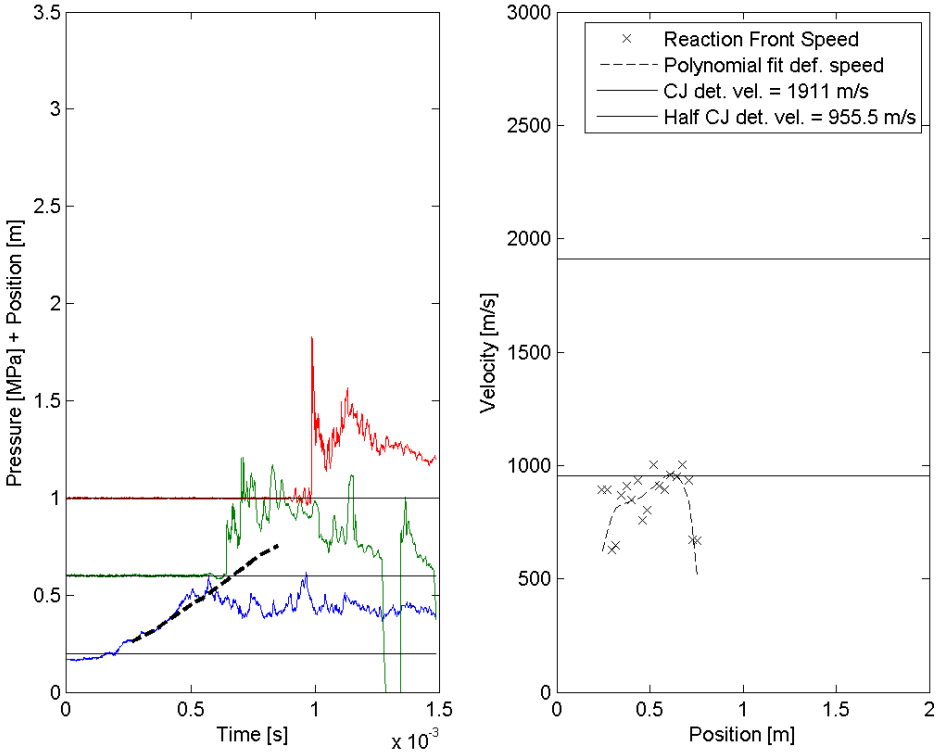

Figure 5.9: $BR = 0.84$ and $27\,\%H_2$ in air. (P115_T7). Fast flame, but no DDT. The pressure oscillations were not as clear as in the experiment shown in Figure 5.10

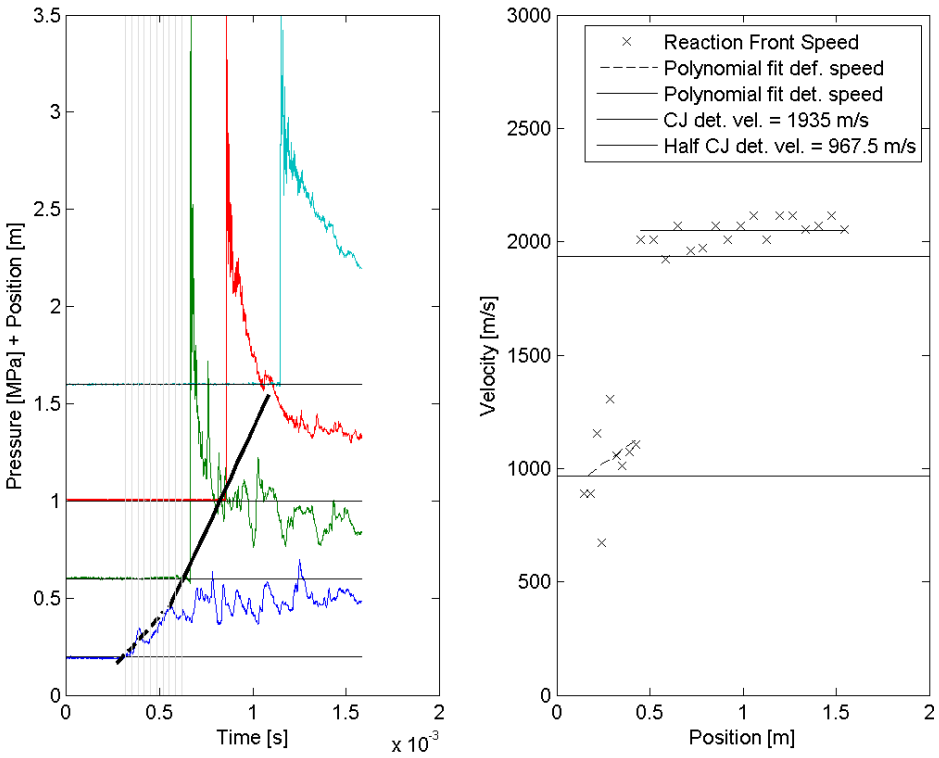

Figure 5.10: $BR = 0.84$ and $28\%H_2$ in air. (P120_T6). The vertical lines correspond to the frame numbers of Figure 5.11. This experiments showed strong pressure oscillations behind the flame front and DDT. The detonation propagated close to CJ velocity in the whole field of view in this experiment.

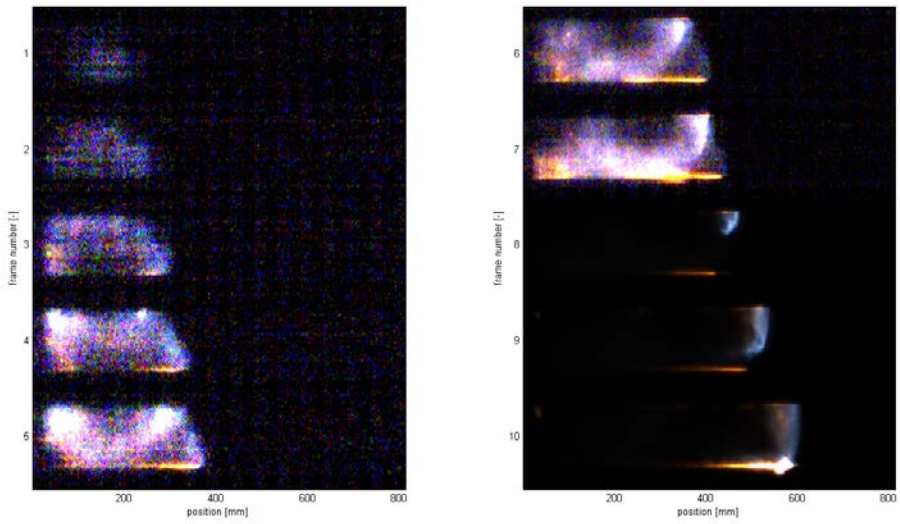

Figure 5.11: $BR = 0.84$ and $28\,\%H_2$ in air. (P120_T6). High speed film frames with various bit-shift. The frame number correspond to the vertical lines in Figure 5.10. Recorded at $30000\,fps$, giving time between frames of $3.33 \cdot 10^{-5}s$

The experiments in this section are summarized in Table 5.3. Concentrations from $27\,\%H_2$ to $35\,\%H_2$ in air were investigated, and the critical detonation concentration was between 27 and 28 %. DDT was observed between 336 and $465\,mm$ behind the obstacle. The P116_T5 experiment did undergo transition to detonation at $168\,mm$, but this experiment had a ignition time delay (ITD) of unknown length (more than five seconds). This experiments was the background for the later study of gas inhomogeneities and the influence on DDT.

Velocities were measured to be about half the CJ detonation velocity or higher in these experiments, also for the experiment that did not detonate ($27\,\%H_2$). In the experiment that did not detonate, about $0.4\,MPa$ were recorded on the second transducer and more than $1\,MPa$ on the third. High peak pressure were recorded for the experiments with DDT, see Figures 5.12 and 5.13. The figures are matched at the vertical lines of the pressure plot, with the high speed frames. Shock waves were recorded at the first transducer at frame 1 and between frame 4 and 5. The last shock is seen on the high speed frames as well.

5.2 Summarized results

This section summarizes the results and gives a qualitative description of the experimental results.

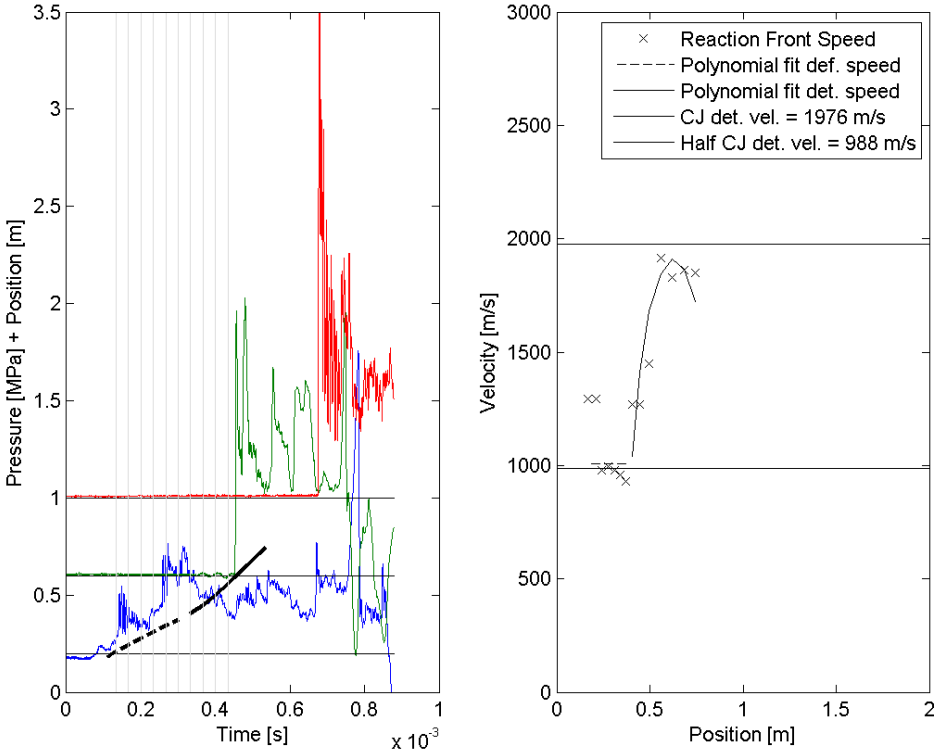

Figure 5.12: $BR = 0.9$ and $30\,\%\,H_2$ in air. (P116_T1). The vertical lines correspond to the frame numbers of Figure 5.13.

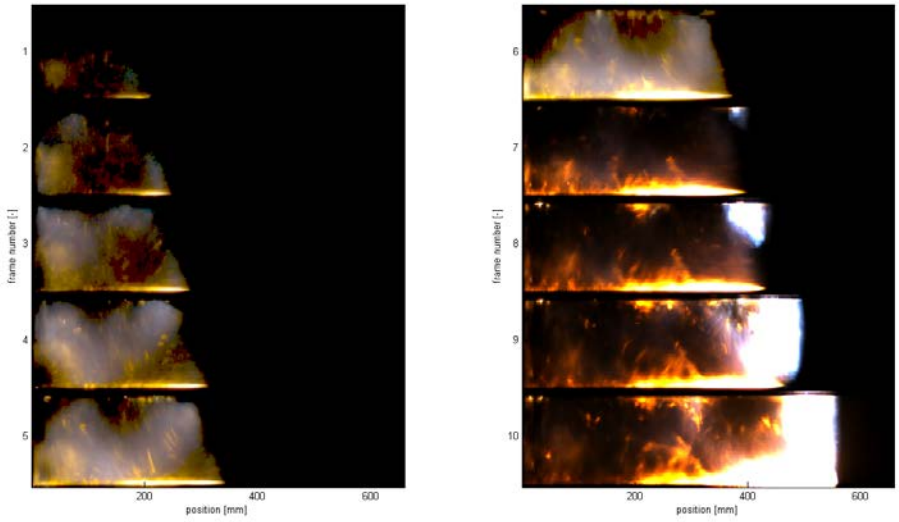

Figure 5.13: $BR = 0.9$ and $30\,\%H_2$ in air. (P116_T1). The frames correspond to the vertical lines in Figure 5.12. Strong pressure oscillation and DDT. Pressure recorded at $1\,m$ exceeds the CJ detonation pressure. Recorded at $30000\,fps$, giving time between frames of $3.33 \cdot 10^{-5} s$

5.2.1 Run up distance

The collection of experimental data shows that the distance behind the obstacle up to the point of DDT varied. There were no DDT observed for blockage ratios of $BR = 0.6$ and lower. The run up distance and concentrations with blockage ratio is summarized in Figure 5.14. The experiments on the right hand side of the vertical line did not detonate. It is shown in the figure that the leanest mixture to detonate was the $28\,\%H_2$ in air, also seen is a decreasing run up distance (x_{DDT}) with increasing hydrogen concentration.

5.2.2 High speed film results

The run up distance presented in Figure 5.14 shows the position along the length axis of the channel the DDT occurs. However it does not present where at the cross section it detonates. This section will more qualitatively present the onset of detonation from selected experiments combined with pressure records and illustrations. The high speed image processing method is described in Chapter 3.

Most experiments followed the same pattern when the flame propagated through the obstacle. The flame speed and reaction rate were much higher in the jet behind the obstacle than in front of the obstacle, see [114]. There was a jet of reactants with intensity depending on the blockage ratio through the obstacle. When the flame reached this jet it burned much faster and propagated down the channel.

In some experiments a spot of bright light appeared at the top or bottom wall in the high

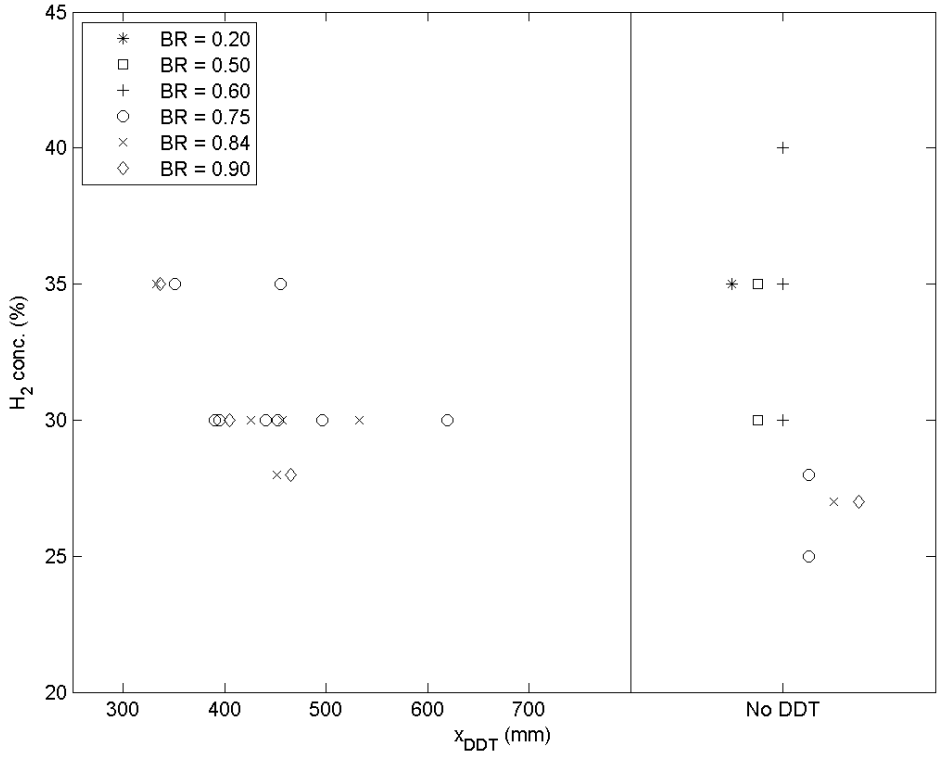

Figure 5.14: The run up distance, behind the obstacle, plotted against the hydrogen concentration, with various blockage ratios. All mixtures on the right hand side of the vertical line did not detonate. Only homogeneous concentrations.

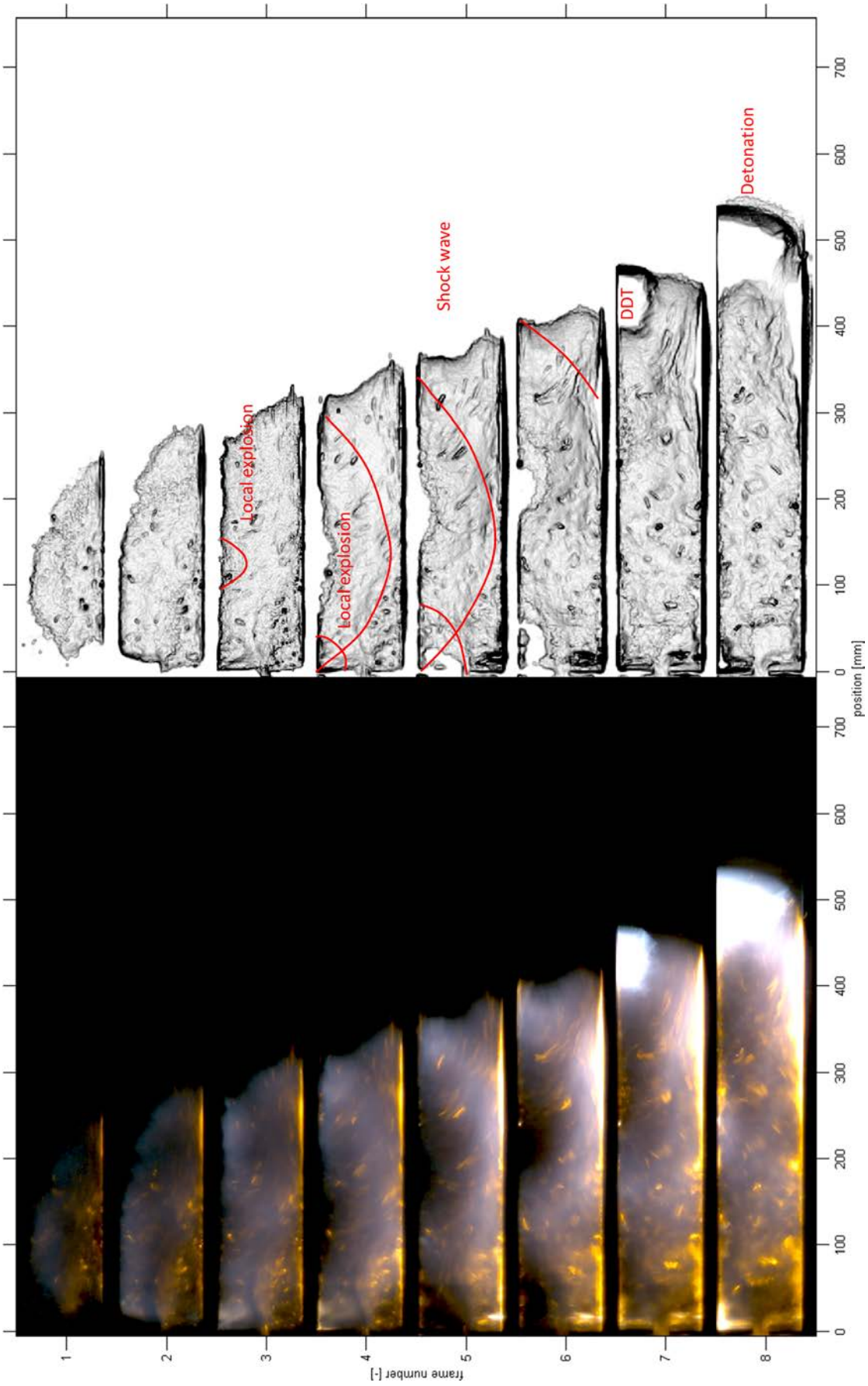

Figure 5.15: Figure is tilted 90^o. This figure shows high speed film frames on the left hand side and sketches to illustrate the interpretation of the film frames. Local explosions and weak shock waves are indicated and the onset of detonation is shown in frame. $BR = 0.84$ and $30\,\%\,H_2$ in air (P115_T5). Recorded at $30000\,fps$, giving time between frames of $3.33 \cdot 10^{-5} s$

speed film. This was interpreted as the DDT or a local explosion. Before the onset of detonation, there were observations of propagating transverse waves in the channel and indications of "explosions within the explosion" (according to A.K. Oppenheim) or local explosions close to the walls. These local explosions occurred far behind the leading edge of the deflagration and are volumes of reactants that burn much faster than the rest of the flame front. These local explosions resulted in propagating pressure waves.

Figure 5.15 shows one experiment with $BR = 0.84$ and $30\,\%\,H_2$ in air (P115_T5). On the left hand side are high speed film frames and on the right hand side are sketches to illustrate the flame propagation. The sketch was created in a image processing software, where the original color photo was converted to gray scale and the contrast and levels were adjusted to give a nice image. The gray scale images are used as a base to draw upon to better illustrate the phenomenon. The actual results are best understood when viewing the moving frames i.e. the film. The frames and sketches are given a short explanation in the list below, according to the interpretation of the author:

1. Flame propagate through the obstacle and burn in the turbulent jet.

2. Flame expands and burns in the turbulent jet. It is assumed to be an enhanced mixing at the flame front.

3. Local explosion in a volume of reactants at the top wall.

4. Shock wave from local explosion reach transducer. There is also a second explosion at the top wall.

5. Transverse waves in the channel.

6. Transverse waves in the channel.

7. DDT at the top wall.

8. Detonation propagate in the channel.

The pressure records from this experiment are shown in Figure 5.16, and the vertical lines corresponds to the frames of Figure 5.15. It is seen in the pressure plot that after frame 2 there is a shock wave recorded at transducer 1 located at the bottom wall. A stronger shock wave was also recorded after frame 3 at the first transducer. This corresponds to the sketches of Figure 5.15.

An example of an experiment without DDT is shown in Figure 5.17 and 5.9 ($BR = 0.84$ and $27\,\%\,H_2$). There are indications of a shock wave on the high speed film (frame 4 to 6) and a weak pressure wave on the pressure records. The flame speed is also shown to first accelerate then decelerate.

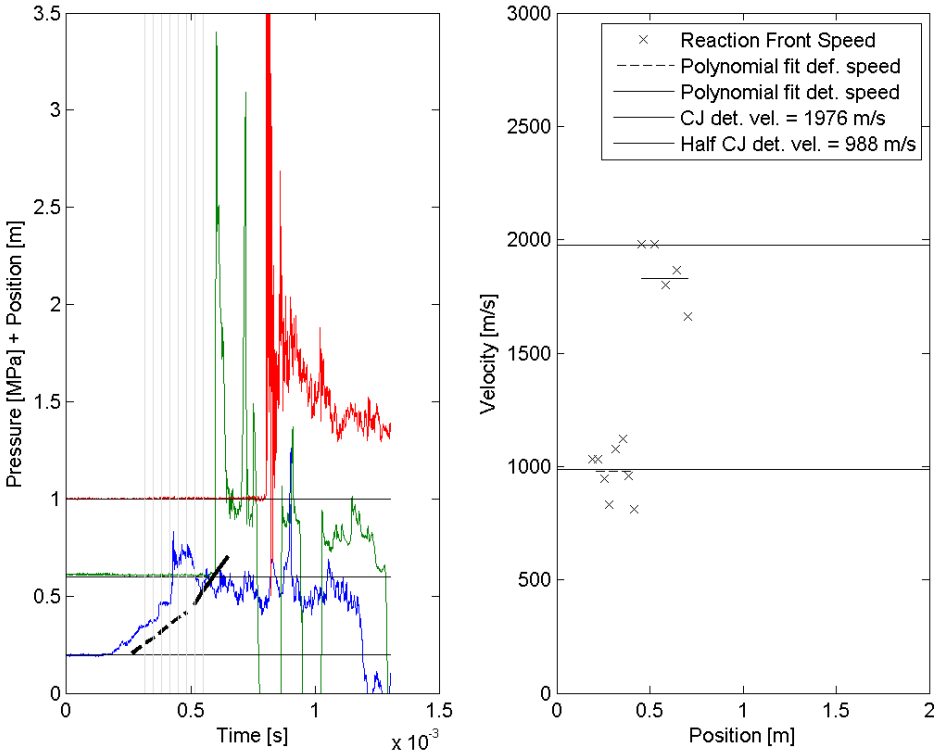

Figure 5.16: $BR = 0.84$ and $30\%H_2$ in air (P115_T5). The vertical lines correspond to the frame numbers of Figure 5.15

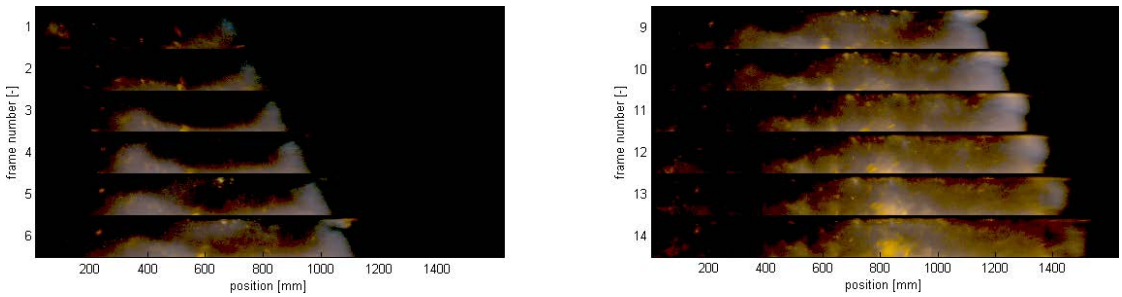

Figure 5.17: $BR = 0.84$ and $27\%H_2$ in air (P115_T7). Recorded at $30000 fps$, giving time between frames of $3.33 \cdot 10^{-5} s$

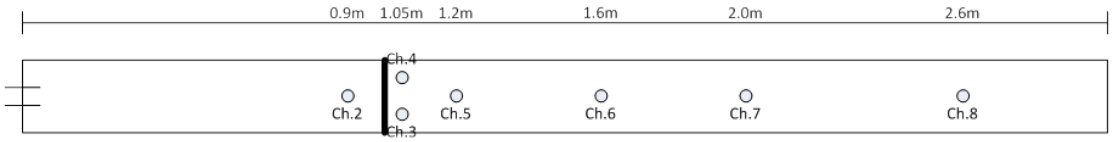

Figure 5.18: The location of the pressure transducers from the experiments (P101) in [21]. Top view of the channel, all transducers are mounted at the bottom wall.

5.3 Schlieren results of DDT in the channel

A z-type schlieren method was used to visualize the details of the deflagration and detonation front in channel. These experiments were part of L. Bjarnason [21] M.Sc. thesis and carried out under supervision of the author. One aim of the study was to investigate the details of the onset of detonation and also investigate the transverse waves in the channel using the schlieren setup. The location of the pressure transducers are shown in Figure 5.18.

The high speed schlieren frames were recorded at 20000 fps and are shown in Figure 5.19 ($BR = 0.75$ and $30\%H_2$). In the last two frames are visible two pressure waves propagating in the channel, most likely from left to right. The corresponding pressure plot from the same experiments are shown in Figure 5.20. Marked by X in the plot are the time instances of the first 9 frames from Figure 5.19. The X's in the plot also indicate the position of the leading tip of the deflagration as seen on the schlieren pictures. After the last X, the leading tip of the deflaration is outside the frames. The clear pressure spike on channel 6 to 8 are clearly a detonation, and by linearly extrapolate the detonation position backwards and extrapolating a linear deflagration position forwards, it is suggested that the transition from deflaration to detonation occur at $t \approx 0.0185s$ and at position $x \approx 0.3m$ behind the obstacle. The pressure records in Figure 5.20 also shows that there are significant pressure waves recorded behind the leading tip of the flame front prior to the detonation transition. These waves are seen on channel 3, 4 and 5. There is a pressure rise as the flame propagates through the obstacle and past the transducers (ch 3 and 4), but also later on channel 5. Then there are pressure spikes recorded on channels 3 to 5 recorded behind the deflagration front. At the estimated time of transition ($t = 0.0185s$) there is a large pressure increase on channel 5 together with several spikes.

A further investigation of the transverse waves in the channel was done by mounting pressure transducers at the same position behind the obstacle but at the top and bottom wall, see Figure 5.21. The mixture is $30\%H_2$ in air and $BR = 0.75$. The same detonation/deflagration extrapolation as previous is used, with a schlieren view from 190mm to 360 mm behind the obstacle. This gives a pressure record as shown in Figure 5.22, with the corresponding (X in pressure plot) high speed schlieren frames in Figure 5.23. A zoom and simplified plot of the same experiment, with only the extrapolated deflagration and detonation trajectories and channel 4 (top wall) and channel 5 (bottom wall) is shown in Figure 5.24. The strong pressure waves recorded at the top wall are seen to reflect at the bottom wall, this presence of transverse waves are seen in the high speed frames of Figure 5.23 as well. In frames 6 to 10 it is seen that there are strong transverse waves in the channel prior to the onset of detonation. In frame 5 there is also a pattern of reflected pressure waves at the top wall. This wave occurred prior to the onset

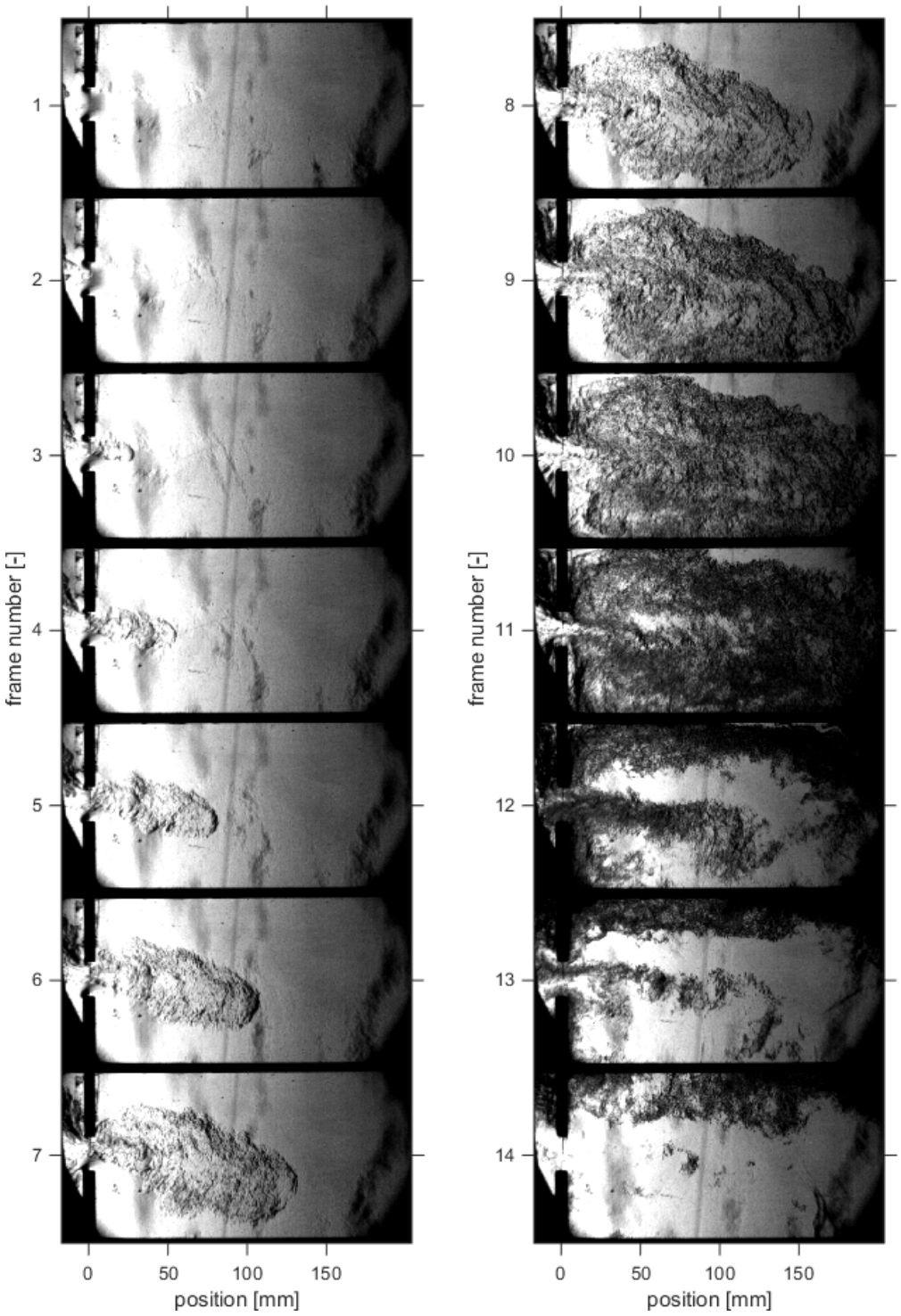

Figure 5.19: High speed schlieren frames from the experiments [21]. Sequence follows top down from left to right. Recorded at $20000 fps$, giving time between frames of $5 \cdot 10^{-5} s$

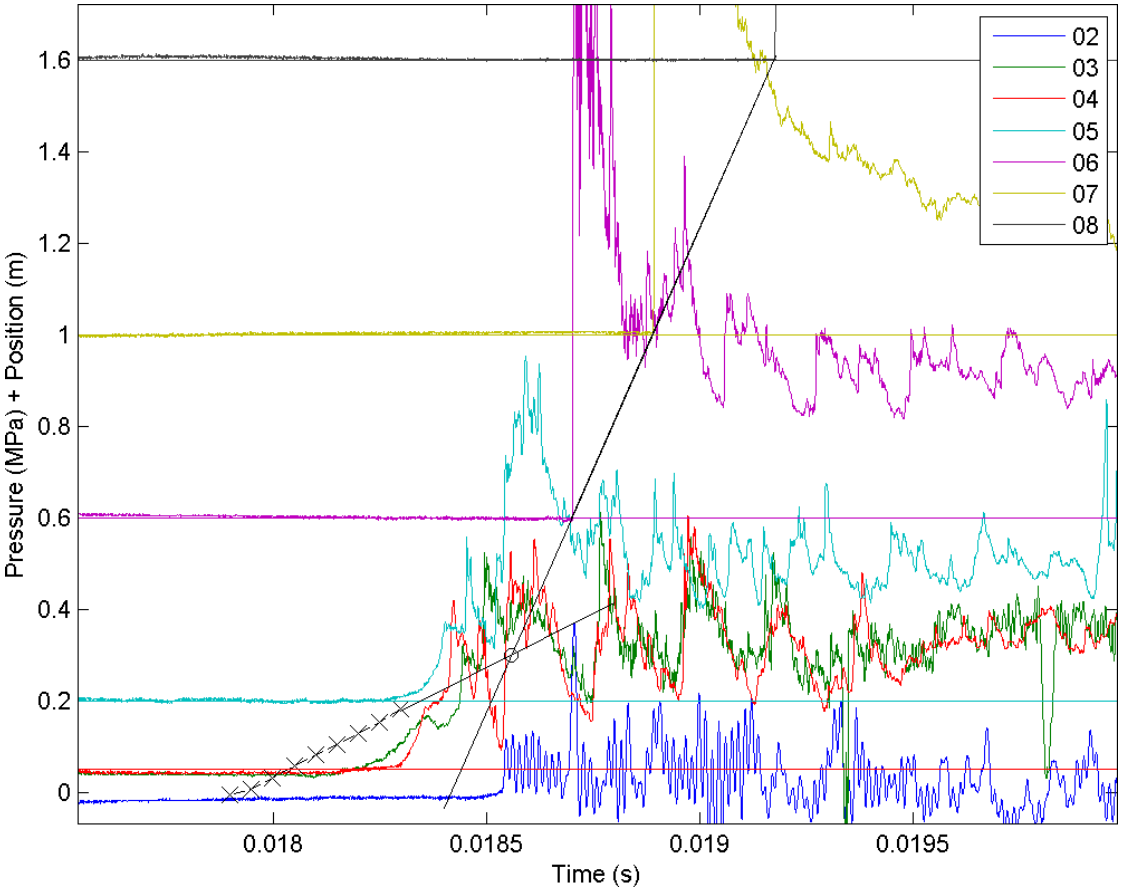

Figure 5.20: Pressure plot from the experiments [21]. X marks the time instance of the first 9 frames in Figure 5.19.

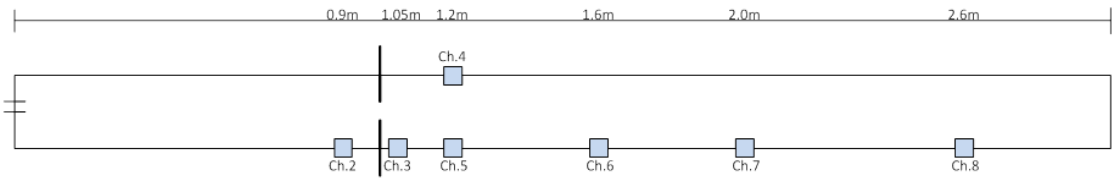

Figure 5.21: The location of the pressure transducers from the experiments (P102) in [21]. Side view.

of detonation accordingly to the extrapolated wave trajectories

The schlieren experiments also showed an example of no DDT is shown in Figure 5.25, but a shock wave propagating at approximately $1000 m/s$. It is an experiment with $BR = 0.75$ and $25\% H_2$ in air.

5.4 Discussion

The goals of this study included:

- Investigate the onset of detonation in a jet behind a single obstacle in a channel. Identify whether it is at the tip of the turbulent flame jet or at the walls.
- Possibly identify the event that lead up to onset of detonation behind the single obstacle.
- Produce experimental results as a basis for validation of numerical simulations.

This discussion will relate the experimental results to other relevant work, and present the main findings of the work.

5.4.1 Discussion on the experimental results

The experimental investigations found the limits of DDT in the present geometry depending on the blockage ratio. It is seen that the blockage ratio is important for the intensity of the jet and the turbulent burning in the jet. Too low blockage ratio gives too low intensity turbulence and no DDT. The reactivity of the mixture is also important, and DDT was not observed for mixtures leaner than $28\% H_2$ in air. Figure 5.14 and Table 5.1 also show that an increase in run up distance (behind obstacle) is observed for decreasing hydrogen concentration. The work of Iijima and Takeno [116] shows that the fastet burning velocity in atmospheric hydrogen-air mixtures are at about $40\% H_2$ in air. This is partly an explanation of the run-up distance. A similar trend is shown by Dorofeev [117], however the results only present lean to stoichiometric results. The paper does give good models for run-up distance in channel with various blockage ratios (for multiple obstacles). The cell size data from the Detonation database in Figure 3.7 [20] also show a minimum detonation cell size at a slightly rich mixture. This is related to a shorter induction time of slightly richer mixtures, thus a higher propensity to generate local explosions.

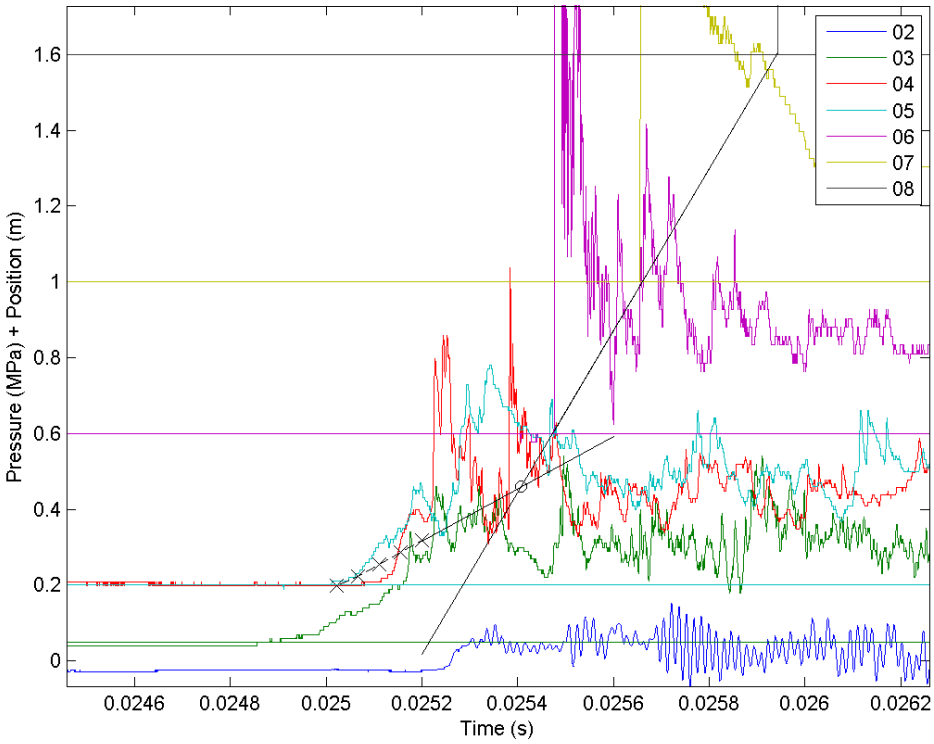

Figure 5.22: Pressure plot from the experiments [21]. X marks the time instance of the first 5 frames in Figure 5.23.

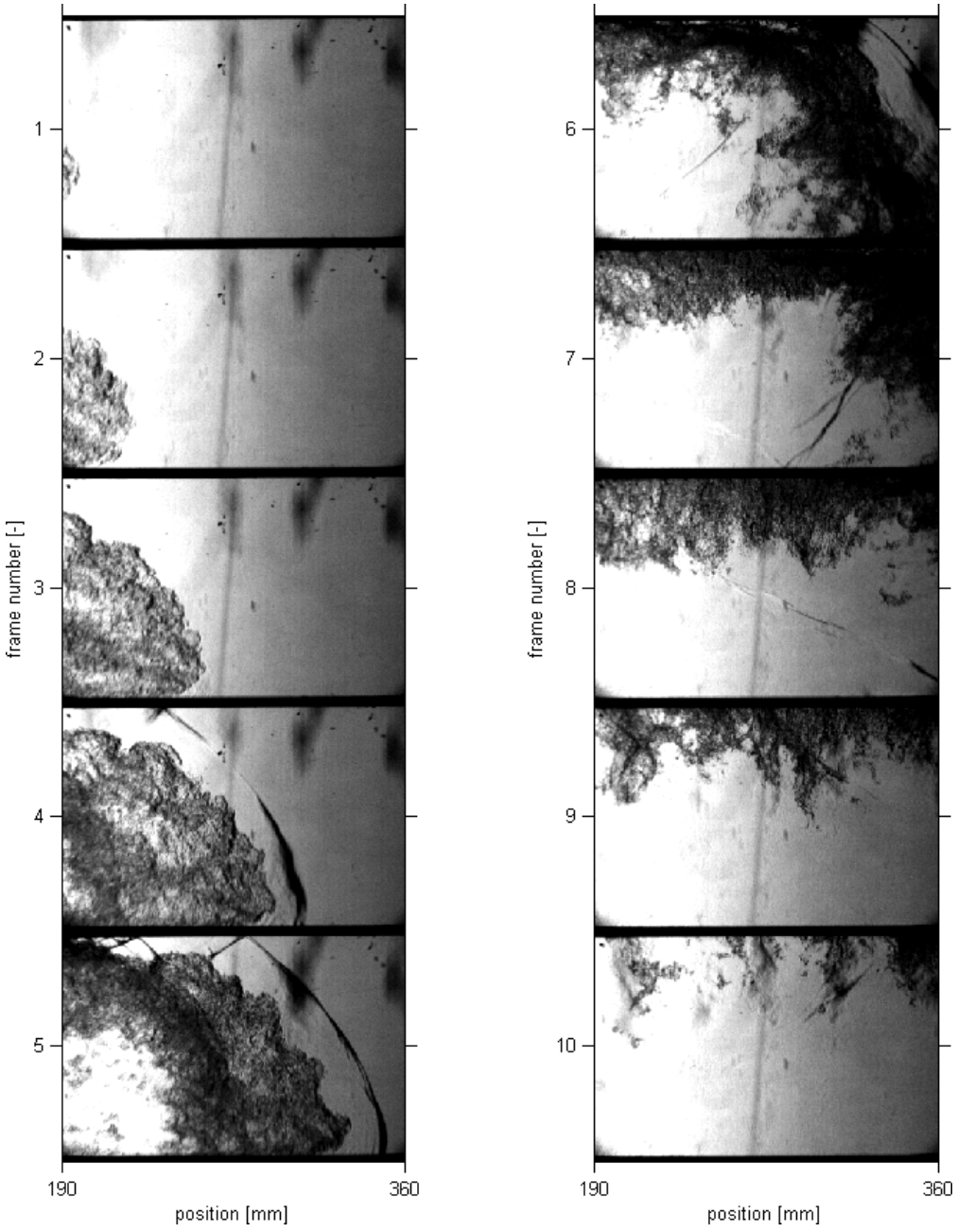

Figure 5.23: High speed schlieren frames from the experiments [21]. Sequence follows top down from left to right. Recorded at $22500 fps$, giving time between frames of $4.44 \cdot 10^{-5} s$

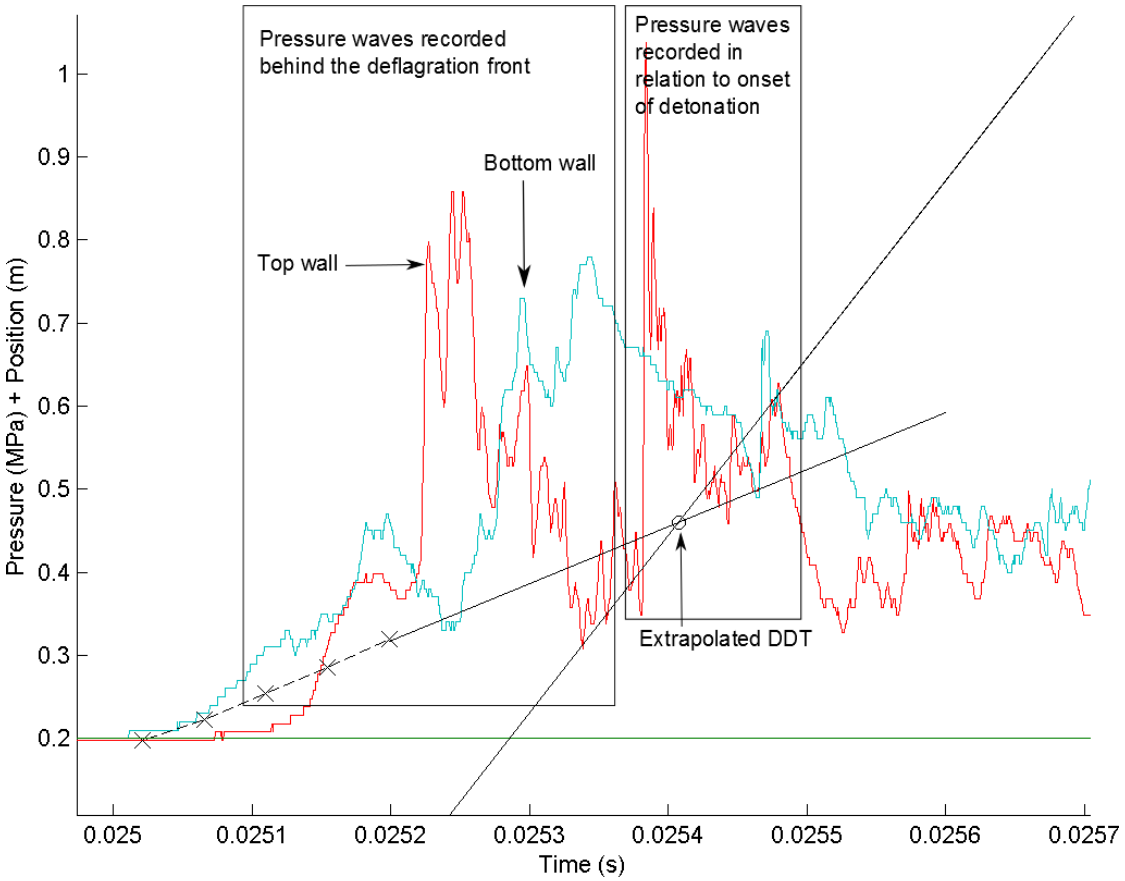

Figure 5.24: Simplified pressure plot from the experiments by [21] with extrapolated wave trajectories and explanations.

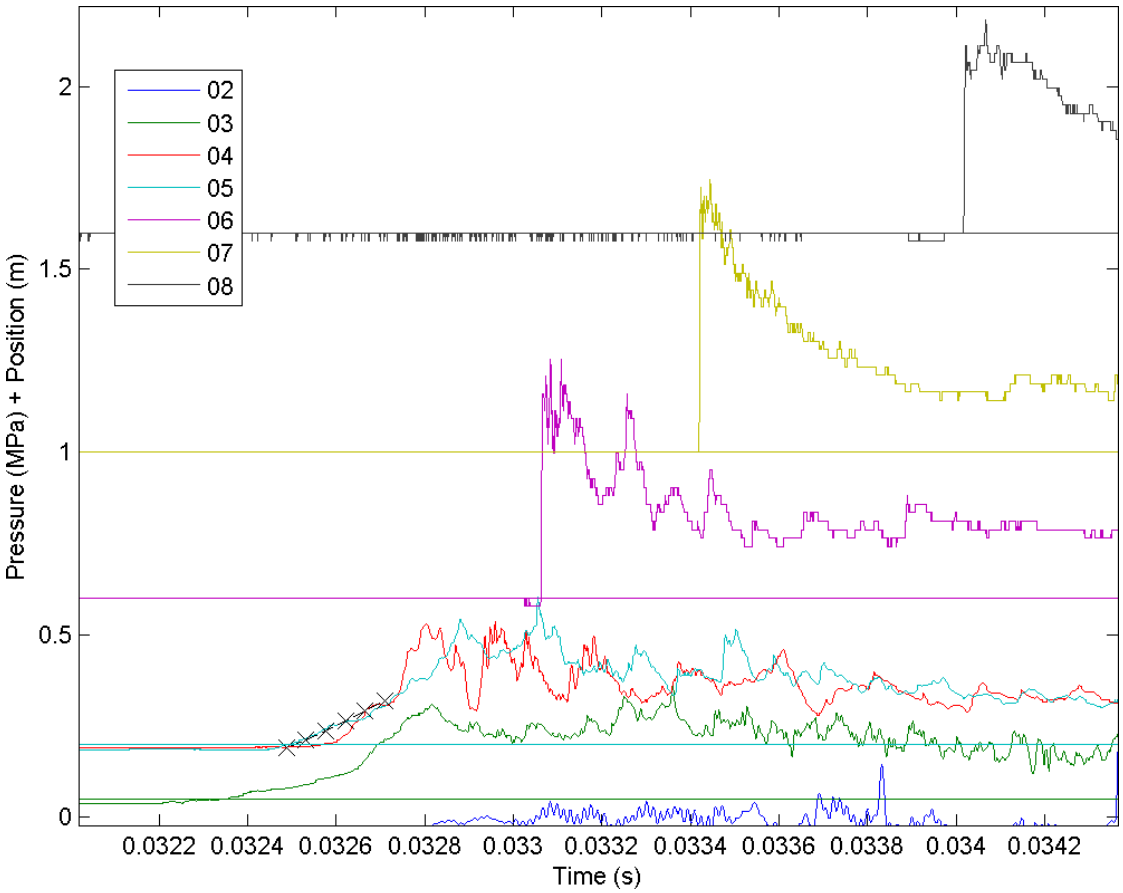

Figure 5.25: Pressure plot from the experiment ($BR = 0.75$ and $25\%H_2$ in air) in [21]. X's mark the position of the leading front of the deflagration.

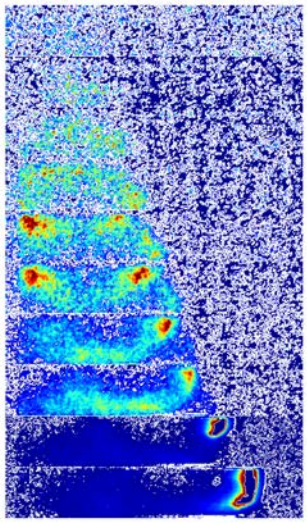

Figure 5.26: The blue channel of the RGB vector of P120_T6, same experiments and frames as Figure 5.11.

The onset of detonation was found to follow a series of local explosions. Volumes of reactants were observed to burn fast, expand and send pressure waves propagating in the channel. These local explosions were observed far behind the leading tip of the deflagration. One local explosion could lead to the reaction in another volume, but the volumes were too small for a detonation to propagate in. The combinations of pressure records and reaction fronts clearly showed that there were strong transverse waves propagating in the channel prior to the onset of detonation. In Figures 5.12 and 5.13 are clear evidence of transverse waves in the channel, as the pressure records and high speed frames show that shock waves were recorded behind the leading edge of the flame front. This experiments lead in turn to an onset of detonation. This is also backed by the schlieren experiments in [21], when close up schlieren photos are combined with pressure transducers located close to each other or top/bottom configuration at the same location behind the obstacle. By processing the self luminescent photos from the experiments and extracting only the blue channel of the RGB vector it is seen in Figure 5.26 that there is a brighter curved section of the flame propagating in the channel prior to the onset of detonation. Close to the critical BR and concentrations it is however not as easy to distinguish between the events prior to DDT or no DDT. This is seen in Figure 5.5 where the hydrogen concentration is near the limit. Very strong shock waves of $2MPa$ were recorded, but no following detonation. This could have been caused by a local explosion at the flame front which failed to develop into a detonation. It is also seen from Figures 5.3 and 5.6 that the pressure waves in the channel were not coupled with the deflagration front for experiments without DDT. This coupling was more prominent in the DDT experiments as seen in Figure 5.10 and Figure 5.12.

Given the square cross section of the channel, it is not clear whether the volumes that burnt

fast were actually the corners of the channel. It is though considered likely that pockets of unreacted hydrogen-air are found in the corners of the experimental setup.

The onset of detonation were observed at the top wall as well, only two experiments showed detonation onset at the bottom wall. This observation might be caused by gravity separation of the fuel and air, but within the (maximum) two seconds from stopped filling until ignition it is believed to be of minor influence. It was clearly given that the onset occurred at the walls and not at the tip of the deflagration or behind any shock wave preceding the deflagration.

5.4.2 Comparison to Knudsen - DDT in circular pipes

The work of Knudsen [34] showed that for circular geometries, parallels of both DDT and no DDT were observed for $25\,\%\,H_2$ in air for $BR = 0.921$. And parallels of DDT and no DDT were observed for $BR = 0.572$ of $35\,\%\,H_2$ in air. This is both lower concentration and lower BR than this study. The work by Knudsen gives a condition for DDT constrained by the $(D_p - D_o)/2\lambda = 1$ and $D_o/\lambda = 1$. where D_o and D_p is the obstacle diameter and the pipe diameter. If the mixture and BR ratio is within these limits transition to detonation could happen.

By scaling the results from this experimental study by similar parameters as the Knudsen [34] study, it is found that it fits the criterion by Knudsen. The work by Knudsen investigated circular geometries and hence the diameter is an defined length scale. In square geometries, Liu et al. [118] suggested that scaling by detonation cell size and hydraulic diameter gave poor results. They suggested an effective diameter D_{eff} as a more suitable scaling length. The effective diameter is a mean of two characteristic lengths (varying depending on geometry). Figure 5.27 shows a comparison of the scaled values from the Knudsen study and this study. The square approximation to the circular problem seems to fit well within the same limits. It is also worth noting that the criteria for DDT is only necessary and not a sufficient one. It is also only validated for hydrogen-air mixtures. In Figure 5.27, a limit for $(D_p - D_o)/3\lambda = 1$ is also given. There are however uncertainties related to detonation cell size measurements and cellular regularity. The circular geometry study of Knudsen and this square geometry does however fit within the same limits and it is reasonable to assume that the phenomenon is also similar. In the circular geometry we can assume that the transition to detonation occur at the wall, which also fit the numerical results by Vaagsaether et al. [119].

5.4.3 Comparison to Dorofeev - length scale of onset of detonation

The experiments in the present study are scaled accordingly to the method proposed by Dorofeev et al. [13]. The length scale (L) for this series of experiments is chosen to be the height of the channel (D_p by Knudsen) which is equal to the width equal to $L = 100\,mm$. Since there is only one length scale in this experimental series, the results are presented with the blockage ratio on the horizontal axis. It is shown in Figure 5.28, and a suggested limit is indicated by the dotted line.

The results in Figure 5.28 agrees quite well with the length scale criterion for onset of detonation by Dorofeev, $L/\lambda > 7$, here the limit is at $L/\lambda > 6.5$. It is important to note that the accuracy of the L/λ criterion is a factor of approx. 2, so it is well within the scale given by Dorofeev [120]. The actual length scale which is valid for this experimental setup is somewhat

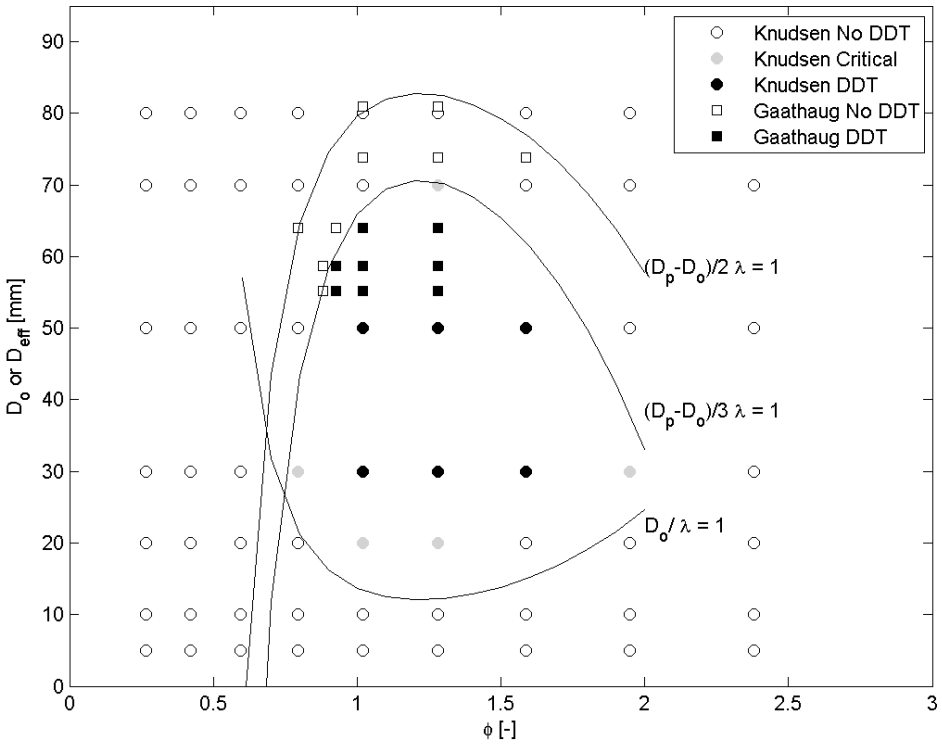

Figure 5.27: The experiments by Knudsen and the experimental results in this work. The current work also follow the Knudsen criteria.

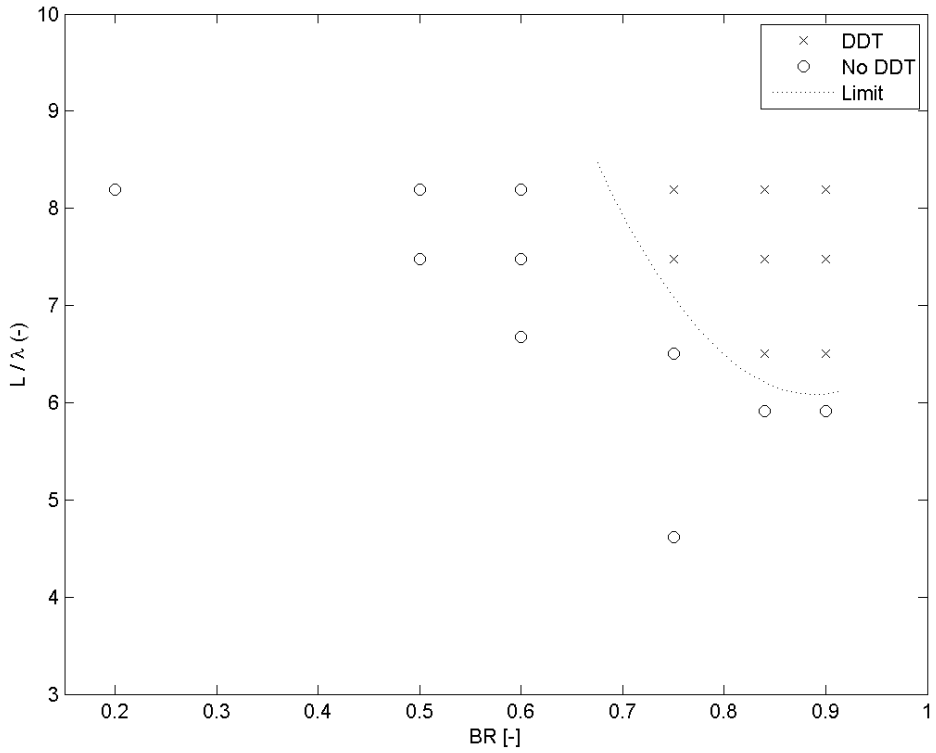

Figure 5.28: The ratio of length scale $L = 100\,mm$ to cell size plotted against the blockage ratio.

difficult to determine. Dorofeev [120] suggested $L = h = w = 100\,mm$ or $L = V^{1/3} = 271\,mm$. It is also important to mention that the length scale is only a necessary criterion, not a sufficient condition for DDT. It is also a criterion of a deflagration velocity of more than the speed of sound in the products. Therefor it is shown that large enough blockage ratio (small opening) is necessary to accelerate the deflagration enough.

5.4.4 Comparison to J. Chao - Critical deflagration waves

The experiments in this work are not directly comparable to the work of Chao [59], where deflagrations down stream a perforated plate were studied, but it is still interesting to compare. Chao observed flame speeds of about the CJ deflagration velocity which is close to half the detonation velocity. This was also observed in this work. Retonation waves which are backwards propagating blast waves from the onset of detonation was observed in some experiments by Chao and in some experiments it was not observed. The same is seen in this work, Figure 5.10 does not show any clear retonation wave recorded on the first transducer, while in Figure 5.12 there is a recorded shock at $0.7\,ms$ which correspond to a retonation wave. Also very strong transverse waves are recorded on the transducers but also seen on the high speed films. The

lack of retonation waves are explained to be because of no hot spot or local explosion onset of detonation but rather an acceleration up to the onset of detonation [86]. The amplification of transverse waves are explained by Lee [86], but are also shown to be important for the transition to detonation. The same importance of transverse waves are seen in this work as explained earlier where it was observed that the pressure spikes are recorded behind the deflagration front. The amplification of transverse waves are also shown by Gaathaug et al. [121]. There are however no clear evidence of several transverse waves in these experiments, but it should be a suggested continuation of this work.

The work by Radulescu [101] also shows similar behavior as a detonation was diffracted over a half sphere and dies. As the shock-deflagration complex propagated further, local explosions were observed at the walls and in the triple points of the shock front.

The study of Bjerketvedt et al. [122] studied the reinitiation of detonation across an inert region. They observed an ignition delay distance behind the inert region. The oscillating pressure waves behind the flame front were also observed in their experiments.

5.4.5 Comparison to Meyer, Urtiew and Oppenheim - DDT in smooth channel

The work by Meyer et al. [56] showed how a local explosion occurred in the turbulent flame brush of a hydrogen oxygen deflagration. In their study the flame followed a series of compression waves, but they found it insufficient to cause ignition and postulated that there had to be other mechanisms as well. The relevance of the study is however the fact that local explosions occurred far behind the leading tip of the deflagration. And some explosions occur in pockets bound by combustion products as seen in the experiments in this work as well. Turbulent mixing in the flame front and the shear flow are believed to lead to the local explosions, as well as shock compression.

5.4.6 Comparison to unconfined jet experiments

The work of Knystautas et al. [14] and Thomas [74] does not agree on the actual mechanism of the deflagration to detonation transition, regarding the importance of heat conduction in the heat transfer and generation of induction time gradients. The experiments in this thesis are not directly comparable to the unconfined jet experiments as these are confined within the channel walls. It is however important to address the mechanism proposed by Thomas that the small scale turbulence in the shear flow could induce mixing at the length scale of the flame thickness.

The flow between the flame and the wall could experience high shear and Kelvin Helmholtz instabilities, thus high shear mixing. The local explosions are observed in this assumed section of high mixing rate, and are likely initiated by the intense small scale mixing of hot products with cold reactants. One could speculate that the high mobility of H-radicals [1] could also be an important factor in the mixing process. If the turbulent length scales are close to the limit where they could influence the laminar structure of the flame, it could influence the thicker H diffusion zone than the diffusion zone for other compounds. It is also important that these explosions occur in a volume large enough to send sufficiently strong transverse waves propagating in the system. Any critical length scale of the turbulence in this study is not possible to define, but the results show that the mixing close to the walls are important.

The generation of transverse waves from local explosions were also observed in the numerical investigations in Chapter 7. There it is observed that several small constant volume explosions add up and amplify each other and lead to the onset of a detonation. It is also pointed out that the volume explosions must be of a sufficient size to generate strong enough transverse waves.

5.4.7 Comment on the importance of detonations in accidental investigation conclusions

Recent comments by Lee [91] states that for the investigations of accidental explosions it is usually not important to determine whether or not a detonation occurred. The blast waves from high speed deflagrations could be as strong as detonations. It is also worth noting that DDT in unconfined geometries are very hard to achieve, even for very reactive gases. This statement does not directly influence this work of DDT in a channel with one obstacle, which is a rather special case. The experimental results does however show that deflagrations could produce very strong over pressures. One example is given in Figure 5.5, where the peak pressure on the second transducer was 2 MPa. DDT is also associated with high pressure peaks as seen in these experiments see Figure 5.24 The comments by Lee [91] also states that without any full three dimensional description of the detonation structure it is still a poorly defined phenomenon in need of more basic research. The paper by Johnson [31] points out that assessing detonation hazards in safety studies has been neglected for a long time and must be given the proper attention. This statement is backed by the results of the Buncefield Explosion Mechanism Joint Industry Project [27].

5.5 Conclusions of the homogeneous experiments

The three goals of this study was to find out where DDT occurred in the channel and possibly identify events that lead up to it. The production of our own numerical results was necessary to use as input to a CFD code.

The conclusion will first be presented by the main goals of the study as given in Chapter 1, and later a general comment.

5.5.1 Investigate the onset of detonation in a jet behind a single obstacle

This aim to identify where at the cross section of the channel the detonation onsets. The run up distance behind the obstacle is shown in Figure 5.14, and a trend of decreasing run up distance with increased hydrogen concentration. This is most likely due to the higher reactivity of slightly richer hydrogen concentrations, this is also seen in Figure 5.27 where the smallest detonation cell size are found in slightly richer mixtures.

All the high speed camera results show that the onset of detonation occur at the walls, see Figures 5.8, 5.11,5.13 and 5.15. Of all the experiments with DDT, only 2 experiments showed onset of detonation at the bottom wall. The bottom wall experiments were P113 T7 and P120 T5 (part of the inhomogeneous experiments presented later).

5.5.2 Identify the events that lead to onset of detonation behind the single obstacle

The deflagration to detonation transition originate far behind the leading edge of the deflagration as it propagates through the obstacle. The high speed films shows local explosions close to the walls and the creation on transverse waves behind the tip of the deflagration. The local explosions are also recorded on the pressure transducer placed closest to the obstacle. The shear layer mixing are believed to heat the reactants in front of the reaction zone, as well as increase the local reaction rate. This is one likely explanation of the origin of the local explosions.

One local explosion could initiate the next explosion as well by compression heating of the already hot reactants. The local explosions amplify each other, and lead to the onset of detonation. The local explosions were observed in volumes, between the flame and the wall, which are too narrow for detonation propagation. These pockets might be located in the corners of the experimental channel. The final onset of detonation occur closer to the front of the flame, but always at the walls.

5.5.3 Produce experimental results as a basis for validation of numerical simulations

The deflagration to detonation transition (DDT) and the onset of detonation have been studied, and experimental results have been made. The deflagration and detonation velocities have been extracted from the high speed film, and the pressure records have been plotted and compared. The reaction wave x-t data together with the pressure records are good for validation of numerical simulations. But the random nature of DDT [53] caused by the large response to small perturbations and the three dimensionality of the flame front as seen in Chapter 4, will most likely not lead to exact reproduction of the experimental results in numerical simulations.

The ignition delay uncertainty described in Chapter 3 must also be considered when doing direct comparison between experimental results and numerical simulations. There is at least an $\pm 10ms$ uncertainty of all measurements relative to time $t = 0s$ (trigger signal). All recorded pressure signals are accurate to the bandwidth of the amplifiers ($200kHz$), and high speed cameras are given by their recording frames per second (fps). The exact time of ignition is not measured in the experiments.

5.5.4 Other concluding remarks of the homogeneous experiments

As shown in Figure 5.27, the current experiments in a square channel fit within the criteria given by Knudsen [34]. Then it is reasonable to assume that in the circular geometries DDT occurs at the walls as well. This is also in agreement with the results of the numerical simulations by Vaagsaether et al. [119] and Gaathaug et al. [123].

Chapter 6

DDT and detonations in inhomogeneous hydrogen air

The gas explosion experiments in inhomogeneous mixture were conducted to assume more real world situations where hydrogen releases seldom are homogeneous in composition. As a part of the IEA HIA task 19 and task 31 this problem should be investigated. The goal of the study was to find out if inhomogeneous gas mixtures could lead to detonation more easily then homogeneous mixtures. A secondary goal of the study was the study of detonation propagation in a layer of reactants above a pocket of air.

Table 6.1: Experimental matrix of the inhomogeneous experiments

Year	Project	Test	BR	$\%H_2$	ϕ	ITD [s]	λ [mm]	X_{DDT} [mm]	CJ_{vel} [m/s]
11	118	1	0.6	35	1.28	7	12.21		2048
11	120	2	0.84	30	1.02	7	13.37	548	1976
11	120	3	0.84	30	1.02	10	13.37		1976
11	120	4	0.84	30	1.02	9	13.37	438	1976
11	120	5	0.84	40	1.59	9	14.98	430	2096
11	120	8	0.84	27	0.88	8.4	16.91		1911

6.1 Experimental results

This section describes the experimental results with pressure plots, x-t diagrams and velocities as described in the experimental setup chapter. The inhomogeneous experiments are presented in Table 6.1. The experiments are organized as projects and test number as seen in Table 6.1. The ITD is the ignition delay time in seconds, and represents the time from filling stop until ignition. This is a measure of how long the air was allowed to flow into the channel before ignition.

The velocity of the inflowing air layer were approximated using the experimental data and model given by Sommersel [107]. There it is given that the velocity of the air layer is about

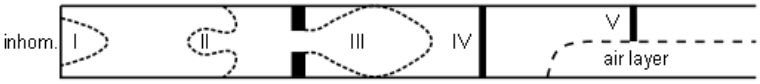

Figure 6.1: Sketch of the combustion wave propagation in the inhomogeneous mixtures

$u_F \approx 0.2 - 0.3 m/s$, it is also assumed no mixing at the front.

The inhomogeneous experiments are a set of 6 experiments, where one was conducted with $BR = 0.6$ while the rest was conducted with $BR = 0.84$. The limits for DDT (with $BR = 0.84$) was found to be $27\% H_2$ in air. The Ignition Time Delay ITD [s] varied in the experiments and the results showed that $ITD = 10 s$ was too long to cause DDT in stoichiometric hydrogen air mixtures.

The inhomogeneous conditions were prepared accordingly to the method described in Chapter 3. A sketch is given in Figure 6.1.

6.1.1 Detonation propagation in stratified layer

This section focuses on the combustion wave propagation behind the obstacle, including the deflagration to detonation transition and the detonation propagation in the stratified layer of reactants above the air layer. After ignition (number I Figure 6.1) the flame propagated up to the obstacle (II Figure 6.1) and displaced reactants in front of the deflagration. A jet of reactants was formed through the obstacle opening (III Figure 6.1). When the flame reached the jet the overall reaction rate increased and the flame speed increased. In the experiments with $BR = 0.84$, concentration above 27% and $ITD < 10$ s DDT was observed in the channel (somewhere between III and IV). The events leading up to detonation transition were similar to the events described in the homogeneous experiments section. The run up distances were not different than for the homogeneous gas mixtures.

When the detonation reached (IV Figure 6.1) the layer of air at the bottom of the channel it continued to propagate in the layer of reactants above the air layer. See V in Figure 6.1.

High speed frames of a detonation propagating in an inhomogeneous mixture are shown in Figure 6.2. The events leading up to the onset of detonation were similar to the events described in the homogeneous section with local explosions and transverse waves. In the first frame of Figure 6.2 the onset of detonation was seen at the top wall.

The propagation of the detonation is seen in the frames 2 - 8. In frame 9 the detonation reached the air layer, and in the subsequent frames it is seen to propagate in the layer of reactant above the air layer. Details of the detonation propagation is shown in Figure 6.3. It is also seen that hot products are displaced downwards behind the detonation front. The detonation front was not planar when it propagated in the reactant layer.

6.1.2 Failure and onset of detonation in the reactant layer

Two of the experiments with inhomogeneous gas mixtures showed a particularly interesting phenomenon, reported here due to its results and relevance to the secondary objective of this study.

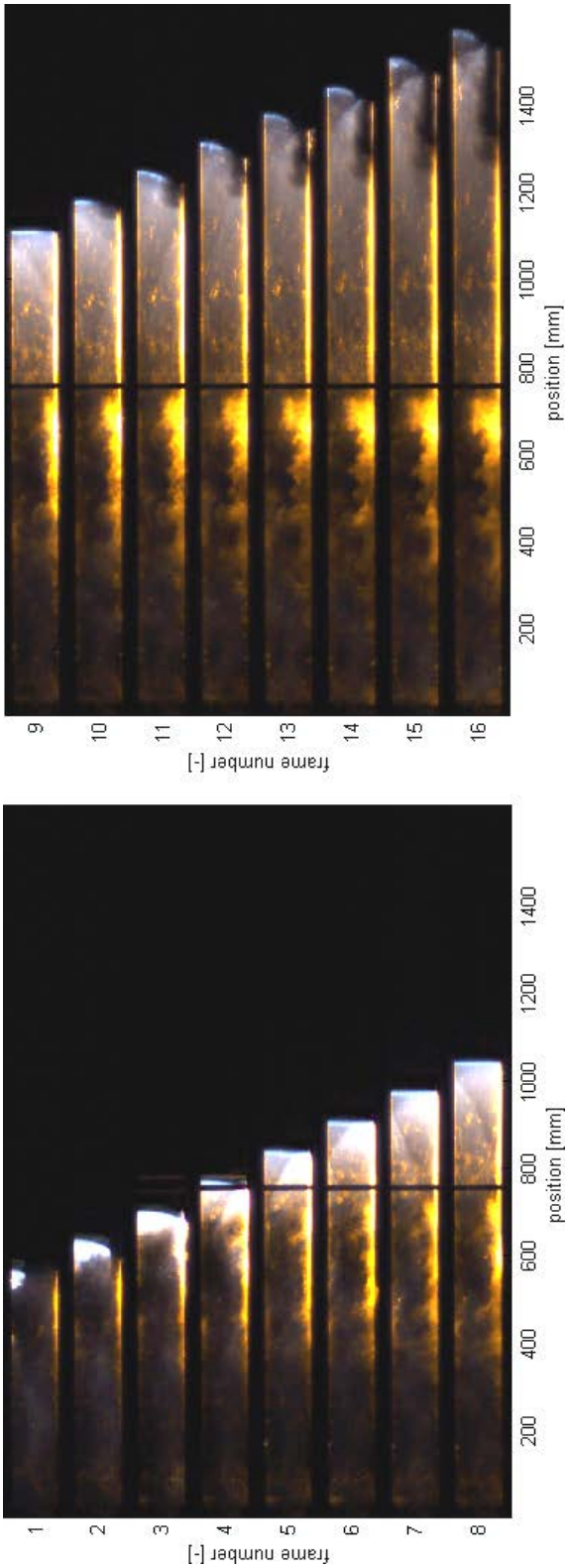

Figure 6.2: High speed frames (P120_T2) of a detonation propagating in inhomogeneous mixture. The detonation reached the air layer in frame 9. Recorded at $30000 fps$, giving time between frames of $3.33 \cdot 10^{-5} s$

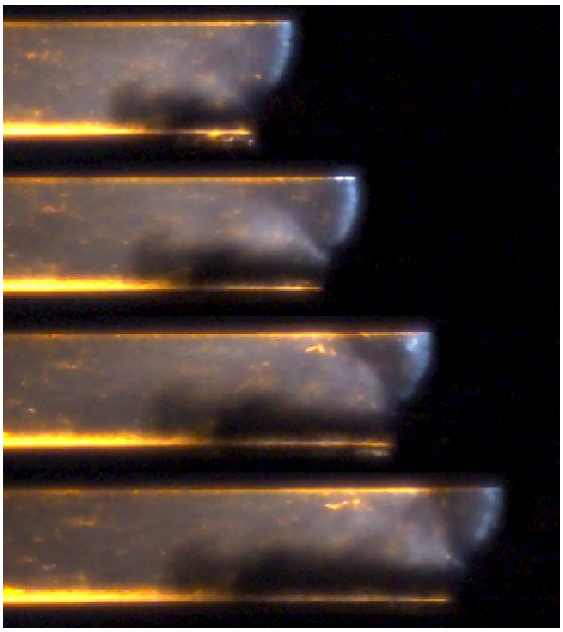

Figure 6.3: Details of the detonation propagating in the reactant layer (P120_T2).

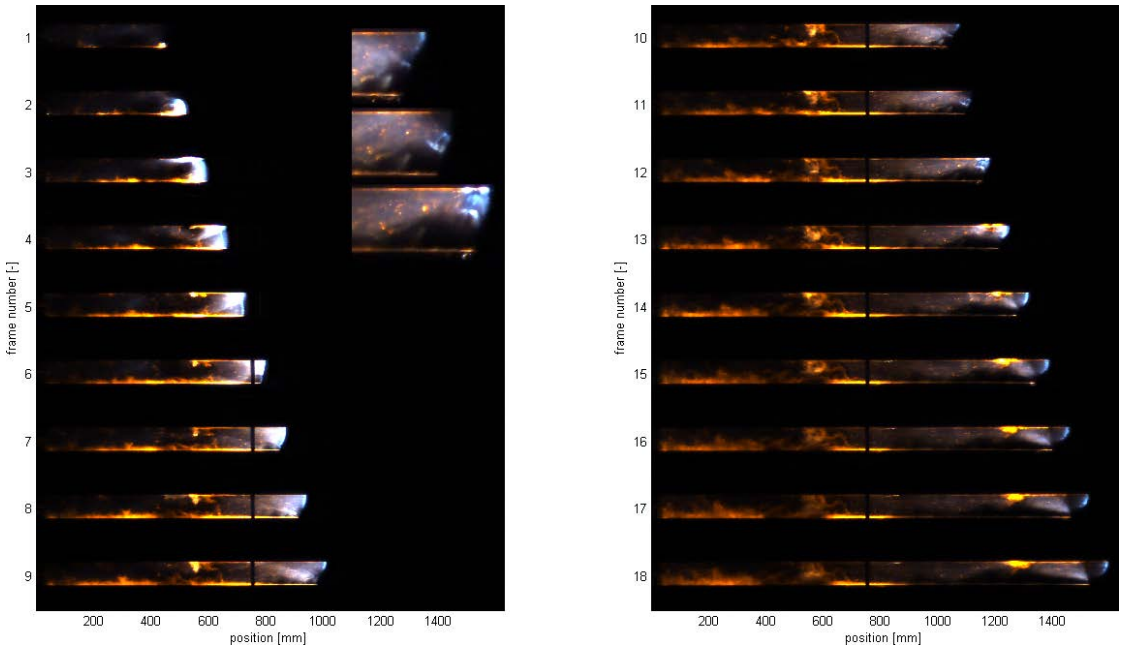

Figure 6.4: High speed frames (P120_T5) of a detonation in inhomogeneous mixture with failure and a second onset of detonation. Three detailed frames of the failure and second onset is given. Recorded at 30000fps, giving time between frames of $3.33 \cdot 10^{-5} s$

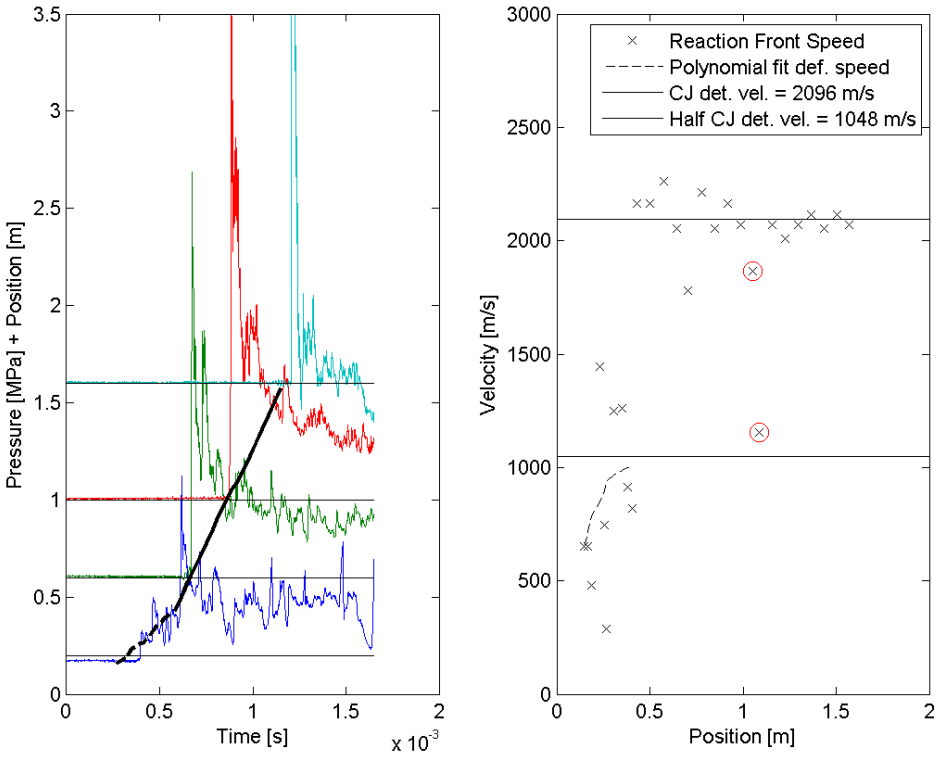

Figure 6.5: This shows an experiment with $BR = 0.84$ and 40 % H_2 in air. The failing detonation is seen in the velocity plot marked by red circles. (P120_T5)

As a detonation propagated in the reactant layer it failed, but a second onset was observed as well. This is shown in Figure 6.4 and 6.6. Figure 6.4 ($BR = 0.84$, 40%H_2 in air) shows the onset on detonation at the bottom wall in the first frame and the arrival at the air pocket in frame 6. The detonation fails in frame 10, which is also shown i detail in the top right corner of Figure 6.4. The next frames shows a second onset of detonation at the interface between the reactants and the air pocket. The next frame shows the developed detonation and it is shown how it propagates through the rest of the reactant layer in the channel.

The pressure plot of experiment P120_T5 is shown in Figure 6.5. The red circles mark the significant velocity drop as the detonation fails, but as it continues if propagate with near CJ velocity.

An other example of a second onset of detonation in the reactant layer is experiment P120_T4 (30% in air). The high speed frames are shown in Figure 6.6 and the pressure and velocity are shown in Figure 6.7

It is also seen that there was a significant drop in detonation velocity as the detonation failed in the reactant layer, but as it did onset again it continued at near CJ velocity. The second onset was observed at the interface between the reactants and the air pocket.

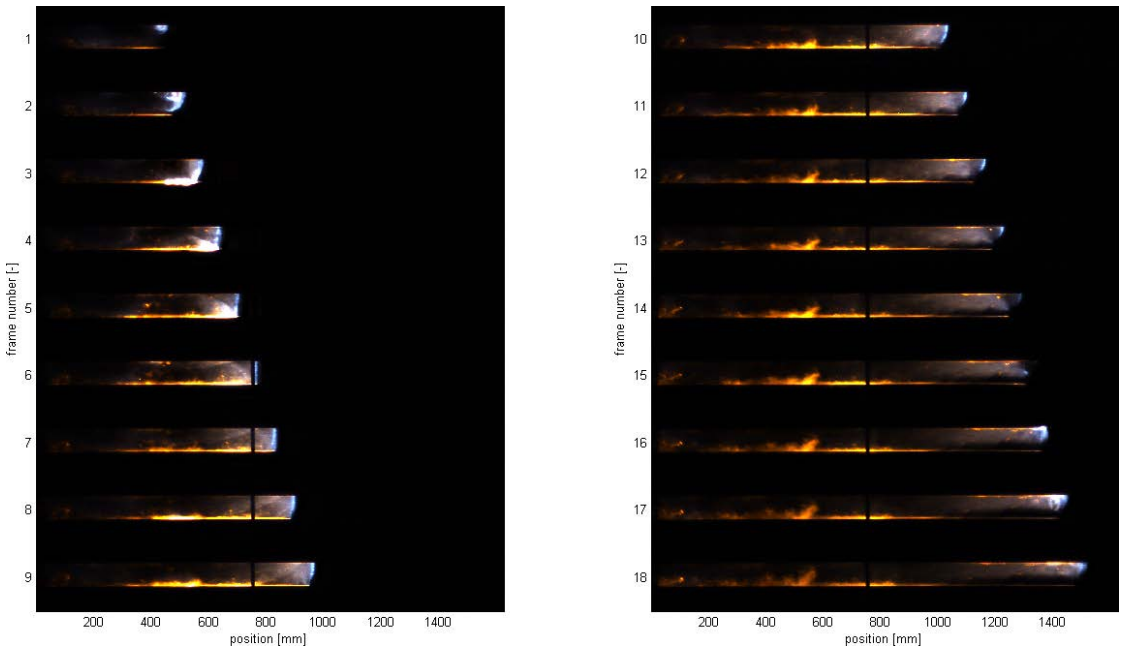

Figure 6.6: High speed frames (P120_T4) of experiment with $BR = 0.8430\%H_2$ in air. The figure shows how the detonation fails in the reactnat layer and the second onset at the interface between the reactants and the air pocket. Recorded at $30000 fps$, giving time between frames of $3.33 \cdot 10^{-5} s$

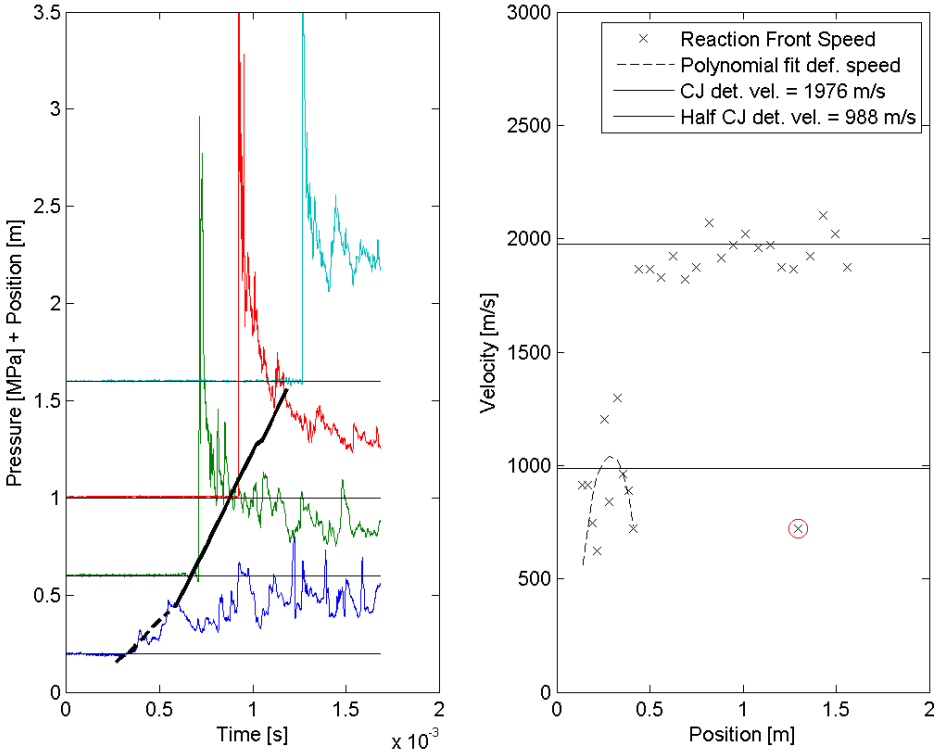

Figure 6.7: This shows an experiment with $BR = 0.84$ and 30 % H_2 in air. The failing detonation is seen in the velocity plot marked by a red circle. (P120_T4)

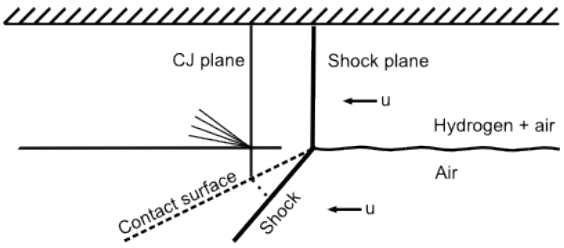

Figure 6.8: Sketch of a detonation with a compressible boundary. Assumed 1D within the reaction zone and 2D behind the CJ plane. From Dabora 1963 [22]

6.2 Discussion

Deflagration to detonation transition (DDT) in the channel with inhomogeneous mixtures followed the same events as the homogeneous mixtures. It followed the same 27% H_2 in air concentration limit for DDT as well. As the flame propagated through the obstacle it burned fast and local explosions were observed at the walls. These explosions generated transverse waves which added up and lead to onset of detonation. The introduction of air into the channel before ignition did not influence the DDT or onset of detonation behind the obstacle. There was no further evidence that inhomogeneous conditions influenced the run up distance behind the obstacle.

A limit of 10 s. Ignition Time Delay was found, as no DDT was observed when the ITD was 10 s, but for 9 s DDT was observed. These times are geometry dependent and no overall criteria, but so far no major influence of inhomogeneous conditions was observed regarding the DDT. As the flame propagated in the first meter between ignition and obstacle, a flow of reactants through the obstacle opening displaced the air pocket towards the open end. The jet through the obstacle displaced fresh reactant ahead of the flame. This jet was assumed also to mix with the airlayer. This lead to unknown gas composition behind the obstacle, but it is believed to be close to the reactants displaced though the opening. When the detonation wave propagated further, the air pocket was visible from the high speed film.

As a detonation propagates in a layer bound by a compressible fluid, the expansion behind the detonation front will be larger than when it is bound by a solid surface due to the increased area behind the front. Dabora investigated this in 1963 [22] and a sketch from the report in given in Figure 6.8. Even though it is simplified and assumed 1D within the reaction zone the sketch shows how the shock angle will increase the area behind the detonation, leading to increased expansion and lower velocity. The increased expansion can be analog to a leaky piston behind the detonation.

Dabora [22] showed that for $H_2 - O_2$ mixtures the critical velocity deficit where the detonation failed was $8 - 10\%$, there were no evidence to quantify the velocity deficit in this study. The more recent work by Rudy et al. [103] showed that $3\,cm$ was the critical layer thickness for stoichiometric hydrogen-air mixtures. This corresponds to a layer thickness of 2 to 3 detonation cell sizes. If the height of the reactant layer above the air layer in this work is assumed to be half the channel height, it should sustain detonations in mixtures between 24% and 43% hydrogen in air [20]. However there are not observed DDT for mixtures leaner than 28% hydrogen in air.

The detonation front is curved as it propagates in the reactant layer. This is assumed to be

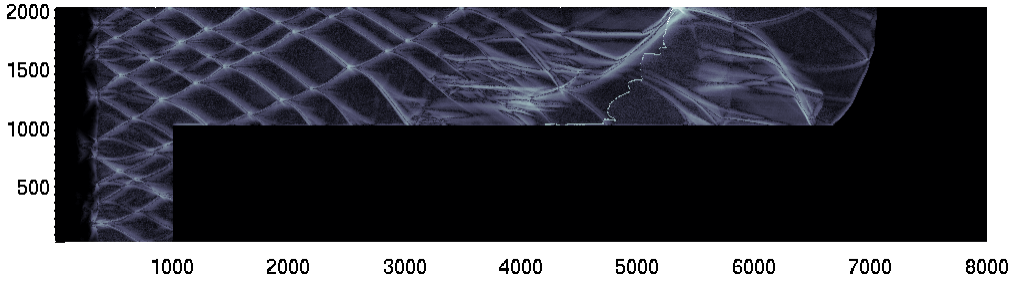

Figure 6.9: Numerical soot foil of a similar case with reactants bound by inert layer and solid wall, from Vågsæther, Gaathaug and Bjerketvedt [23].

partly due to lower hydrogen concentration closer to the interface caused by mass diffusion. The concentration effect was also observed by Boeck et al. [124] and Rudy et al. [103].

The expansion behind the oblique shock, see Figure 6.8, will also expand the products more close to the reactant/air interface. This will lead to a lower detonation velocity close to the interface. In Figure 6.3, the details of the detonation front is given. The lowest section of the reaction front has less illumination and could indicate a failed detonation and a resulting shock and deflagration propagating there. Further investigations of this limit phenomena is needed.

The work by Kuznetsov et al. [104] showed that a critical height of the partially confined layer of reactants had to be 13 times the detonation cell size to get DDT. This was investigated for stratified layers of hydrogen and air with obstacles, but the critical height was much higher than the layer investigated in this study. In this study the height of the reactant layer was about half the channel height, i.e. reactant height of ~ 5 cm. This gives a ratio of about 3.3 to 3.7 cell sizes. DDT was not observed in the reactant layer in this study, but in a nearer to homogeneous mixture made by the jet through the obstacle opening.

A failing detonation was observed in two experiments, but also a new onset near the interface between fuel-air and inert. The cause of this is unclear, and earlier work [125] presented a theory that it was a second DDT at the interface between inert and reactants. More recent numerical simulations of a similar but simplified case showed a similar phenomena. The work by Vaagsaether et al. [23] (see Appendix D.1) investigated the role of activation energy, and hence detonation front stability, for a detonation propagating in a layer of reactants above a layer of inert. The setup is dimensionless and set to a mesh resolution of 10 control volumes in the induction zone length. The details are given in the paper (see appendix D.1). The results are presented as numerical soot foils in Figure 6.9. The left side of the figure shows a detonation propagating towards the inert layer. All the wave patterns in the inert layer is removed to clarify the phenomena. The figure shows a pattern of triple point in the reactants which are expanded into the inert layer below. These triple point make up a cellular pattern which widens and “die” towards the top wall. There are also a merging of triple points at about 4000 control volumes in the horizontal direction. This could be similar to the experimental results shown in Figures 6.4 and 6.6. There is still however no conclusive explaination of the phenomena of a “dying” detonation and a “second onset”.

6.3 Conclusion

The conclusion is divided in two sections where the first section concludes on the main goal given in Chapter 1. The second conclusion regards the secondary goal to investigate detonation propagation in the reactant layer.

6.3.1 Investigate if inhomogeneous mixtures behind the obstacle influence the onset of detonation

The goal of this part of the study was to investigate if and possibly how the inhomogeneous mixtures influence the deflagration to detonation transition in the reactants behind the obstacle. Did inhomogeneous mixtures make it easier or harder to onset detonation?

The results of the limited experimental study showed no evidence of DDT occurring significantly closer to the obstacle than the homogeneous mixtures. In the experiments where DDT was observed it followed the same set of events as the homogeneous mixture experiments with local explosions and generation of transverse waves. DDT was observed when the concentration was $28\% H_2$ in air and higher and the Ignition Time Delay was below 10 s.

Due to the displacement of reactants no air pocket was observed right behind the obstacle, and the actual reactant composition in the section behind the obstacle is unknown.

6.3.2 Other concluding remarks of the inhomogeneous experiments

When the ITD was 9 s. a failing detonation in the reactant layer was observed, but a second onset at the reactant/air interface followed the failing detonation. This observation is important from a safety perspective as stratified layers of hydrogen and air would likely follow and accidental leakage of hydrogen. Ignition of the fuel/air cloud could lead to a detonation, and the mechanisms of detonations propagating in layers still needs further investigations. The study by Vaagsaether et al. [23] showed that a likely explanation of the new emerging detonation or second onset is due to an expanding detonation and merging of triple points close to the channel top wall. A part of this further investigation has been initiated by the author and co-workers as more knowledge is necessary to understand this phenomena.

Chapter 7

Simulations of DDT in hydrogen air

The aim of this study was to investigate numerically the same setup as was investigated experimentally. As shown previously in Chapter 4 it was hard to reproduce the same flame propagation in the first meter of the setup with a two dimensional approach. It was however interesting to find qualitatively similar results as the experimental investigation. These results has previously been published as "Experimental and numerical investigation of DDT in hydrogen-Air behind a single obstacle" in the International Journal of Hydrogen Energy in 2012.

This chapter includes selected numerical results and also a introductory study of the influence on different induction time models for the onset of detonation in the simulations. The two induction time models investigated were one by Sichel et al. [126] and one by del Alamo e. al. [127]

7.1 Numerical method

The numerical investigations were conducted with Vaagsaether's FLIC code, which is a flux limited centred TVD method. The specific details are given in the paper in appendix A.2, and a further detailed background on the method is provided by Toro [88] and Vaagsaether [12]. The development of this method is not included in this work.

FLIC solves the Euler equations with the ideal gas equation of state. The turbulence is solved by conserving the turbulent kinetic energy k, with sources and sinks [12]. The turbulence is only used for the turbulent burning velocity. The combustion model is a progress variable method where β is conserved and can represent a normalized concentration, see Equation 7.1. β varies between 1 and 0, where 0 is burnt gas and 1 is fresh gas.

$$\frac{\partial \rho \beta}{\partial t} + \bigtriangledown \cdot (\rho \vec{u} \beta) = \dot{\omega} \tag{7.1}$$

$$\frac{\partial \rho \alpha}{\partial t} + \bigtriangledown \cdot (\rho \vec{u} \alpha) = \dot{\vartheta} \tag{7.2}$$

Another progress variable, α, varies from 0 to 1 and represents the induction time, see Equation 7.2. The induction time variable is not connected to the conservation of energy, as

it is assumed that the induction reaction's heat of reaction is zero. The reaction rate $\dot{\omega}$ is a combination of a turbulence controlled rate and a chemical kinetic rate, see Equation 7.3.

$$\begin{aligned} \dot{\omega} &= max\left[\dot{\omega}_T, \dot{\omega}_k\right] \\ \dot{\omega}_T &= \rho_u S_T \sqrt{\left(\frac{\partial \beta}{\partial x}\right)^2 + \left(\frac{\partial \beta}{\partial y}\right)^2} \end{aligned} \tag{7.3}$$

The turbulent burning velocity S_T uses Flohr and Pitsch's model, Equation 7.4, [128]. This model includes a constant A set to 0.52.

$$\begin{aligned} S_T &= S_L\left(1 + A\frac{\sqrt{RePr}}{Da^{0.25}}\right) \\ Re &= \frac{\sqrt{k}l}{\nu} \\ Da &= \frac{S_L^2 l}{\sqrt{k}\kappa} \end{aligned} \tag{7.4}$$

Re and *Da* are the turbulent Reynolds and Damköhler numbers, respectively, where l is the turbulent length scale proportional to the grid size and κ is the thermal conductivity. Pr is the Prandtl number. The Iijima and Takeno [129] model for the laminar burning velocity S_L is used. The chemical kinetic rate is a two step model by Korobeinikov et al. [130] in which the first step has zero heat of reaction and the second step is exothermic. The model constants for the Korobeinikov model (Equation 7.6) is given in Table 7.1.

$$\dot{\vartheta} = f(p,T) = \frac{\rho}{\tau} \tag{7.5}$$

Table 7.1: Model constants

A_β	$1.05 * 10^{-5}[s^{-1}Pa^{-2}]$
$T_{a,\beta}$	$2000[K]$
A_α	$6.2335 * 10^{10}[PaK^{-1}s]$
B_α	$35.1715[-]$
C_α	$8530.6[K]$
D_α	$7.22 * 10^{-11}[-]$
$T_{a,\alpha}$	$21205[K]$

$$\dot{\omega}_k = \begin{cases} 0 & \text{if } \alpha < 0 \\ \rho\left(A_\beta p^2 \beta^2 e^{\left[-\frac{T_{\alpha\beta}}{T}\right]} - A_\beta p^2 (1-\beta)^2 e^{\left[-\frac{T_{\alpha\beta}}{T} + \frac{q}{RT}\right]}\right) & \text{if } \alpha = 0 \end{cases} \tag{7.6}$$

The present work uses two induction time models for $\dot{\vartheta}$, see Equations 7.5, 7.7 and 7.8. One model was presented by Sichel et al. [31] and the other by del Alamo et al. [127]. The Sichel model is an experimental fit while the DelAlamo is theoretically derived from detail chemistry.

$$\tau_{Sich} = A_\alpha \frac{T}{p}\left[-B_\alpha + \frac{C_\alpha}{T} + D_\alpha\left(\frac{p}{p_{atm}}\right)^2 exp\left[\frac{T_{a,\alpha}}{T}\right]\right] \tag{7.7}$$

$$\tau_{delAlamo} = \frac{1}{c_{O_2}(2k_1 - k_{10}c_M)} ln\left[(2k_1 - k_{10}c_M)\frac{c_{H_2}k_2k_3}{2c_{O_2}k_1k_{12b}}\right] \tag{7.8}$$

The model constants for the del Alamo model are given in [127], and the constants for the Sichel model is given in Table 7.1.

Two step kinetics is selected for the modelling of DDT and detonations. If the unburned mixture is sufficiently heated and/or compressed, then the induction time progress variable will increas. And when α reaches 1, the exothermic reaction starts. It is important to model the induction time for detonations, since the detonation wave consists of shock compression and a subsequent reaction zone. The author would like to mention that detonations and DDT have also been studied successfully with one step chemical kinetics in cases where the spatial resolution is high [131]. The spatial resolution of the present work is assumed to be too coarse for one step kinetics [12].

7.2 Numerical setup

The geometry of the numerical setup was similar to that of the experimental setup. The domain had to be simplified to 2D due to computational recourses. It was 3 m in length, with solid reflecting top and bottom boundaries. The outlet was a zero gradient boundary. The internal geometry (i.e., the obstacle) was solid and reflecting. The initial conditions and parameters are listed in Table 7.2. The subscripts u and b refer to unburned and burned. A relatively coarse mesh of 0.5 mm in 2D was chosen due to computational time and resource constraints. This gave a total of 1.2 million cells, and calculated on a single-core setup resulted in a CPU time of about 3 days for the run up (flame propagation in the first meter of the channel), and about 20 hours from obstacle to end of the channel.

7.3 Numerical results

As stated earlier, the scope of this paper focuses on DDT in the flow and the reactions behind the obstacle. However, the numerical simulation included the entire channel geometry and time from ignition until all reactants were burned. Only the results from behind the obstacle is presented in this chapter.

The numerical results were visualized using numerical schlieren-like frames (H). These were calculated from the density field at a single time instance, using Equation 7.9.

$$H = |\nabla\rho| \cdot exp\left[-25\frac{|\nabla\rho|}{|\nabla\rho|_{max}}\right] \tag{7.9}$$

Results for a section of the channel starting from the obstacle, from one numerical simulation with BR = 0.84 and H2 conc. 35% are shown in Figure 7.1. As the flame propagated through the

Table 7.2: Parameters for the numerical simulation.

Symbol	Parameter	30% H2	35% H2
$M_{w,u}$	Unburned Molecular weight [kg/mol]	$20.9 * 10^{-3}$	$19.5 * 10^{-3}$
$M_{w,b}$	Burned Molecular weight [kg/mol]	$24.1 * 10^{-3}$	$22.4 * 10^{-3}$
ρ_0	Initial density [kg/m3]	0.85	0.8
γ_u	Unburned adiabatic index [-]	1.4	1.4
γ_b	Burned adiabatic index [-]	1.242	1.243
q	Change of enthalpy of reactants [J/kg]	$3.01 * 10^6$	$3.21 * 10^6$
p_0	Initial pressure [Pa]	$1 * 10^5$	
$u_x = u_y$	Initial velocity [m/s]	0	
α_0	Initial induction progress variable [-]	0	
β_0	Initial reaction progress variable (except ignition) [-]	0	
dx	Size of computational cell [mm]	0.5	

obstacle it became elongated. There was a thin layer between the flame and the wall in which several small local explosions were seen. The first explosion was seen at time 14.121 ms, and it was followed by several small local explosions occurring in the volume between the walls and the flame. At time 15.165 ms and 15.865 ms a fast reaction wave propagated in the bottom layer, and an oblique shock wave reflected at the top wall; this in turn started a fast reaction wave at the top wall (17.794 ms). The last two frames show a detonation.

Figure 7.2 shows an x-t plot of $\frac{\frac{\partial p}{\partial x}}{\frac{\partial p}{\partial x}_{max}}$ along the bottom wall, where x is the length axis of the channel. The figure can be interpreted as a numerical streak-schlieren images at the bottom wall, for simulations where BR = 0.75 and 35% H2. First the constant velocity line originating from 500 mm at t = 0 ms is a shock propagating through the channel far ahead of the flame, it is not very strong but has a sharp gradient. This wave is produced when the flame propagate in the first meter of the setup. Two cases with two different induction models are presented in Figure 7.2; one developed into a detonation while the other did not. The two cases used the same run up before the obstacle, but compared different induction models (del Alamo and Sichel) for the process behind the obstacle. There were many local explosions in both cases. The del Alamo model simulations exploded earlier than the Sichel model simulations. Also, for a given setup, the del Alamo simulations developed into a detonation while the Sichel model did not. The left image in Figure 7.2 shows, among several smaller, three local explosions that failed to develop into a detonation, at 300 mm (1.3 ms), 500 mm (1.42 ms), and 650 mm (1.5 ms) behind the obstacle. In the right hand side image there are explosions at 250 mm and (1.0 ms), and one at about 450 mm (time 1.1 ms). The last one develops into a detonation. Similar behaviours were observed in other cases of detonation failure or success.

In the simulated cases where DDT was not observed, there were still local explosions in the layer between the flame and the walls. However, this did not develop into a detonation.

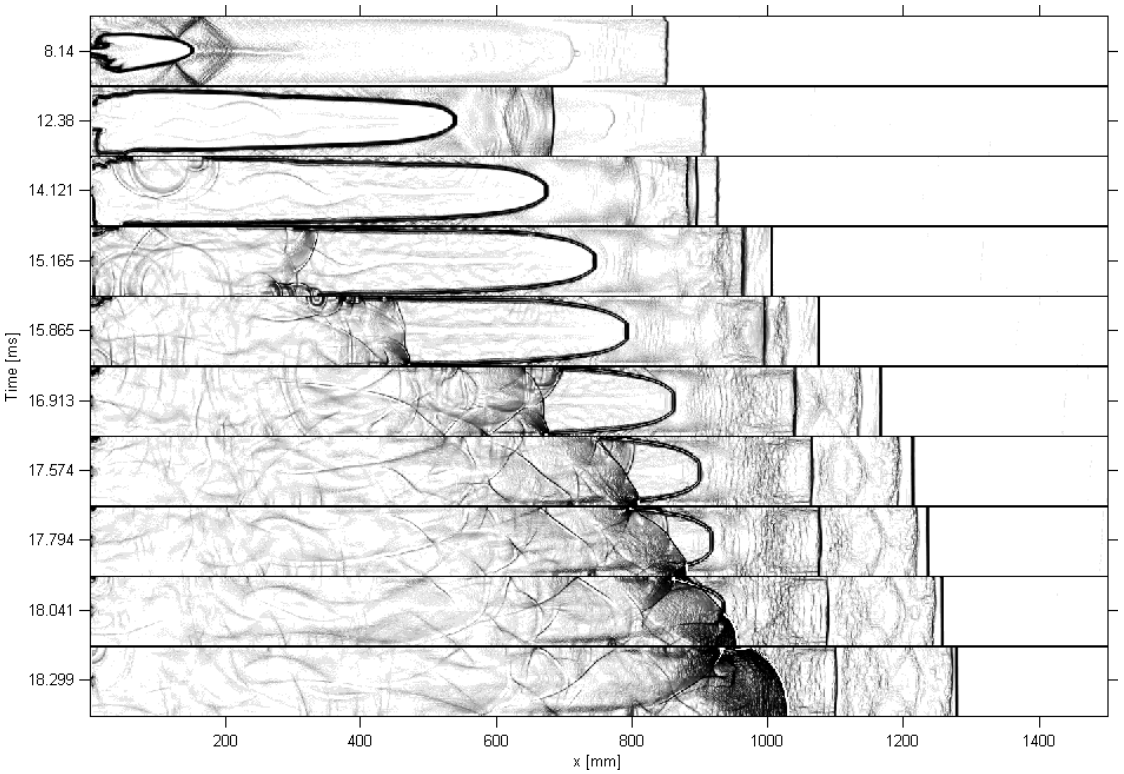

Figure 7.1: Numerical schlieren pictures from the simulation with $BR = 0.84$ and $35\% H_2$ in air. This result is from a simulation using the DelAlamo model.

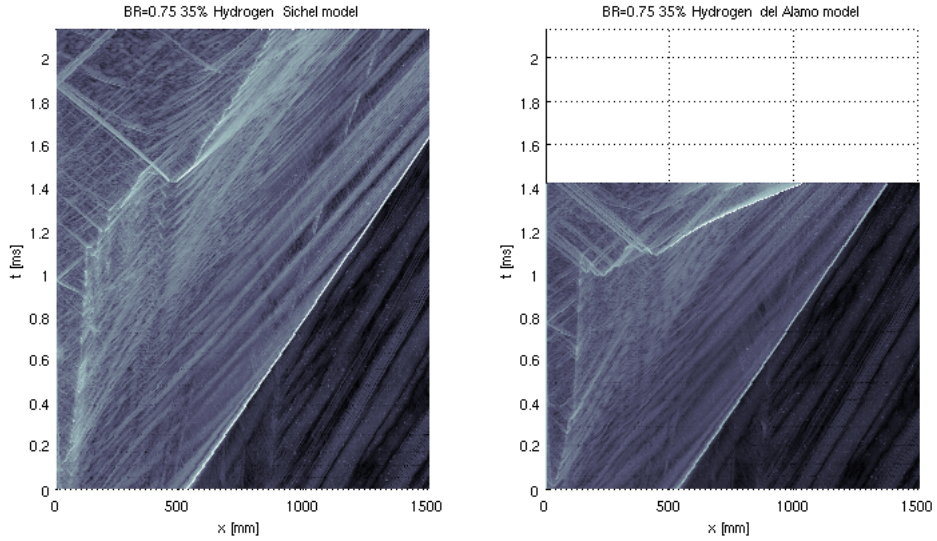

Figure 7.2: Numerical simulation results of the normalized pressure gradient along the top wall

7.4 Discussion

Within the numerical simulations, local explosions can be described using the induction progress variable α that reaches α=1 in one cell, thus initiating the exothermic reaction. The relatively high temperatures in the layer between the wall and the flame are caused by the mixing of products and reactants, which leads to a reduced induction time. Another likely cause to the local explosion or hot spot is shock compression. These local explosions usually develop in a gradient of β, but at the "cold side". In this flame front gradient, the induction time variable α reaches 1 and then the kinetic (much faster) mechanism takes over the turbulent mechanism, see Equation 7.3. A high reaction rate follows and could result in a shock wave. Shock compression of the neighboring cells could in turn result in the onset of detonation. Some of these explosions were observed in isolated islands of reactants or in too narrow layers of reactants with no detonation seen, but several explosions were observed and they "added up" and eventually lead to a detonation. Interactions between the top and bottom wall explosions were observed in simulations which lead to detonation. The detonations originated from the layer between the flame front and the walls, and fast accelerating waves were observed in these layers. Local explosions were also seen in simulations which did not detonate, and there were fast reaction waves (It is hard to categorize these waves as either detonation or deflagration) in the layer between the flame and the wall. The waves died out however because they were too weak or occurred in layers which were too narrow or did not have the top/bottom wall interaction. Some fast reaction waves in the layers stopped because they occurred in isolated pockets of reactants.

The experimental study in Chapter 5 showed some pressure waves recorded at the first transducer behind the obstacle prior to DDT. Usually there was one stronger wave and several smaller variations in pressure, which were still larger than the recorded noise. These could originate from small explosions similar to those seen in the simulations. The waves were also seen in experiments without DDT, but they could have been too weak to result in the onset of detonation. Oran [53] pointed out that high speed reactive flows are very sensitive to minute changes; this is why we can see a detonation in some experiments and no detonation the next time.

A more detailed study of the phenomenon is required to draw further conclusions. This should also include a full three dimensional simulation of the setup.

A bright layer along the bottom wall seen on the high speed film was common to all experiments with DDT and near the DDT limits (Figure 5.13). One could speculate that this is similar to the fast reaction wave seen in the simulations. The study of detonations in layers could be similar to the study by Dabora et al. [132] in which they studied detonations bounded by a wall and a compressible layer. They concluded that the velocity loss due to the expanding compressible layer could cause failure to propagate as a detonation. This loss was dependent on the density ratio of the gases used. As seen in the simulations, there is an oblique shock behind the fast reaction wave in the layer between the flame and the wall, which is similar to the case by Dabora et al. [132].

There is an obvious limitation to the 2D approximation used in the simulations, as the influence of corners is not considered in the simulations. The results from Chapter 4 shows that the run up and flame propagation through the obstacle is three-dimensional. Buoyancy effects and non-uniform concentrations behind the obstacle were also not included. The influence and

validity of the induction models should also be investigated further.

7.5 Summary

- Simulations of DDT in hydrogen air mixtures were performed, using a grid size $\Delta x = 0.5$ mm.
- Two different induction time models were tested and they gave different results.
- DDT was observed in the simulations at the walls between 1200 mm and 2000 mm from the ignition end (200 mm and 1000 mm behind obstacle).
- Local explosions far behind the leading edge of the flame were observed in simulations . These explosions initiated the process of DDT. The simulations showed that the explosions occurred in a layer between the flame and the walls.
- Several local explosions followed the first, and the fast reaction wave propagated along the walls and resulted in DDT in some simulations. In other simulations DDT was not observed; there were local explosions but the fast reaction wave died after several attempts. In some simulations the fast reaction wave accelerated in an isolated layer of reactants, where the wave died as it ran out of fresh combustible gas.
- The local explosions must have sufficient strength and must propagate in a layer of sufficient height. The blast (pressure wave) from an explosion at one wall can initiate a new explosion at the other wall.

Chapter 8

Conclusions

The conclusions are presented in the same order as the flame in Figure 8.1 and follow the main goals of the study as given in Chapter 1.

8.1 From ignition up to obstacle

This work is presented in the paper "Experiments with Flame Propagation in a channel with a Single Obstacle and Premixed Stoichiometric H_2-air' [114]'. The aim of the study was to investigate the shape of the flame front by using a line ignition and point ignition source. The line ignition was assumed to produce a two dimensional flame front as the ignition was almost invariant in the direction normal to the view. This was also backed by the shape of the obstacle which was also invariant in the same direction. Both ignition sources produced pressure waves propagating in the channel and reflecting at the obstacle and the closed ignition end. These pressure waves correspond with the times of flame front stagnation and inversion or tulip front formation. This flame front inversion was observed several times in this study. The same phenomena has later been reported by Xiao et al. [51] and called the distorted tulip flame. The coincidence with the tulip shape formation and the pressure waves gives a good argument for the baroclinic effect on the tulip flame formation. The flame front did not change back to its initial shape.

The other main conclusion from the study was that the flame could only be assumed to be two dimensional by using the line ignition and only up to the point where it changes to inverted flame front. After that the flame front is variant in all directions. This is important for the assumptions or simplifications of 2D numerical investigations of these deflagrations.

The flame propagation through the obstacle was also investigated and showed that the actual

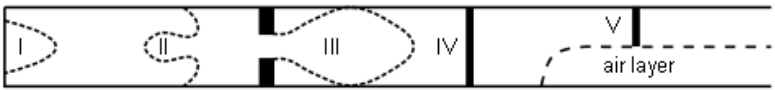

Figure 8.1: A sketch of the experimental setup.

shape of the flame as it propagated through the obstacle was quite complex and probably only possible to simulate if the flame front propagation up to the obstacle was nearly identical to the experiment.

8.2 The onset of detonation

The run up distance behind the obstacle is reported and shown to slightly decrease with increased hydrogen concentration. A concentration of 28% hydrogen in air, which is slightly lean, was found to be the limit of DDT in this particular experimental setup. All experiments showed that the onset of detonation occurred at the walls, mostly at the top wall. This was also seen in the numerical investigations in the paper "Experimental and numerical investigation of DDT in hydrogen-Air behind a single obstacle" [121]. High speed schlieren photography [21] also showed that DDT occurred at the walls, following an oblique shock wave reflection.

The criteria proposed by Knudsen [34] was also valid for the square setup when the geometry was scaled properly.

8.3 Local explosions behind the front

The schlieren photography, the pressure records and the numerical investigations all show that there are transverse waves in the channel prior to the onset of detonation. This was in good agreement with Chao [59] and Radulescu [101]. This study has shown that these waves originate from local explosions relatively far behind the leading edge of the flame front. The numerical investigation show that there were many local explosions, while the experimental study showed that there were at least one before DDT was observed. The local explosions occurred in layers of reactants between the flame and the wall. An explosion sends pressure waves propagating in the channel and might onset other explosions (hot spots) which in turn lead to onset of detonation.

8.4 Inhomogeneous gas mixtures

A layer of hydrogen-air on top of an inert layer of air was produced in the channel. This setup was investigated to see if it would influence DDT in the channel. Because of the displacement of reactants through the obstacle opening there was no effect on DDT in this particular setup. The same $28\% H_2$ in air limit still applied, while the maximum time air was able to flow into the channel (while still achieving DDT) was 9 seconds.

There were other interesting results from the study on inhomogeneous gas mixtures, as the detonation propagated in the layer of reactants on top of the inert. In some cases the detonation failed only to start again. This was first speculated to be a second onset of detonation at the interface between reactants and inert, while more recent numerical results showed that it might be caused by a widening effect on the cellular pattern and a merging of weak triple points to continue the propagation of the detonation.

8.5 Produce experimental results for validation

The combined work in this thesis is a collection of data for validation of numerical methods. There is a large set of data with combined flame position, velocity and pressure records. The novelty of the data are given by the large spacial size of the data, where many experimental results are given for ranges of more than 1 meter and combined with pressure records. When ever it is possible it is therefore important to relate both the pressure and the velocity and also the shape of the reaction fronts for a correct reproduction by numerical simulations. The experimental results are also conducted at atmospheric conditions which are most relevant for safety studies and modeling of realistic scenarios.

The two dimensional simulation of the deflagration to detonation transition behind the obstacle, did not exactly reproduce the experimental shape, velocity and pressure. It did however show very similar qualitatively results with local explosions and transverse waves in the channel. The lack of reproduction is however in good agreement with the first conclusion of this work (see Section 8.1).

Bibliography

[1] C.K. Law. *Combustion Physics*. Cambridge University Press, New York, 2006.

[2] G. Ciccarelli and S.B. Dorofeev. Flame acceleration and transition to detonation in ducts. *Progress in Energy and Combustion Science*, 34(4):499–550, August 2008.

[3] C.K. Law. Propagation, structure, and limit phenomena of laminar flames at elevated pressures. *Combustion Science and Technology*, 178(April 2013):335–360, 2006.

[4] K. Rai, D. Bjerketvedt, and O.K. Sommersel. Experimental study of the initial flame propagation of premixed H 2 -air explosion in a channel . In *International Colloquium on the Dynamics of Explosions and Reactive Systems*, number 1, pages 4–7, 2009.

[5] J. Oakley. Rayleigh-Taylor Instability Notes, 2004.

[6] G.H. Markstein. A shock-tube study of flame front-pressure wave interaction. In *6th. Symposium (International) on Combustion*, pages 387–398, 1957.

[7] M. Gonzalez, R. Borghi, and a. Saouab. Interaction of a flame front with its self-generated flow in an enclosure: The "tulip flame" phenomenon. *Combustion and Flame*, 88(2):201–220, February 1992.

[8] D. Dunn-Rankin and R.F. Sawyer. Tulip flames: changes in shape of premixed flames propagating in closed tubes. *Experiments in Fluids*, 24(2):130–140, February 1998.

[9] S.B. Dorofeev, M.S. Kuznetsov, V.I. Alekseev, A.A. Efimenko, and W. Breitung. Evaluation of limits for effective flame acceleration in hydrogen mixtures. *Journal of Loss Prevention in the Process Industries*, 14(6):583–589, November 2001.

[10] Jerzy Chomiak. *Combustion: A Study in Theory, Fact and Application (Energy & Engineering Sciences)*. Taylor & Francis Ltd, 1987.

[11] J. Warnatz, U. Maas, and R.W. Dibble. *Combustion: Physical and Chemical Fundamentals, Modeling and Simulation, Experiments, Pollutant Formation*. Springer-Verlag, Berlin Heidelberg, 3rd. edition, 2001.

[12] K. Vaagsaether. *Modelling of Gas Explosions*. PhD thesis, Telemark University College – NTNU, Norway, 2010.

[13] S.B. Dorofeev, V.P. Sidorov, M.S. Kuznetsov, I.D. Matsukov, and V.I. Alekseev. Effect of scale on the onset of detonations. *Shock Waves*, 10(2):137–149, May 2000.

[14] R. Knystautas, J.H.S. Lee, I.O. Moen, and H.Gg. Wagner. Direct initiation of speherical Detonation by a Hot Turbulent Gas Jet. In *17th Symp. (Int.) on Combustion*, pages 1235–1245, 1979.

[15] I.O. Moen, D. Bjerketvedt, T. Engebretsen, A. Jenssen, B.H. Hjertager, and J.R. Bakke. Transition to detonation in a flame jet. *Combustion and Flame*, 75(3-4):297–308, March 1989.

[16] H.D. Ng, A Higgins, C Kiyanda, M Radulescu, J.H.S. Lee, and K Bates. Nonlinear dynamics and chaos analysis of one-dimensional pulsating detonations. *Combustion Theory and Modelling*, 9(1):159–170, 2005.

[17] I.O. Moen, A. Sulmistras, G.O. Thomas, D. Bjerketvedt, and P.A. Thibault. Influence of Cellular Regularity on the Behavior of Gaseous Detonations. *Progress in Astronautics and Aeronautics*, 106:220–243, 1986.

[18] H.I. Lee and D.S. Stewart. Calculation of linear detonation instability : one-dimensional instability of plane detonation. *Journal of fluid mechanics*, 216:103–132, 1990.

[19] W.P Sommers. *The Interaction of a Detonation Wave with an Inert Boundary*. PhD thesis, 1961.

[20] J.E. Shepherd. Detonation Database, 2005.

[21] L. Bjarnason. *Experimental investigation of hydrogen-air explosions with a schlieren set-up*. PhD thesis, Telemark University College, 2013.

[22] E. Dabora. The Influence of a Compressible Boundary on the Propagation of Gaseous Detonations. Technical report, University of Michigan, College of Engineering, Department of Aeronautical and Astronautical Engineering, Aircraft Propulsion Laboratory, 1963.

[23] K. Vaagsaether, A.V. Gaathaug, and D. Bjerketvedt. Detonation propagation in a reactive layer; the role of detonation front stability. In *International Symposium on Hazard, Prevention and Mitigation of Industrial Explosions*, number June, 2014.

[24] J.E. Shepherd. Detonation in gases. *Proceedings of the Combustion Institute*, 32(1):83–98, 2009.

[25] Peter O. K. Krehl. *History of Shock Waves, Explosions and Impact: A Chronological and Biographical Reference*. Springer, 2009.

[26] D.M. Johnson, G.B. Tomlin, and D.G. Walker. Journal of Loss Prevention in the Process Industries Detonations and vapor cloud explosions : Why it matters. *Journal of Loss Prevention in the Process Industries*, pages 1–7, 2015.

[27] B.A. Burgan. Dispersion & Explosion Characteristics of Large Vapour Clouds. Technical report, 2014.

[28] D.S. Burgess and M.G. Zabetakis. Detonation of a flammable cloud following a propane pipeline break: the December 9, 1970, explosion in Port Hudson, Mo. Technical report, US Bureau of Mines, January 1973.

[29] D. Bjerketvedt and A. Mjaavatten. A hydrogen-air explosion in a process plant: a case history, 2005.

[30] D. Bradley, G.A. Chamberlain, and D.D. Drysdale. Large vapour cloud explosions, with particular reference to that at Buncefield. *Philosophical transactions. Series A, Mathematical, physical, and engineering sciences*, 370(1960):544–66, February 2012.

[31] M. Johnson, B.G. Tomlin, and D.G. Walker. Detonations and Vapour Cloud Explosions : Why it Matters. In *International Symposium on Hazard, Prevention and Mitigation of Industrial Explosions*, number June, pages 19–30, 2014.

[32] Takashi Tsuruda. Hydrogen Explosion Hazards in Degraded Core Accidents in Nuclear Power Plants. In D. Bradley, G.M. Makhviladze, V. Molkov, P. Sunderland, and F. Tamanini, editors, *Proceedings of the Seventh International Seminar on Fire and Explosion Hazards*, pages 8–15. Research Publishing, 2013.

[33] IAEA. Mitigation of Hydrogen Hazards in Nuclear Power Plants. Technical report, 2011.

[34] V. Knudsen. *Hydrogen gas explosions in pipelines - modeling and experimental investigations*. PhD thesis, Telemark University College/NTNU, 2006.

[35] L. Landau. On the Theory of Slow Combustion. *Acta Physicochimica U.R.S.S.*, 19(1):76–85, 1944.

[36] L. Rayleigh. On the stability or instability of certain fluid motions. *Proc. R. Soc. Lond. Ser*, 13:5–12, 1895.

[37] G. Sir Taylor. The instability of liquid surfaces when accelerated in a direction perpendicular to their planes. *Proceedings of the Royal Society A: Mathematical, Physical and Engineering Sciences*, 201(1065):192–196, 1949.

[38] R.D. Richtmyer. Taylor instability in shock acceleration of compressible fluids. Technical report, Los alamos Scientific Laboratory of the University of California, 1954.

[39] E. E. Meshkov. Instability of the interface of two gases accelerated by a shock wave. *Fluid Dynamics*, 4(5):101–104, 1972.

[40] H.v. Helmholtz. On the discontinuous movements of fluids. *Monthly Reports of the Royal Prussian Academy of Philosophy in Berlin*, 23:215–228, 1868.

[41] H.W. Thompson. Hydrokinetic solutions and observations. *Philosophical Magazine*, 42:362–377, 1871.

[42] E. Mallard and H. Le Chatelier. On the Propagation Velocity of Burning in Gaseous Explosive Mixtures. *Comptes Rendus Hebdomadaires des Seances de l Academie des Sciences*, 93:145–148, 1881.

[43] O.C. Ellis and H.A. Robinson. New method of flame analysis. *Journal of the chemical society*, 127:760–767, 1925.

[44] G.D. Salamandra, T.V. Bazhenova, and I.M. Naboko. Formation of detonation wave during combustion of gas in combustible tube. *Proceedings of the Combustion Institute*, 7:851–855, 1958.

[45] C. Clanet and G. Searby. On the "Tulip Flame" Phenomenon. *Combustion and Flame*, 105(95):225–238, 1996.

[46] T. Kratzel, E. Pantow, and M. Fischer. On the transition from a highly turbulent curved flame into a tulip flame. *International Journal of Hydrogen Energy*, 23(1):45–51, 1998.

[47] D. Dunn-Rankin. Tulip flames: The shape of deflagrations in closed tubes. In J. Jarosinski and B. Veyssiere, editors, *Combustion Phenomena, Selected Mechanisms of Flame Formation, Propagation, and Extinction*. CRC Press, New York, 1 edition, 2009.

[48] P. Metzener and M. Matalon. Premixed flames in closed cylindrical tubes. *Combustion Theory and Modelling*, 5:463–483, 2006.

[49] A.K. Kaltayev, U.R. Riedel, and J. Warnatz. The Hydrodynamic Structure of a Methane-Air Tulip Flame. *Combustion Science and Technology*, 158:53–69, 2000.

[50] H. Xiao, Q. Wang, X. He, J. Sun, and X. Shen. Experimental study on the behaviors and shape changes of premixed hydrogen–air flames propagating in horizontal duct. *International Journal of Hydrogen Energy*, 36(10):6325–6336, May 2011.

[51] H. Xiao, D.V. Makarov, J. Sun, and V. Molkov. Experimental and numerical investigation of premixed flame propagation with distorted tulip shape in a closed duct. *Combustion and Flame*, 159(4):1523–1538, April 2012.

[52] S.B. Dorofeev. Flame acceleration and explosion safety applications. *Proceedings of the Combustion Institute*, 33(2):2161–2175, January 2011.

[53] E.S. Oran. Turbulence and Stochasticity in High-Speed Reactive Flows. In *Proceeding of the Sixth International Conference on Fluid Mechanics*, 2011.

[54] G.O. Thomas. Some observations on the initiation and onset of detonation. *Philosophical transactions. Series A, Mathematical, physical, and engineering sciences*, 370(1960):715–39, February 2012.

[55] P.A. Urtiew and A.K. Oppenheim. Experimental observations of the transition to detonation in an explosive gas. *Proc. R. Soc. Lond. Ser*, 195(A):13–28, 1966.

[56] J.W. Meyer, P.A. Urtiew, and A.K. Oppenheim. On the inadequacy of gasdynamic processes for triggering the transition to detonation. *Combustion and Flame*, 14(1):13–20, February 1970.

[57] O. Peraldi, R. Knystautas, and J.H.S. Lee. Criteria for transition to detonation in tubes. 21:1629–1637, 1986.

[58] R.P. Lindstedt and H.J. Michels. Deflagration to Detonation Transition and strong Deflagrations in Alkane and Alkene Air Mixtures. 76:169–181, 1989.

[59] J. Chao. *Critical Deflagration Waves that Lead to the Onset of Detonation*. PhD thesis, McGill University, 2006.

[60] J.H.S. Lee and I.O. Moen. The Mechanism of transition From Deflagration to Detonation in Vapour Cloud Explosions. *Progress in Energy and Combustion Science*, 6:359–389, 1980.

[61] J.H.S. Lee, R. Knystautas, and C.K. Chan. Turbulent flame propagation in obstacle-filled tubes. *Twentieth Symposium (international) on Combustion*, pages 1663–1672, 1984.

[62] A. Teodorczyk, J.H.S. Lee, and R. Knystautas. Propagation mechanism of quasi-detonations. *Symposium (International) on Combustion*, 22(1):1723–1731, 1988.

[63] A. Teodorczyk. The structure of fast turbulent flames in very rough, obstacle-filled channels. *Symposium (International) on Combustion*, 23(1):735–741, 1991.

[64] A. Teodorczyk. Scale effects on hydrogen–air fast deflagrations and detonations in small obstructed channels. *Journal of Loss Prevention in the Process Industries*, 21(2):147–153, March 2008.

[65] S.M. Frolov. Acceleration of the deflagration-to-detonation transition in gases: From Shchelkin to our days. *Combustion, Explosion, and Shock Waves*, 48(3):258–268, July 2012.

[66] C.K. Chan. Collision of a shock wave with obstacles in a combustible mixture. *Combustion and Flame*, 100(1-2):341–348, January 1995.

[67] V.N. Gamezo, T. Ogawa, and E.S. Oran. Numerical simulations of flame propagation and DDT in obstructed channels filled with hydrogen–air mixture. *Proceedings of the Combustion Institute*, 31(2):2463–2471, January 2007.

[68] Explosion Dynamics Laborotory. EDL Shock and Detonation Toolbox.

[69] M.P. Sherman, Tieszen. S.R., and W.B. Benedick. FLAME Facility - The Effect of Obstacles and transverse Venting on Flame Acceleration and transition to Detonation for Hydrogen-air Mixtures at Large Scale. Technical report, Sandia National Laboratories, Albuquerque, 1989.

[70] C.K. Chan and W.a. Dewit. Deflagration-to-detonation transition in end gases. *Symposium (International) on Combustion*, 26(2):2679–2684, January 1996.

[71] G. Ciccarelli and J.L. Boccio. Detonation wave propagation through a single orifice plate in a circular tube. *Symposium (International) on Combustion*, 27(2):2233–2239, January 1998.

[72] M.S. Kuznetsov, V.I. Alekseev, and S.B. Dorofeev. Comparison of critical conditions for DDT in regular and irregular cellular detonation systems. In *Proceedings of the 22nd ISSW*, page 180, London, 1999.

[73] A.I. Gavrikov, A.A. Efimenko, and S.B. Dorofeev. A model for detonation cell size prediction from chemical kinetics. *Combustion and Flame*, 120(1-2):19–33, January 2000.

[74] G.O. Thomas and A. Jones. Some observations of the jet initiation of detonation. *Combustion and Flame*, 120(3):392–398, February 2000.

[75] R.K. Eckhoff, K. Fuhre, O. Krest, C.M. Guirao, and J.H.S. Lee. Some recent large scale gas explosion experiments in Norway. Technical report, The Chr. Michelsen Institute, Bergen, 1980.

[76] V.V. Mitrofanov and Soloukhin R.I. The diffraction of multifront detonation waves. *Sovjet Physics*, 9(12):1055, 1965.

[77] R. Knystautas, J.H.S. Lee, and C.M. Guirao. The critical tube diameter for detonation failure in hydrocarbon-air mixtures. *Combustion and Flame*, 48:63–83, January 1982.

[78] D.J. Mackay, S.B. Murray, I.O. Moen, and P.A. Thibault. Flame-Jet Ignition of Large Fuel-Air Clouds. *Proceeding of the Twenty-Second International Conference on Combustion*, pages 1339–1353, 1988.

[79] A. Ungut and P.J. Shuff. Deflagration to Detonation transition from a Venting Pipe. *Combustion Science and Technology*, 63:75–87, 1989.

[80] M. Berthelot and P. Vielle. On Explosive Waves. *Comptes Rendus Hebdomadaires des Seances de l Academie des Sciences*, 94:149–152, 1882.

[81] W.J.M Rankine. On the thermodynamic theory of waves of finite longitudinal disturbance. *Philosophical Transactions of the Royal Society*, 160:277–288, 1870.

[82] P.H. Hugoniot. Sur la propagation du mouvement dans les corps et spécialement dans les. *Journal de l'École Polytechnique*, 57:3–97, 1887.

[83] P.H. Hugoniot. Mémoire sur la propagation des mouvements dans les corps et spécialement dans les gaz parfaits (deuxième partie). *Journal de l'École Polytechnique*, 58:1–125, 1889.

[84] D.L. Chapman. On the Rate of Explosion in Gases. *Philos. Mag*, 47:90–104, 1899.

[85] E Jouguet. On the Propagation of Chemical Reactions in Gases. *Journal de Mathématiques Pures et Appliquées*, 1:347–425, 1905.

[86] J.H.S. Lee. *The Detonation Phenomenon*. Cambridge University Press, 2008.

[87] W. Fickett and W.C. Davis. *Detonation: Theory and Experiment (Dover Books on Physics)*. Dover Publications Inc., 2003.

[88] Eleuterio F. Toro. *Riemann Solvers and Numerical Methods for Fluid Dynamics: A Practical Introduction*. Springer, 2010.

[89] Ya.B. Zel'dovich. On the theory of the propagation of detonations on gaseous system. *Journal of Experimental and Theoretical Physics*, 10:542–568, 1940.

[90] W. Döring. Über Detonationsvorgang in Gasen [On detonation processes in gases]. *Annals of Physics*, 1943.

[91] J.H.S. Lee. Plenary – Comment on Detonations in Accidental Explosions. In *International Seminar on Fire and Explosion Hazards*, pages 3–7, 2013.

[92] F. Zhang. *Shock Waves Science and Technology Library, Vol. 6: Detonation Dynamics*. Springer, 2012.

[93] R.A. Strehlow. Detonation and the hydrodynamics of reactive shock waves, 1963.

[94] S.B. Murray. *The influence of initial and boundary conditions on gaseous Detonation waves*. PhD thesis, McGill university, 1985.

[95] J.E. Shepherd, I.O. Moen, and S.B. Murray. Analyses of the cellular structure of detonations. *Twenty-first Symposium on Combustion(int.)*, page 1649, 1986.

[96] J.M. Austin, F. Pintgen, and J.E. Shepherd. Reaction zones in highly unstable detonations. *Proceedings of the Combustion Institute*, 30(2):1849–1857, January 2005.

[97] E.S. Oran, T.R. Young, J.P. Boris, J.M. Picone, and D.H. Edwards. A study of detonation structure: The formation of unreacted gas pockets. In *Ninetheenth Symposium (International) on Combustion*, pages 573–582, 1982.

[98] R. Guirguis, E.S. Oran, and K. Kailasanath. Numerical Simulations of the Cellular Structure of Detonations in Liquid NitromethanemRegularity of the Cell Structure. *Combustion and Flame*, 365:339–365, 1986.

[99] V.N. Gamezo, D. Desbordes, and E.S. Oran. Formation and evolution of two-dimensional cellular detonations. *Combustion and Flame*, 116(1-2):154–165, January 1999.

[100] F. Ettner, K.G. Vollmer, and T. Sattelmayer. Simulating Deflagrations and Detonations with Detailed Chemistry. In *International Colloquium on the Dynamics of Explosions and Reactive Systems*, number 1, pages 1–4, 2009.

[101] M.I. Radulescu, G.J. Sharpe, and D. Bradley. A Universal Parameter Quantifying Explosion Hazards , Detonability and Hot Spot Formation : the χ Number. In *International Seminar on Fire and Explosion Hazards*, pages 617–626, 2013.

[102] F.A. Williams. *Combustion theory*. The Benjamin/Cummings Publishing Company, Inc, Menlo Park, California, 2nd edition, 1982.

[103] W. Rudy, M.S. Kuznetsov, R. Porowski, a. Teodorczyk, J. Grune, and K. Sempert. Critical conditions of hydrogen-air detonation in partially confined geometry. *Proceedings of the Combustion Institute*, 34(2):1965–1972, January 2013.

[104] M.S. Kuznetsov, J. Grune, A. Friedrich, K. Sempert, W. Breitung, and T. Jordan. Hydrogen-Air Deflagrations and Detonations in a Semi-Confined Flat Layer. In *Sixth International Seminar on Fire and Explosion Hazards*, pages 978–981, 2011.

[105] J. Grune, K. Sempert, H. Haberstroh, M.S. Kuznetsov, and T. Jordan. Experimental investigation of hydrogen–air deflagrations and detonations in semi-confined flat layers. *Journal of Loss Prevention in the Process Industries*, pages 7–13, October 2011.

[106] L.R. Boeck. Personal communication.

[107] O.K. Sommersel, D. Bjerketvedt, K. Vaagsaether, and T.K. Fannelop. Experiments with release and ignition of hydrogen gas in a 3m long channel. *International Journal of Hydrogen Energy*, 34(14):5869–5874, July 2009.

[108] G.S. Settles. *Schlieren & Shadowgraph Techniques*. Springer; Corrected edition, 2006.

[109] D.G. Goodwin. Cantera.

[110] C.M. Guirao, R. Knystautas, J.H.S. Lee, W.B. Benedick, and M. Berman. Hydrogen-air detonations. In *Symposium (International) on Combustion*, pages 583–590, 1982.

[111] S.R. Tieszen, M.P. Sherman, W.B. Benedick, J.E. Shepherd, R. Knystautas, and J.H.S. Lee. Detonation cell size measurements in hydrogen-air-steam mixtures. *Progress in Astronautics and Aeronautics*, 106:205–219, 1986.

[112] G. Ciccarelli, T. Ginsberg, J.L. Boccio, C. Economos, K. Sato, and M. Kinoshita. Detonation cell size measurements and predictions in hydrogen-air-steam mixtures at elevated temperatures. *Combustion and Flame*, 99(2):212–220, 1994.

[113] W.B. Benedick, R. Knystautas, and J.H.S. Lee. Large-Scale Experiments on the Transmission of Fuel-Air Detonations from Two-Dimensional Channels. In J.R. Bowen, N. Manson, A.K. Oppenheim, and R.I. Soloukhin, editors, *Dynamics of Shock waves, explosion and detonation*, pages 546–555. American Institute of Aeronautics and Astronautics, 1985.

[114] A.V. Gaathaug, D. Bjerketvedt, and K. Vaagsaether. Experiments with Flame Propagation in a Channel with a Single Obstacle and Premixed Stoichiometric H2 -Air. *Combustion Science and Technology*, 182(11-12):1693–1706, October 2010.

[115] D. Bradley, M. Lawes, Kexin Liu, S. Verhelst, and R. Woolley. Laminar burning velocities of lean hydrogen–air mixtures at pressures up to 1.0 MPa. *Combustion and Flame*, 149(1-2):162–172, April 2007.

[116] T. Iijima and T. Takeno. Effects of temperature and pressure on burning velocity. *Combustion and Flame*, 65(1):35–43, July 1986.

[117] S.B. Dorofeev. Hydrogen flames in tubes: Critical run-up distances. *International Journal of Hydrogen Energy*, pages 1–11, 2009.

[118] Y. K. Liu, J.H.S. Lee, and R. Knystautas. Effect of Geometry on the Transmission of Detonation through an Orifice. *Combustion and Flame*, 225:215–225, 1984.

[119] K. Vaagsaether and D. Bjerketvedt. Simulation of flame acceleration in an obstructed tube with LES. In *International Colloquium on the Dynamics of Explosions and Reactive Systems*, 2007.

[120] S.B. Dorofeev. Personal communication, 2013.

[121] A. V. Gaathaug, K. Vaagsaether, and D. Bjerketvedt. Experimental and numerical investigation of DDT in hydrogen–Air behind a single obstacle. *International Journal of Hydrogen Energy*, pages 1–10, June 2012.

[122] D. Bjerketvedt, O.K. Sonju, and I.O. Moen. The Influence of Experimental Condition on the Reinitiation of Detonation Across an Inert Region. *Progress in Astronautics and Aeronautics*, 106:109–130, 1986.

[123] A.V. Gaathaug, K. Vaagsaether, and D. Bjerketvedt. Simulation of DDT in Hydrogen-air behind a single obstacle. In *The 4th International Conference on Hydrogen Safety (ICHS)*, 2011.

[124] L.R. Boeck, J. Hasselberger, F. Ettner, and T. Sattelmayer. Investigation of Peak Pressures during Explosive Combustion of Inhomogeneous Hydrogen-Air Mixtures. In *International Seminar on Fire and Explosion Hazards*, pages 959–965, 2013.

[125] A.V. Gaathaug, D. Bjerketvedt, and K. Vaagsaether. DDT in Homogeneous and Inhomogeneous Hydrogen-Air Mixtures. In *Proceedings of the Seventh International Seminar on Fire and Explosion Hazards*, pages 739–748, 2013.

[126] M. Sichel, N.A. Tonello, E.S. Oran, and D.A. Jones. A two-step kinetics model for numerical simulation of explosions and detonations in H2-O2 mixtures. *Proceedings of the Royal Society A: Mathematical, Physical and Engineering Sciences*, 458(2017):49–82, January 2002.

[127] G. Del Alamo, F.A. Williams, and A.L. Sanchez. Hydrogen-oxygen induction times above crossover temperatures. *Combustion Science and Technology*, 176:1599–1626, 2004.

[128] P. Flohr and H. Pitsch. A turbulent flame speed closure model for LES of industrial burner flows. *Proceedings of the Summer Program*, pages 169–179, 2000.

[129] T. Iijima and T. Takeno. Effects of Temperature and Pressure on Burning Velocity. In *Proceedings of the Faculty of Engineering, Tokai Univ*, volume 65, pages 53–67, July 1984.

[130] V.P. Korobeinikov, G.G. Chernyi, V.V. Markov, and V.A. Levin. Propagation of Blast Waves in a Combustible Gas. *Astronautica Acta*, 17:529–537, 1972.

[131] E.S. Oran and V.N. Gamezo. Origins of the deflagration-to-detonation transition in gas-phase combustion. *Combustion and Flame*, 148(1-2):4–47, January 2007.

[132] E. Dabora, J.A. Nicholls, and R.B. Morrison. The influence of a compressible boundary on the propagation of gaseous detonations. In *Tenth Symposium (int) on Combustion*, volume 10, pages 817–830, 1965.

Appendix A

Journal published papers - First author

A.1 Experiments with Flame Propagation in a Channel with a Single Obstacle and Premixed Stoichiometric H_2-air

This paper is presented as a Chapter 4. Here is the original paper from "Combustion Science and Technology" 182, 2010.

A.2 Experimental and numerical investigation of DDT in hydrogen-Air behind a single obstacle

This paper is presented as a Chapter 7. Here is the original paper from “International journal of hydrogen energy” 2012.

Appendix B

Conference proceeding papers - First author

B.1 DDT in Homogeneous and Inhomogeneous Hydrogen-Air Mixtures

This conference paper was presented at ISFEH7 2013 in Providence, USA. It was selected to the “Best paper presentation at the ISFEH7”.

DDT in Homogeneous and Inhomogeneous Hydrogen-Air Mixtures

Gaathaug, A. V.[1*], Bjerketvedt, D.[1,2], and Vaagsaether, K.[1]

[1]Telemark University College, Faculty of Technology, Porsgrunn, Norway.
[2]Tel-Tek, Porsgrunn, Norway
**Corresponding author email: andre.v.gaathaug@hit.no*

ABSTRACT

Detonations and deflagration to detonation transition (DDT) represent a major hazard to process industry and fuel infrastructure. The main objective of this study was to experimentally investigate the location where DDT occurs behind one obstacle. A second objective was to identify the events leading up to DDT as well as the effects of inhomogeneous gas mixtures. High speed film and pressure records were the main diagnostic tools. Local explosions were observed at the walls and pressure waves oscillated between the walls, as seen on high speed film and recorded by pressure transducers. These transverse pressure waves were assumed to amplify and couple with the reaction zone of the deflagration, leading up to DDT. The onset of detonation was always observed at the walls for all homogeneous experiments. Inhomogeneous gas mixtures are very relevant for safety applications, as real gas leakages are typically inhomogeneous in composition. This paper shows that DDT occurred at the interface between reactants and air layer.

KEYWORDS: Hydrogen, DDT, inhomogeneous, detonation.

INTRODUCTION

This paper reports experimental data from studies of deflagration to detonation transition (DDT) in hydrogen-air mixtures. The main goal of the study was to investigate the location of the onset of detonation. Additionally the effects of inhomogeneous gas mixtures were investigated. High speed film and pressure records were used to analyze the results. Fig. 1 shows the experimental setup, in which the dotted lines are deflagrations and the solid lines are detonations. Both homogeneous and inhomogeneous gas mixtures are shown.

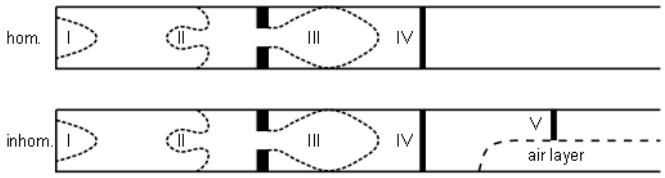

Figure 1. Schematic of the experimental setup.

BACKGROUND

DDT has been widely studied, with early work performed by Shelkin (1940) [1] and Urtiew and Oppenheim (1966) [2]. The latter study is well-known and describes the onset of detonation in smooth tubes. The authors reported DDT at the turbulent flame brush, occurring behind the precursor shock wave or at the contact surface.

The criterion for DDT is very dependent on boundary conditions, thus it is hard to generalize. Lee [3] summarized previous work and found that the ratio of detonation cell size (λ) to tube diameter (d) is $\lambda/d \approx 1$. The deflagration must accelerate to about half the detonation Chapman-

Proc. of the Seventh International Seminar on Fire & Explosion Hazards (ISFEH7), pp. xx-xx
Edited by D. Bradley, G. Makhviladze, V. Molkov, P. Sunderland, and F. Tamanini

ISBN: 978-981-08-7724-8 :: doi: 10.3850/978-981-08-7724-8_0x-0x

B.2 Experiments with flame propagation in a channel with one obstacle and premixed H_2-air

This conference paper was presented at ICDERS 2009 in Minsk Belarus

Experiments with flame propagation in a channel with one obstacle and premixed H_2-air

Andre Vagner Gaathaug[1], **Dag Bjerketvedt**[1], **Knut Vaagsaether**[1]

[1]Faculty of Technology, Telemark University College
Kjolnes ring 56, 3901 Porsgrunn, Norway

1 Introduction

Flame propagation and flame inversion in tubes and channels has been studied by many researchers. Clanet and Searby [1] divided flame propagation into four stages. During the third stage the flame changed curvature to an inverted shape. D. Dunn-Rankin and R. F. Sawyer [2] investigated tulip flames in closed tubes. They recognized that the tulip formation was initiated when the flame quenched at the walls.

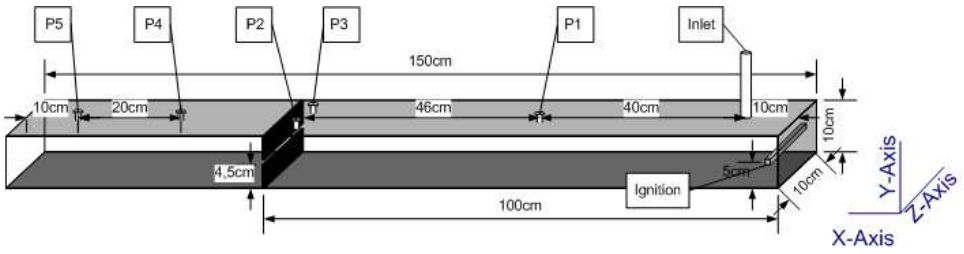

Figure 1: The experimental setup. Showing inlet, pressure transducers, distributed ignition and obstacle.

T. Kratzel, E. Pantow, M. Fischer [3] investigated the transition of a curved flame into a tulip shape for hydrogen/air mixtures. They pointed out the baroclinic effect on the formation of an inverted flame front, due to reflected pressure waves generated by the flame.

This abstract presents experimental results of flame propagation in a square channel with a single obstacle. The background for the experimental study was to investigate how a flame propagated when and after the flame inverted. The experiments could also be used to verify numerical calculations. The results presented are a part of over 100 experiments.

2 Setup

The experimental setup was a square channel with 10 cm by 10 cm cross section and 150 cm long with a single obstacle. An axis system was defined to ease the description of the results. The axis system

Correspondence to : andre.v.gaathaug@hit.no

B.3 Experimental study of DDT in homogeneous and inhomogeneous Hydrogen-Air behind a single obstacle

This conference paper was presented at ICDERS 2013 in Taipei, Taiwan

Experimental Study of DDT in Homogeneous and Inhomogeneous Hydrogen-Air Behind a Single Obstacle

Gaathaug A. V., Bjerketvedt D. and Vaagsaether K.
Telemark University College
Faculty of Technology
Department of Process, Energy and Environmental Technology
Norway

1 Introduction

This paper reports an experimental study of detonation deflagration transition in a square channel. The gas mixtures used were hydrogen and air with varying concentrations. The channel had one obstacle with adjustable blockage ratio, see figure 1. After ignition the flame propagated as laminar and tulip flame (I and II). A jet was formed behind the obstacle as the flame expanded and pushed the reactants ahead of itself (III). After the flame propagated through the obstacle it detonated (IV) in some experiments. Inhomogeneous conditions were made by letting air flow into the channel before ignition, and the detonation propagated in a layer of reactants bound by a layer of air. The main objective of this study was to investigate where the detonation started. The experimental results showed a series of local explosions at the walls which added up to DDT. The detonation propagated through the rest of the channel, also in inhomogeneous cases where the reactants were bound by a layer of air.

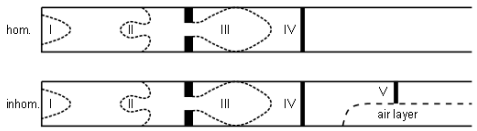

Figure 1: A sketch of the experimental setup, homogeneous on top and inhomogeneous below.

2 Background and motivation

Urtiew and Oppenheim [1] showed in 1966 the transition from deflagration to detonation in a channel. They showed that DDT could occur at the turbulent flame brush, behind a precursor shock wave or at the contact surface behind a shock wave. Oppenheim also introduced the term *"an explosion within the explosion"*. Meyer *et. al.* [3] showed that an explosion could occur in a layer of unburned mixture behind the leading edge of a turbulent flame. Lee [2] pointed out that a detonation could originate from the explosion, but there must be an amplification mechanism between the reaction zone and the shock wave. An other possibility is the continuous amplification of transverse waves that progress into

Correspondence to: andre.v.gaathaug@hit.no

B.4 Simulations of DDT in hydrogen-air behind a single obstacle

This conference paper was presented at ICHS 2011 in San Francisco, USA

SIMULATION OF DDT IN HYDROGEN-AIR BEHIND A SINGLE OBSTACLE

Gaathaug A.V.[1], Vaagsaether K.[1] and Bjerketvedt, D.[1]
[1] Telemark University College, Faculty of Technology, P.O.Box 203, Porsgrunn, 3901, Norway, andre.v.gaathaug@ hit.no

ABSTRACT

Two-dimensional numerical simulations of detonation deflagration transition (DDT) in hydrogen-air mixtures are presented and compared with experiments. The investigated geometry was a 3 meter long square channel. One end was closed and had a single obstacle placed 1 m from the end, and the other end was open to the atmosphere. The mixture was ignited at the closed end. Experiments and simulations showed that DDT occurred within 1 meter behind the obstacle. The onset of detonation followed a series of local explosions occurring far behind the leading edge of the flame in a layer of unburned reactants between the flame and the walls. A local explosion was also seen in the experiments, and the pressure records indicated that there may have been more. Furthermore, local explosions were observed in the experiments and simulations which did not detonate. The explosions should have sufficient strength and should explode in a layer of sufficient height to result in a detonation.

The numerical resolution was 0.5 mm per square cell, and further details of the combustion model used are provided in the paper.

1.0 BACKGROUND

This paper describes a numerical study of detonation deflagration transition (DDT) in a turbulent jet behind an obstacle. Numerical and experimental results were compared for similar cases. Fig. 1 shows the dimensions for the geometry used in this investigation. The 3 meter long channel had a 0.1 x 0.1 m^2 square cross section with transparent sidewalls and smooth top and bottom walls made of painted steel. One end was closed and one end was open to the atmosphere. The channel was filled with a mixture of hydrogen and air. The gas mixture was ignited at the closed end, and the combustion propagated one meter before reaching an obstacle. A jet formed at the obstacle opening and DDT was observed behind the obstacle. Prior to DDT some local explosions occurred in a layer between the flame and the walls.

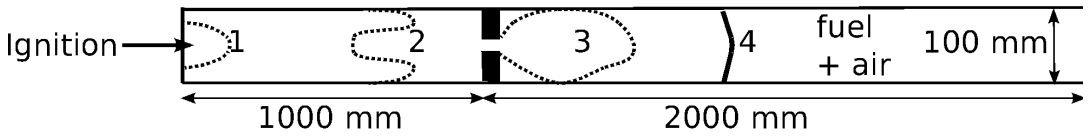

Figure 1. Investigated geometry. 1-3 represent the deflagration, while 4 represents the detonation. In some experiments DDT was observed behind the obstacle.

The earliest observations of detonations were conducted by Mallard and Le Chatelier in 1881 [1] and by Berthelot and Vielle [2] about the same time. Chapman [3] and Jouguet [4] formulated the so-called CJ theory of detonations, a one-dimensional theory combining the conservation of mass, momentum, and energy with an equation of state and an assumption of an infinitely fast reaction. The CJ theory results in two limiting solutions, one for detonations and one for deflagrations.

An expansion of the CJ theory for detonations was developed almost simultaneously by Zeldovich, von Neumann, and Döring [5]. Known as the one-dimensional ZND theory, it accounts for the chemical reaction time and length of a shock wave that propagates in front of the reaction. The shock

Appendix C

Journal papers - Co-author

C.1 Gas explosion field test with release of hydrogen from a high pressure reservoir into a channel

This conference paper was presented at ISHPMIE 2010 in Yokohama, Japan. The author contributed to the experimental planning, setup and execution.

Appendix D

Conference proceeding papers -Co-author

D.1 Detonation propagation in a reactive layer; the role of detonation front stability

This paper was presented at the "The Tenth International Symposium on Hazards, Prevention, and Mitigation of Industrial Explosions" (X ISHPMIE) in Bergen, Norway, on 10-14 June 2014. The author has been a major contributor to the work together with first author K. Vaagsaether PhD.

Detonation propagation in a reactive layer; the role of detonation front stability.

Knut Vaagsaether [a], André V. Gaathaug [a] & Dag Bjerketvedt [a]

E-mail: *knut.vagsather@hit.no*

[a] Telemark University College, Porsgrunn, Norway

Abstract

The objective of the presented work is to investigate the propagation mechanisms of a detonation in an explosive gas with a neighbouring inert gas layer. The role of stability or regularity of the detonation cells is assumed to influence the method of propagation. The mechanisms are investigated by numerical simulations with a two-step reaction "mock-up" gas. The induction zone length of the detonation front is varied by increase the activation energy of the iso-thermic reaction mechanism. The irregularity of the detonation cells increase as the induction zone length increases. For moderately stable detonation fronts the detonation propagates in the layer with a height of three detonation cell widths or more. For highly unstable detonation fronts the propagation mechanism is considerably different than for the moderately stable detonation. The detonation fails and is re-initiated as it propagates in a layer smaller than 3 detonation cell widths.

Keywords: *Detonation, detonation cells, inhomogeneous gas, simulation.*

1. Introduction

Detonations in layers of reactants bound by an inert gas were studied by Sommers (1961) and Dabora (1963). Sommers (1961) investigated H2-O2 reactants and air/He/Ar as inert. Even though the work was largely motivated by a study of yielding boundary conditions of high explosives it is relevant for industrial accidents where light or dense gas could stratify along the floor or ceiling of industrial buildings. Dabora (1963) presented a sketch of a detonation propagating in the layered fuel-inert as seen in figure 1. In figure 1 it is shown how the expansion behind the detonation front expands both backwards into the products but also downwards into the inert gas. This double expansion leads to a slight curvature of the detonation wave front, and might lead to lower detonation velocity. Sommers and Dabora investigated how the velocity deficit of the front would lead to failure of the detonation. There was no investigation of the stability of cells/pattern detonation in this work.

More recent work has been done by Kuznetsov et. al. (2011), Rudy et. al. (2013) and Grune et. al. (2013) where flame propagation, DDT and detonations in stratified layers of hydrogen and air was investigated. They showed that a detonation could propagate in a layer if the height of the layer was more than three times the detonation cell size.

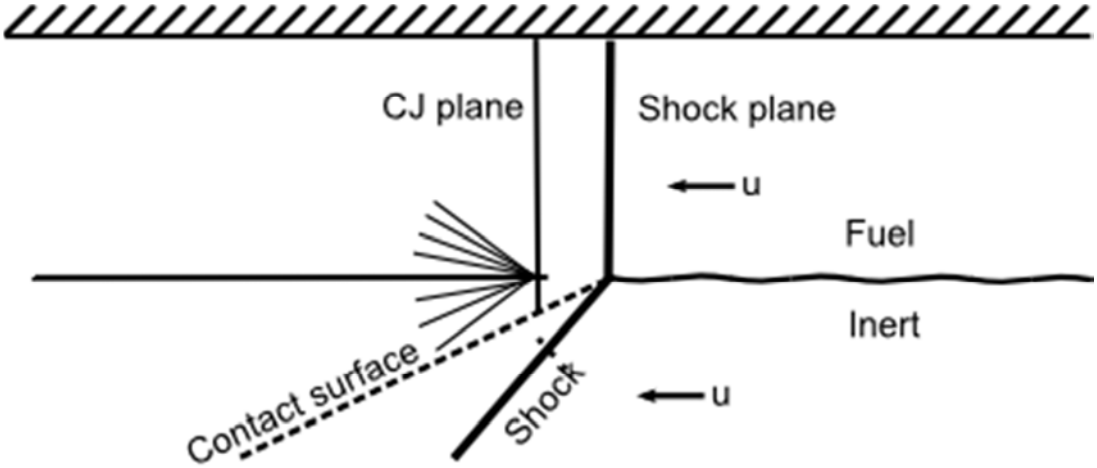

Figure 1: Schematic of a detonation propagating in a layer of fuel bounded by an inert layer, after Dabora (1963).

Böck et. al. (2013) also reported experimental results of detonations in vertical concentration gradients of hydrogen and air. There it was shown that concentration gradients could potentially be more hazardous than homogeneous mixtures as they were more prone to deflagration to detonation transition.

The influence on the propagation of a detonation of regularity or level of instability in the reaction zone was studied by Austin (2003).

Stability criteria for the cellular detonation front can be made from the reduced activation energy:

$$\theta = \frac{E_a}{RT_{vN}}$$

Where T_{vN} is the temperature just behind the incident shock wave in the detonation front. The propagation of the front had different propagation mechanisms based on the level of instability where a clear boundary between moderately stable and Lee Stewart neutral stability boundary of $\theta = 4.5$ for sufficiently high CJ-Mach numbers.

The weakly unstable detonation fronts exhibits structured detonation cells with equal size while highly unstable or unstructured detonation fronts show detonation cells with several characteristic cell sizes as seen in figure 2.

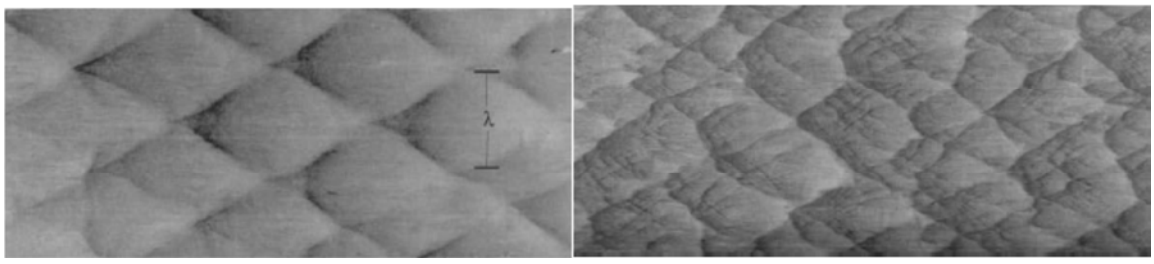

Figure 2: Example of detonation cellular structure on a smoked foil by Austin (2003). Left: structured $2H_2+O_2+17Ar$ at 20 kPa initial pressure. Right: unstructured$C_3H_8 + 5O_2+ 9N_2$ at 20 kPa initial pressure.

An experimental study by Moen et. al. (1986) showed that the velocity deficit relative to CJ-velocity in an acetylene-air detonation in small tubes was much less that the deficit in

detonations in acetylene-oxygen or argon-diluted acetylene-oxygen. The regularity of the detonation cells is highest for the argon diluted mixture and irregular for acetylene-air.

The objective of the presented work is to investigate the propagation mechanisms of a detonation in an explosive gas with a neighbouring inert gas layer. The role of stability or regularity of the detonation cells is assumed to influence the method of propagation.

2. Numerical method

The numerical method solves the reactive Euler equations with ideal gas law as EOS. The hyperbolic equation solver is a centred 2. order flux-limiter method. The method is a simplified version of the code presented by Gaathaug et. al (2012) where the turbulent reaction rate is omitted in the present simulations. Three species are conserved with two reaction rates as shown in eq. (1).

$$\boldsymbol{\alpha \rightarrow \alpha'} \qquad \textbf{Step 1} \qquad \textbf{(1)}$$
$$\boldsymbol{\alpha' \rightarrow \beta} \qquad \textbf{Step 2}$$

Where step 1 is an isothermal reaction for the induction zone and step 2 is an exothermic reaction. The species variables are modelled as reaction progress variables and all values are between 0 and 1 and only equations for α and β need to be solved. The reaction rates are modelled as:

$$\frac{d\alpha}{dt} = -Aexp\left(\frac{E_\alpha}{RT}\right)$$
$$\frac{d\beta}{dt} = B(1-\beta)exp\left(\frac{E_\beta}{RT}\right)\cdot\mathcal{H}(\alpha'-1)$$

$\mathcal{H}$is the Heaviside step function which explains that α need to be completely reacted before step 2 can start. This two-step model separates the detonation front into an induction zone and an exothermic reaction zone. The reason for

2.1 Simulation set-up.

To study the effect of structure of the detonation front the CJ-states and the steady ZND-states are kept constant for all simulations. Also the length of the exothermal reaction zone is kept constant. The only difference in the simulations is the induction zone length. Two levels of unstable detonation fronts are studied where one is moderately stable and produces structured detonation cells. The two has a higher degree of instability. The dimensionless activation energies of the induction zone model are 15 and 90. The half-length exothermic reaction zone for all simulations is equal to the induction zone length of $E_\alpha = 15$.

Table 1 summarizes the constants for the reaction model and initial values.

Table 1: Constants and initial values for variables

Variable	Symbol	Value
Dimensionless heat of reaction	q	30
Heat capacity ration	γ	1.4
Dimensionless activation energy 2. step	E_β	15
Pre-exponential factor 2. step	B	4.9738
Initial dimensionless pressure	p0	1
Initial dimensionless temperature	T0	1

Dimensionless gas constant	R	1

An initial detonation front is produced numerically by running a simulation of a detonation front into the reactive gas for a sufficiently long time i.e. until the number of detonation cells does not change. The detonation front is then mapped into a simulation domain as seen in figure 3, where the detonation front interacts with a layer of inert gas. The inert gas has the same temperature, pressure and density as the fuel gas. The simulations are scaled by the induction zone length at CJ-velocity. The mesh resolution is 10 control volumes for the induction zone length (Δ_i) and the height h of both the reactive and inert layer is 100, 75 and 50 Δ_i.

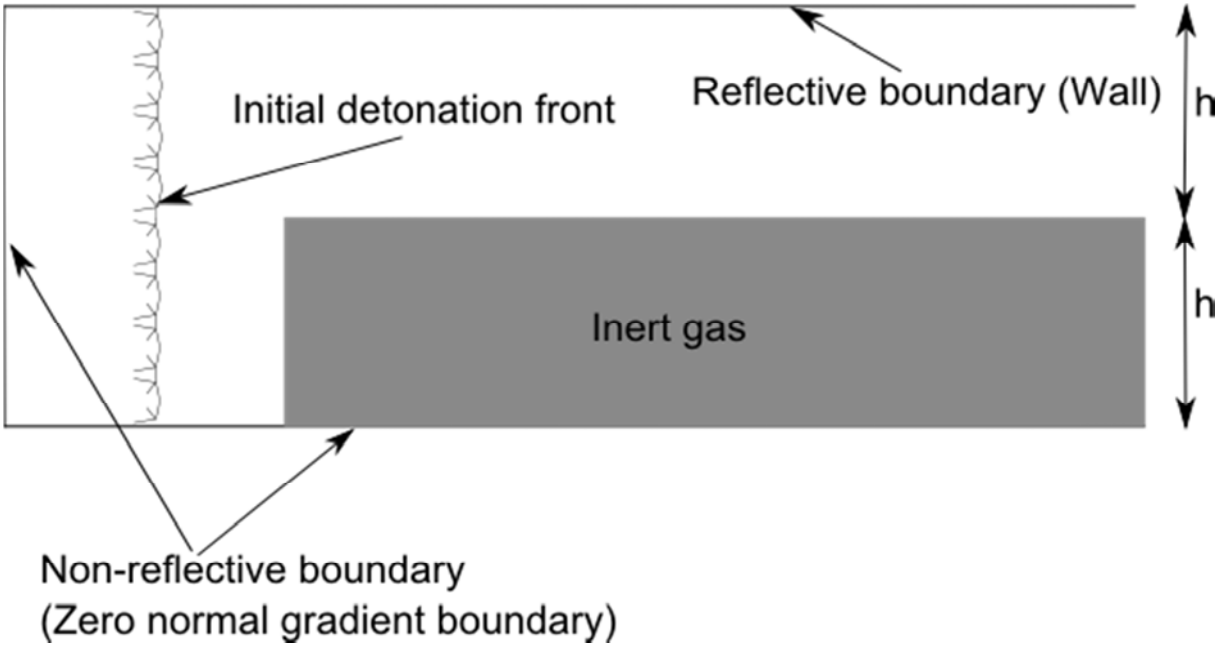

Figure 3: Simulation set-up. The height h is 100, 75 or 50 induction zone lengths. The inert gas has the same density, pressure and molecular weight as the reactive gas.

Figure 4 shows a stability diagram with reduced activation energy on the vertical axis and detonation front Mach-number on the horizontal axis. The simulation cases presented in this paper is shown as points in the diagram. The $E_\alpha = 15$ case is below the curve and is characterized as moderately stable detonation. The other investigated cases are classified as more unstable.

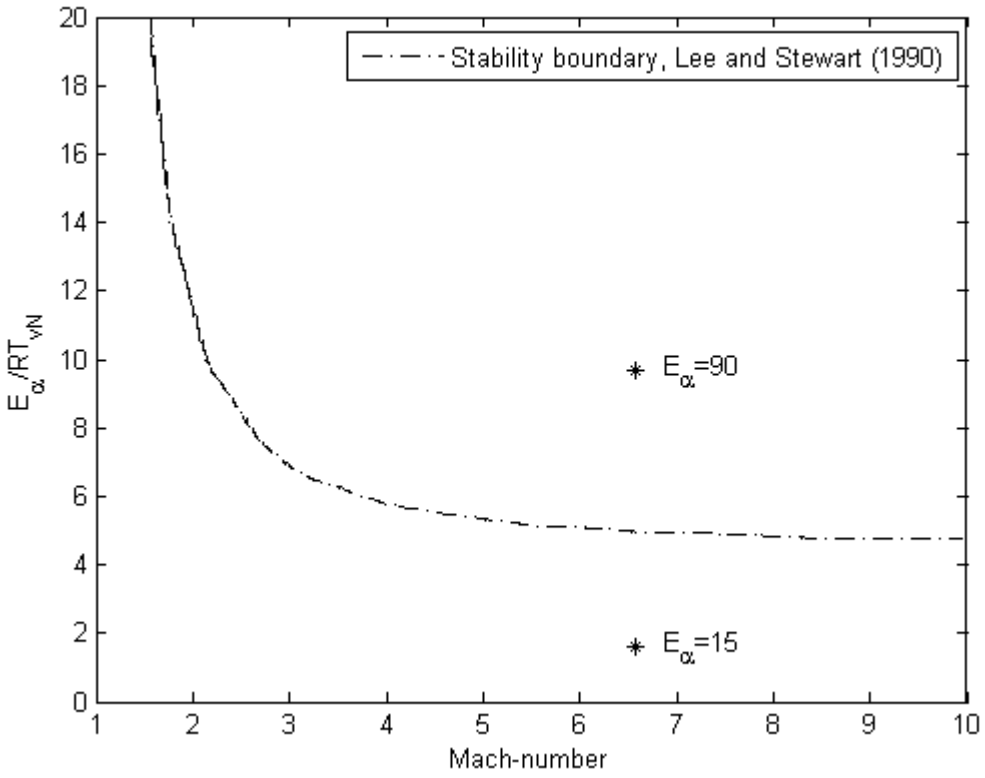

Figure 4: Stability boundary with the present simulation activation energies. Values above the curve display irregular cellular structure. Reproduced from Austin (2003), originally presented by Lee and Stewart (1990).

Figure 5 shows the detonation front structure of the initial detonation before the front reaches the inert layer. There it can be seen how the wave pattern of the $E_\alpha = 15$ is more regular than the $E_\alpha = 90$ case.

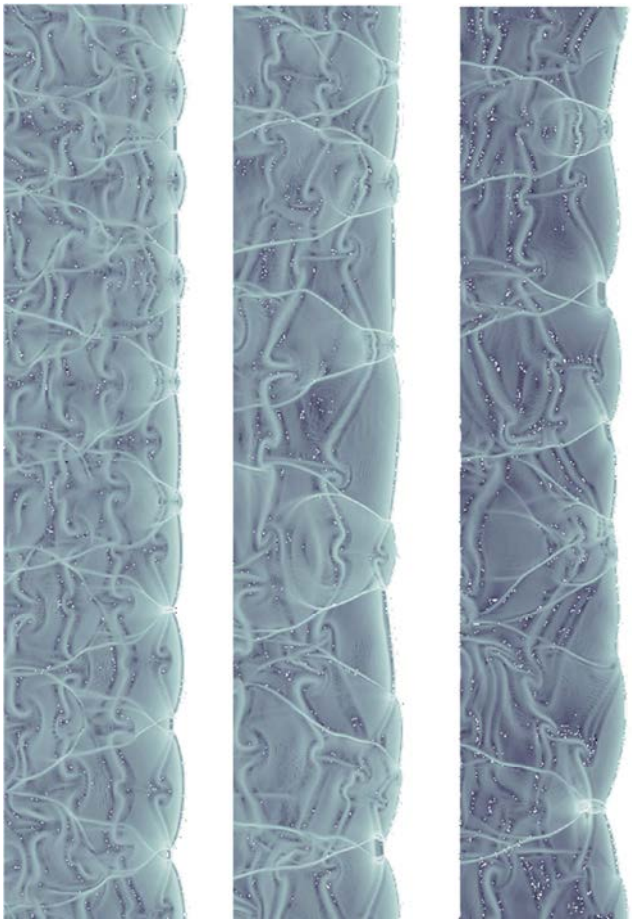

Figure 5: Density gradients for the initial detonation front for the three different E_α. The height for all fronts is 200 Δ_i. Left: E_α = 15. Middle: E_α = 90. Right: E_α = 120, included for reference.

3. Results and discussion

Figure 6 shows a sequence of density contours from the simulation with E_α = 15 and h = 100 Δ_i. It is clear that the propagation mechanism in this simulation is by several detonation cells in the layer and several triple point collisions occurs in the combustible layer height. Also seen is the curvature of the bottom section of the detonation front due to the expansion into the inert gas.

Other results are presented as numerical smoke foils to show the trajectories of the triple points in the detonation front. The numerical smoke foils are calculated as:

$$I = \log\left(\left|\nabla\left(\int (p - p_0)(1 - \beta)dt\right)\right|\right)$$

Figure 7 shows the numerical smoke foils also for E_α = 15 with three different reactive layer heights (100, 75 and 50).

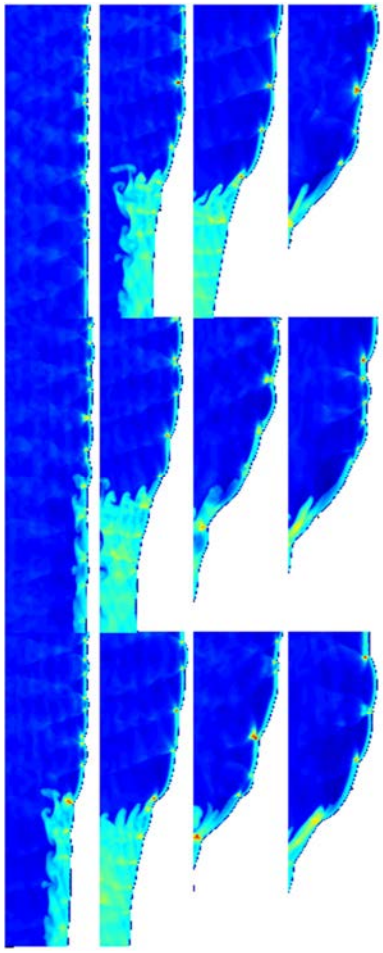

Figure 6: Sequence of details of detonation front for E_α = 15 and layer height of 100 Δ_i. The contours are of density. The sequence is from top to bottom and left to right.

For both the 100 and 75 Δ_i several triple point trajectories is seen in the combustible layer. These collisions form Mach-stems that keep the reaction front propagating as a detonation. The detonation propagating in the 50 Δ_i layer fails as the last transverse wave forming the triple point propagates into the inert layer. The two cases where the detonation can propagate in the layer have initially 3 detonation cells or more.

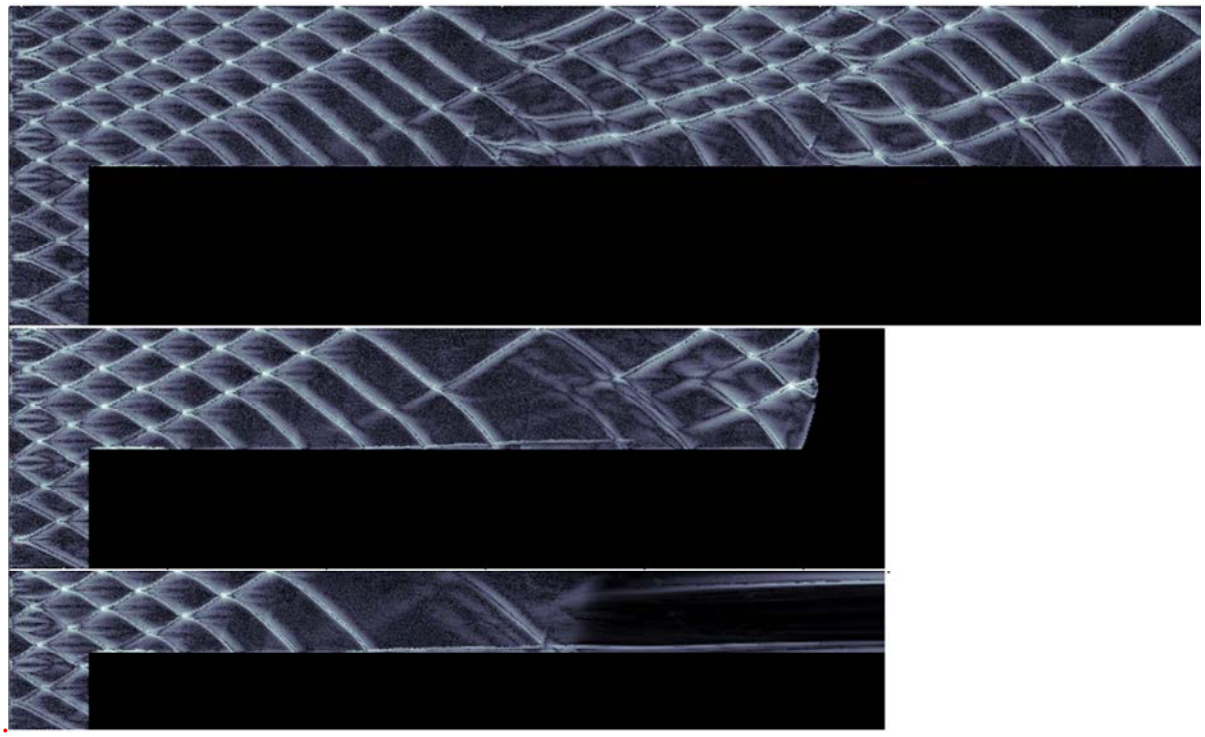

Figure 7: Numerical smoke foil for E_α = 15, and height of layer h = 100, 75 and 50 Δ_i from top to bottom.

A sequence of the detonation front propagation from E_α = 90 and h =100 Δ_i is shown in figure 8. Initially the detonation propagates in the layer with several detonation cells stemming from the initial detonation front. After some length the typical cellular front disappears and the reaction front and shock wave is decoupled. The gas is reacted as a transverse combustion wave propagates in the zone between the shock and reaction zone. This propagation mechanism is similar to a DDT event.

The triple point trajectories as numerical smoke foils for E_α = 90 is shown in figure 9. For the two tallest layers the detonation propagates due to shock reflections and strong transverse waves. In the low velocity part of the detonation cell cycle the detonation fails and the shock decouples from the reaction front. For the layer height of 75 Δ_i the initial number of detonation cells in the layer is lower than 3 but it is still able to propagate as a detonation or in a similar manner as a detonation. The transverse shock waves form a transverse detonation wave propagating in the zone between the shock wave and reaction front.

Figure 8: Sequence of details of detonation front for E_α = 90 and layer height of 100 Δ_i. The contours are of density. The sequence is from top to bottom and left to right.

4. Conclusions

The moderately stable detonation front where E_α = 15 propagates in the reactive layer as a detonation when the layer height is 75 Δ_i which corresponds to about 3 detonation cell widths, as reported earlier. A layer height of 50 Δ_i (2 cells) results in failure of detonation. Typical cellular structures in the detonation front is seen as the front propagates in the combustible layer.

The more unstable detonation front of E_α = 90 and higher has a typical failure-re-initiation mode of propagation, where shock diffraction decouples the shock and flame. The transverse shock waves propagate in the compressed zone behind the shock wave and react the gas forming a transverse combustion wave. A layer height of 75 Δ_i corresponds to 2 detonation cells as seen in figure 9, but no total failure of detonation is observed in the simulations.

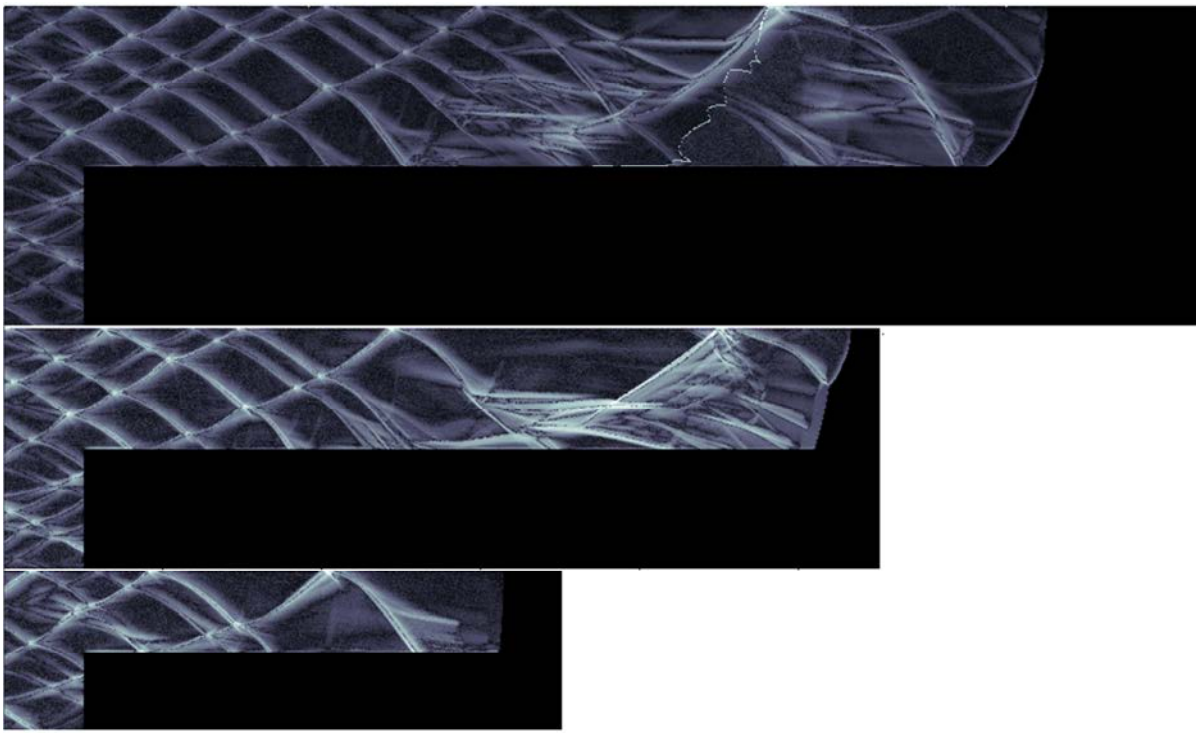

Figure 9: Numerical smoke foil for E_α = 90, and height of layer h = 100, 75 and 50 Δ_i from top to bottom.

References

Austin, J. (2003), *The Role of Instability in Gaseous Detonation*, PhD. Thesis, California Institute of Thechnology.

Dabora, E. (1963) *The Influence of a Compressible Boundary on the Propagation of Gaseous Detonations*. Technical report, University of Michigan, College of Engineering, Department of Aeronautical and Astronautical Engineering, Aircraft Propulsion Laboratory.

Gaathaug A.V, Vaagsaether K. and Bjerketvedt D. (2012), *Experimental and numerical investigation of DDT in hydrogen-Air behind a single obstacle.* International Journal of Hydrogen Energy 37 pp. 17606-17615.

Grune, J., Sempert, J., Haberstroh, H., Kuznetsov, M., and Jordan, T. (2013) *Experimental investigation of hydrogen-air deflagrations and detonations in semi-confined flat layers*. Journal of Loss Prevention in the Process Industries 26 (2): 317-323.

Kuznetsov, M.S., Grune, J., Friedrich, A., Sempert, K., Breitung, W.,and Jordan, T. (2011) *Hydrogen-Air Deagrations and Detonations in a Semi-Confined Flat Layer*. In Sixth International Seminar on Fire and Explosion Hazards, pp 978-981.

Moen, I. O., Sulmistras, A., Thomas, G. O., Bjerketvedt, D., Thibault, P.A. (1986), Influence of Cellular Regularity on the Behaviour og Gaseous Detonations, Dynamics of Explosions, Progress in Astronautics and Aeronautics series Vol. 106, 220-243.

Rudy, W, Kuznetsov, M, Porowski, R, Teodorczyk, A, Grune, J and Sempert, K. (2013) Critical conditions of hydrogen-air detonation in partially confined geometry. *Proceedings of the Combustion Institute*, 34(2):1965-1972.

Sommers, W.P.(1961) *The Interaction of a Detonation Wave with an Inert Boundary*. PhD thesis, University of Michigan.

D.2 Mach-stem formation and DDT in atmospheric Hydrogen-Air behind a single obstacle

This conference paper was presented at the Joint meeting of the British and Scandinavian-Nordic section of the Combustion Institute in Cambridge England. The author contributed with the experimental planning, setup and execution

MACH-STEM FORMATION AND DDT IN ATMOSPHERIC HYDROGEN-AIR BEHIND A SINGLE OBSTACLE

K. Vaagsaether[1], A.V. Gaathhaug[1], L. Bjarnason[1] and D. Bjerketvedt[1]

[1]Telemark University College, Porsgrunn, Norway

Introduction

The objective of the work presented is to experimentally investigate the mechanisms of flame acceleration and the eventual transition from deflagration to detonation behind a single obstacle where the deflagration is initiated by a spark. The aim is to show how the formation of the initial shock and subsequent Mach-stem causes transition to detonation in a channel with one obstacle. The experimental gas mixture is hydrogen-air at atmospheric pressure and room temperature.

It is known in industrial accidents that jets can cause flame acceleration and transition from deflagration to detonation [1] and [2]. In these examples a possible ignition in a semi-closed compartment produced a strong jet in which the flame propagated. Mach-stems formed from oblique shock reflections are possible causes of the transition to detonation. Several studies [3], [4], [5] of the effects of solid boundary-shock interactions show that the increased temperature behind a Mach-stem from moderately strong shocks can cause transition to detonation. The interaction between the Mach-stem and boundary layer may cause DDT for even weaker incident shocks. Thibault et. al. [6] studied the transmission of a detonation through an annulus orifice where shock reflection played an important part in the re-initiation of the detonation. Bhattacharjee et. al. [4] discussed five mechanisms that could lead to transition to detonation behind a Mach-stem including flow instabilities.

Experimental set-up

The experimental set-up is shown in Figure 1. It consists of a 3 m long channel with .1 x .1 m^2 cross section. The channel was closed in the ignition end and an obstacle was placed 1 m from ignition. The side walls of the channel were made of transparent polycarbonate. The obstruction was a baffle type obstacle creating an open slit with a blockage ratio of 0.75. A Z-type schlieren setup was used for imaging and the film was captured on a Photron APX-RS high speed camera at 22500 fps. Kistler 603b transducers were used for pressure measurements. The gas mixture in the experiments was 15% to 40% hydrogen in air

Figure 1: Experimental set-up.

Results and Discussion

With the present geometry DDT was not observed in the tip of the jet but in Mach-reflections some distance behind the obstacle.

The formation of the shock wave in front of the leading flame front is caused by the rapid combustion behind the obstruction. A pressure wave, not being a shock-wave, is formed due to the high total reaction rate in the area and the wave propagates in the products as discussed earlier. When the pressure wave interacts with the flame front from the product side the wave is reflected due to the density difference across the flame front forming a shock wave in the reactants. The formed shock is important for transition to detonation due to the Mach- reflection at the wall. The shock-flame interaction can also increase flame surface area due to instabilities like the Richtmyer-Meshkov instability. The importance of the formed instabilities due to the shock-flame interaction is difficult to determine in these experiments with the present diagnostics. The Mach-reflection in the experiment with 25% hydrogen causes a moderately fast reaction front behind itself. For 28% hydrogen-air the Mach-stem is followed by a reaction front which is not fast enough to cause DDT directly. For 30 % hydrogen in air the DDT occurs behind or in the Mach-stem as seen in the right column of Figure 2. The shape of the appearing shock in the reactants is dependant of the shape of the flame since the pressure wave propagates much faster in the products. In the presented experiments the flame passes the obstacle in such a way that the shape of the flame front is non-symmetric in the plane of view. The asymmetry of the flame front might be due to geometrical asym-

[1] Corresponding author: knut.vagsather@hit.no

metry. The flame is pushed down and forms a large volume of unreacted gas in the top half of the channel. The effect of the asymmetry produces larger volumes of unreacted gas that can either be consumed by the flame in a strong vortex as is seen behind the obstacle and larger volumes can be compressed by shock reflections behind the Mach-stem. Previous simulations [7] show that symmetrical flame shapes need longer distances to achieve transition to detonation and need to form several Mach-reflections before transition to detonation. In inhomogeneous gas mixtures asymmetry may be caused by local higher or lower burning velocities due to spatially varying concentrations. Flame acceleration and DDT experiments in inhomogeneous hydrogen-air mixtures [8] has shown that inhomogeneity in the concentration can promote transition to detonation.

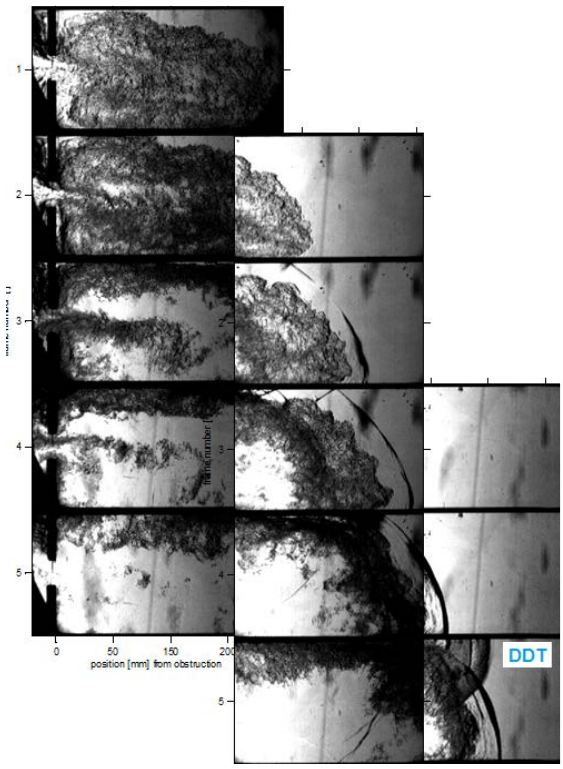

Figure 2: DDT in 30 % H_2.

Conclusions

From high speed schlieren images together with pressure records the flame propagation leading up to DDT or flame-shock coupling under atmospheric conditions in hydrogen-air has been identified. To be able to visualize the shock-wall interactions the high speed images show the full channel height. The mechanisms seen in the present study is similar to mechanisms reported in earlier work with transmission of detonations and in pipes. The mechanism of fast flame propagation and DDT in the presented experimental set-up is may be initiated by a local explosion due to a backwards propagating flame just behind the obstacle. It appears that the following pressure wave reflects in the dense reactants when it reaches the leading flame front and thereby forms a shock wave in the unburned gas. Mach reflections of the formed shock cause locally very high reaction rates and can cause transition to detonation. The flame shape in the present experiments promotes DDT since the asymmetrical shape of the flame front creates larger volumes of unreacted gas between the flame and the wall than a symmetrical flame front.

Acknowledgements

This work have been supported financially by the Norwegian Research Council (RENERGI and ENERGIX programs) as part of the IEA HIA Task 19 and 31

References

[1] Burgess, D. S. Zabetakis, M. G. Detonation of a Flammable Cloud Following a Propane Pipe Break. The December 9, 1970, Explosion in Port Hudson, MO. US Bureau of Mines.

[2] Bjerketvedt, D. Mjaavatten, A. A Hydrogen-Air Explosion in a Process Plant: A Case History. International Conference on Hydrogen Safety, 2005, Pisa, Italy.

[3] G. Thomas, R. Bambrey, C. Brown, Combust. Theory and Modelling 5 (2001) 573-594.

[4] R.R. Bhattacharjee, S.S.M. Lau-Chapdelaine, G. Maines, L. Maley, M.I. Radulescu, Proc. Combust. Inst. 34 (2013) 1893-1901.

[5] E. Dzieminska, A. K. Hayashi, Intl. J. of Hydrogen Energy 38 (2013) 4185-4193.

[6] P. A. Thibault, D. Bjerketvedt, A. Sulmistras, G. O. Thomas, A. Jenssen, I. O. Moen, Proc. 10th Intl. Colloquium on the Dynamics of Explosions and Reactive Systems, Berkeley, (1985).

[7] A. V. Gaathaug, K. Vaagsaether, D. Bjerketvedt, Intl. J. of Hydrogen Energy 37 (2012) 17606-17615.

[8] L. R. Boeck, J. Hasselberger, F. Ettner, T. Sattelmayer, Proc. 7th International Seminar on Fire and Explosion Hazards, (2013), 959-965.

Appendix E

Other appendices

E.1 Angular schlieren. Premixed combustion from a new perspective

This appendix is short presentation of the angular schlieren setup and some results of the method.

Angular schlieren. Premixed combustion from a new perspective.

A.V. Gaathaug

August 26, 2014

Abstract

The schlieren technique has been used for combustion diagnostics since the 17^{th} century and has been a very valuable tool. This paper presents a method of visualising premixed hydrogen air combustion in a channel. The angular schlieren method is a simple modification of the traditional z-type schlieren method where the viewing window of the test section is not perpendicular to the light. This method gives a depth perspective to the schlieren pictures.

1 Introduction

Schlieren photography of premixed flames has been done many times and has been, and still is a very important diagnostic tool. Schlieren photos visualizes gradient of refractive index. It allows us to see density gradient in transparent media and it is excellent for investigating many combustion phenomena. As summarized by G.S.Settles (2001), the technique started in the 17^{th} century with Robert Hook as he investigated candle plumes and combustion research has ever since used schlieren methods for diagnostics. G.H.Markstein (1964) visualized the shock and flame interaction with the schlieren method, and Urtiew and Oppenheim (1966) showed schlieren records of deflagration detonation transition in hydrogen oxygen mixture.

Flame propagation in pipes and channels has been studied with the emphasis on the formation of inverted or tulip flames. The formation of tulip flames has been studied experimentally in open (Clanet and Searby 1996) and closed geometries (Dunn-Rankin and Sawyer 1998). Gonzalez et. al. (1992) have pointed out that numerical studies of flame inversion have been done with several methods with and without viscosity and heat loss, and for reaction sheet models.

The focus of this paper is not to explain the formation of the inverted flame, but rather show the tulip shape formation from a semi frontal perspective. Other studies have investigated flame propagation and tulip flames based upon a traditional perpendicular schlieren setup. This does not give a full understanding of the depth perspective of the flame motion. This paper will present a method and results of visualization the flame and tulip formation in a new way. The method is easy with only minor changes to the

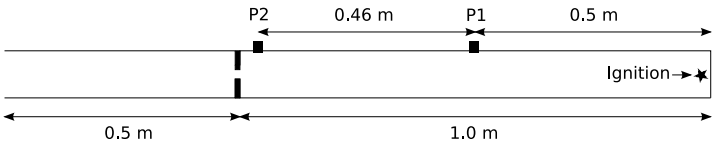

Figure 1: The experimental setup (side view). Showing the obstacle and the line ignition which is normal to the plane of this figure.

well known z-type schlieren setup (Settles 2001). The new clarity of the experiments eases the understanding and confirm the already established explanations.

2 Experimental setup

The experimental setup was a 100 *by* 100 mm^2 cross sectional area and 1500 mm long channel. One end was open to the atmosphere and one end was closed. An obstacle was placed 1000 mm from the closed end. Figure 1 shows an illustration of the setup. The top an bottom walls were made of steel and painted to give a smooth surface. The side walls were transparent 10 mm polycarbonate allowing schlieren filming of the experiment. The obstacle was made of two adjustable steel plates set to a constant ratio of blocked to total cross sectional area of $BR = 0.9$. An ignition device was installed at the closed end of the channel and consisted of a plastic rod with five evenly distributed gaps giving five electrical sparks as a 10 kV voltage was applied to the igniter. The orientation of the igniter was normal to the plane of figure 1. It ignited a homogeneous, stoichiometric hydrogen-air mixture at 1 atm and about 20^oC.

3 Schlieren setup

Two types of schlieren setup was used, and the difference between them will be described in this section (see figure 2). Both of them used an ordinary z-type configuration with one light source, two parabolic mirrors, one knife edge, one lens and a high speed camera recording at 5000 fps. For the ordinary perpendicular setup the direction of the parallel light from the first parabolic mirror was perpendicular to the transparent walls of the channel. Some irregularities in the plastic material caused light refraction in the transparent walls. The angular schlieren setup was made by tilting the channel 30^o relative to the light, see figure 2. Polycarbonate has a refractive index of $n = 1.5849$ and air has $n = 1.0003$. Snell's law gives an offset of 3.3 mm for each transparent wall, as light bends at gradients of refractive index, and this had to be compensated for by sliding the second parabolic mirror 6.6 mm sideways, see figure 2. The critical angle for total reflection was calculated to be $a_{crit} = 39^o$, but $a = 30^o$ was the highest practical angle for this setup. Higher angles of incident caused to much light to reflect and too poor quality of the schlieren photos.

As the light pass through the experiment, the angle of deflection in x and y direction is, according to Settles, given by:

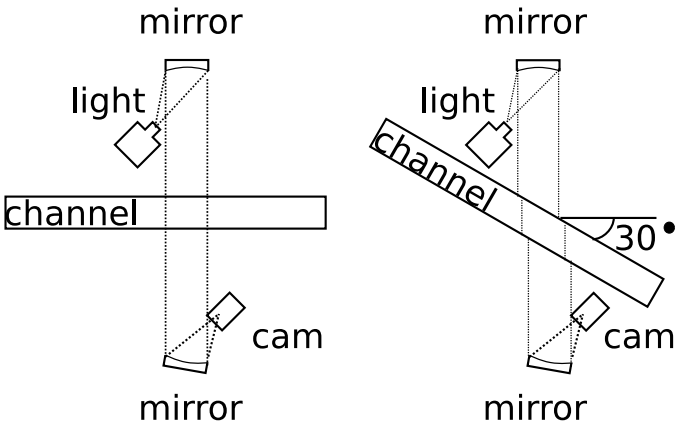

Figure 2: Perpendicular and angular schlieren setup.

$$\epsilon_x = \frac{1}{n}\int_0^L \frac{\partial n}{\partial x}\,dz, \qquad \epsilon_y = \frac{1}{n}\int_0^L \frac{\partial n}{\partial y}\,dz \tag{1}$$

Where z is along the optical axis which is path of the unrefracted light through the experiment, i.e inside the channel. L is the width of the channel. For the perpendicular setup the length of the optical axis equals L, while for the angular setup the length of the optical axis is given by $L \cdot \sin 30$. By letting n_0 equal the refractive index of the surroundings, the deflection angle becomes:

$$\epsilon_x = \frac{L \cdot \sin 30}{n_0}\frac{\partial n}{\partial x}, \qquad \epsilon_y = \frac{L \cdot \sin 30}{n_0}\frac{\partial n}{\partial y} \tag{2}$$

The gradient of refractive index is high at the flame front and related to the density gradient (Settles 2001)and we assume that the light is only refracted at the flame front. As it is integrated along the optical axis it cannot be determined where along the axis the flame front is located, and if there are several flame fronts along one optical axis they cannot be uniquely determined.

4 Results

After the hydrogen mixture was ignited by the five sparks, five spherical flames expanded and join together as one parabolic cylinder which propagated towards the obstacle. The expanding flame generated pressure waves in front of the flame. As the flame quenched at the top and bottom walls it interacted with a pressure wave reflected at the obstacle. This caused the flame front to change curvature and invert as explained by Clanet and Searby (1996). This is often referred to as the Rayleigh-Taylor instability all though Sir G. Taylor (1950) stated that the amplitude should be small compared to the wavelength. Perpendicular schlieren pictures in figure 3 show the flame as it changed shape from a parabolic cylinder to an inverted or funnel shaped flame. As the deflection angle is

integrated along the whole optical axis it is not clear where the gradients of the refractive index are. Frame 62 and 66 of figure 3 are clear and understandable, while frame 70 to 82 shows a growing flame front in the x/y projection but schlieren pictures does not give a depth perspective along the optical axis. It is commonly understood that this process creates a funnel in the middle of the flame, and a little imagination visualizes a funnel shape in the perpendicular schlieren pictures. It is however insufficient to uniquely determine the shape as the optical axis crosses two flame fronts.

The angular schlieren setup give a view of the inversion of the flame front from an angle. This reveals more of the actual shape as the optical axis is not parallel to the initial axis of symmetry i.e along the line of ignition. The angular schlieren pictures are shown in figure 4, remember that the view of the angular schlieren pictures are as seen from the bottom mirror of figure 2. The flame propagation should be viewed as if the flame approach you from the front right and pass over your left shoulder. In frame 78 there are four lines curving from the top to the bottom. These lines and one more behind them originated from the five sparks of the ignition source. In frame 82 and 86 the flame quenched at the top and bottom walls and interacted with the reflected pressure wave. As it changed curvature it also corrugated rapidly creating a cellular structure of the flame front. Frame 90 shows how the flame was almost flat but cellular and frame 94 and 98 shows how the funnel shape developed and how the thickness of the flame at the walls grew and basically changed the almost symmetrical initial shape of the flame to a highly 3D flame front (Gaathaug et.al 2009). The angular schlieren pictures also show that as the flame inverted a center square of the flame front was pushed back relative to the flame at the walls.

The difference between the perpendicular and angular schlieren methods is the path of the optical axis. This difference is illustrated in figure 5, where a sketch of a flame at two time instances t_1 and t_2 is shown for a top and side view. We assume that the flame shape was convex towards the reactants and shaped as a parabolic cylinder. The gradient of refractive index in the burned gas was assumed to be much smaller than the gradients at the flame front, implying that the bent light of the schlieren pictures represent the flame front. For the perpendicular setup we see that the arrow in the top view which correspond to the dot in the side view passes through a section of uniformity. When the light passed through the flame front it is also clear that the thickness of the area of refracted light is relatively thin. This was also shown in frame 62 if figure 3. As the flame changed shape and inverted its shape was no longer clear. The inverted shape of figure 5 shows that two areas of light refraction, i.e flame front, given as point A and B could coincide at the same x and y coordinates along the z axis. Since the perpendicular schlieren picture is a projection on to the x/y plane there is no possibility to determine where along the z axis the light is refracted and therefore where the flame front is located.

The angular schlieren setup of figure 5 shows that the light pass through the flame from an angle and the elliptic shape on the side view sketch represent the path of the arrow of the top view sketch. This clearly shows that the shape of the flame is visible, but the thickness of the flame front is not visible with the angular schlieren setup. During

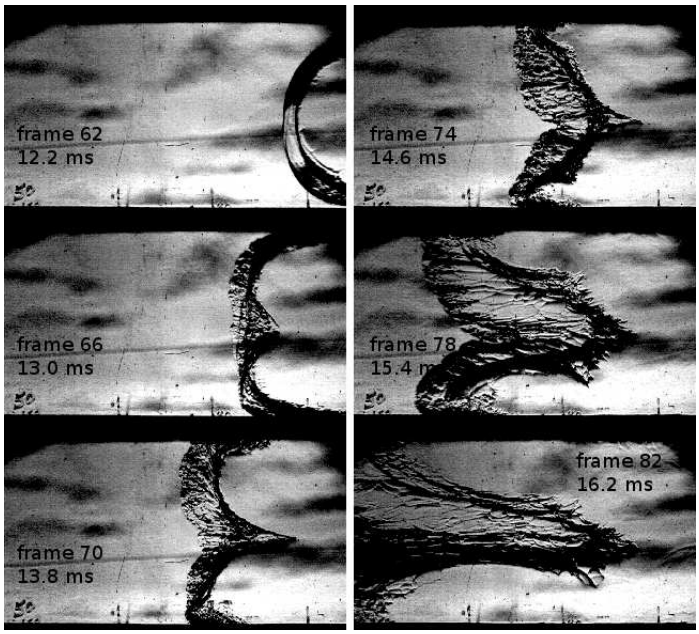

Figure 3: Perpendicular schlieren pictures of the formation of the inverted flame front. There is no clear understanding of the depth perspective of the picture.

and after the inversion of the flame it is best visualized using the angular setup since point A and B does not coincide on the same x and y coordinates. It is however not possible to visualize the whole funnel shape since at a given length of the funnel two points of refracting light will overlap each other, see figure 6. The lines p_1 and p_2 cross the flame front once along the optical axis, while p_{-1} and p_{-2} are optical axis were the light passes through the flame front two or three times. The line p_1 is the critical optical axis where the light passes through the flam once. This can be seen in figure 7 where the area within the full line is the area where the light passes through the flame two or three times, while the area within the dotted line is the area where the light refracts once. The area between them is within the funnel shape but still uniquely described. The maximum length of the funnel (l) before two points coincide is dependent on the width of the funnel (w) and the angle of the light (a). The width of the funnel must be determined where the curvature of the flame is equal to the angle of the light. The angle of light must be smaller than the critical angle a_{crit}, and as the flame burn normal to its own surface the width w decreases with time unless other mechanisms influence the shape of the inverted flame.

5 Summary

- By comparing the two schlieren methods the angular schlieren setup gives additional understanding of the phenomena of premixed combustion as the flame can

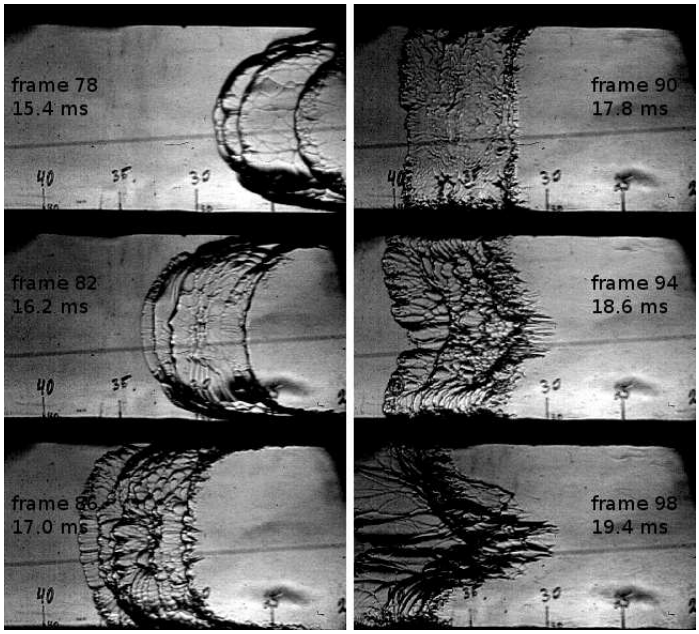

Figure 4: Angular schlieren pictures of the formation of the inverted flame front. The understanding of the depth perspective is improved compared to the perpendicular schlieren setup.

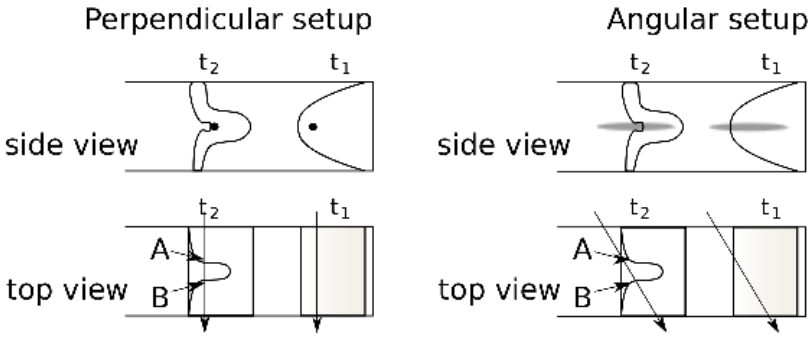

Figure 5: The difference between the perpendicular and angular schlieren setup. Notice how it is difficult to determine where the light bends (point A and B) in the perpendicular setup compared to the angular setup.

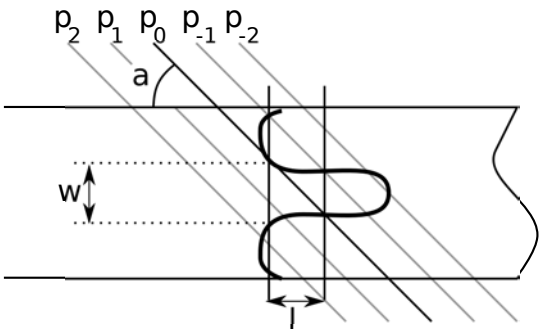

Figure 6: The maximum length l of the funnel shape at which no points coincide along the optical axis.

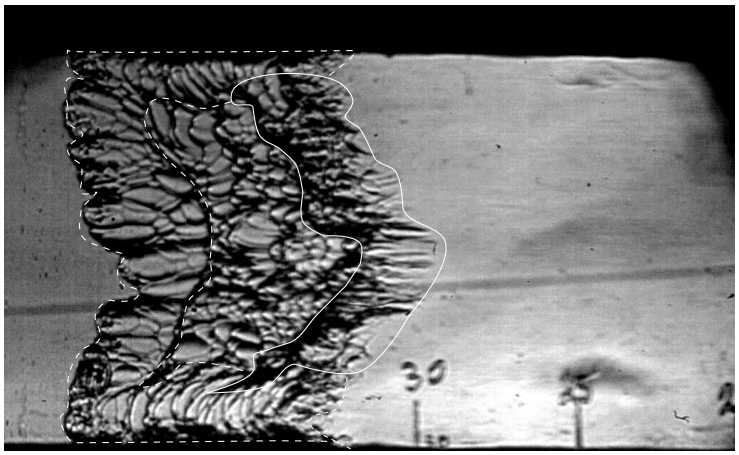

Figure 7: Angular schlieren picture of a developing funnel shape. The area within the dotted lines are uniquely described. The area within the full drawn line cannot be uniquely described. The area between them is the part of the funnel which can be uniquely described.

be viewed from a angle.

- Only small changes of the normal perpendicular setup is needed to use the angular schlieren method.
- If the flame has two or more coinciding points of flame front along the optical axis when using the perpendicular setup it is hard to determined where along the optical axis the flame fronts are located. The angular schlieren method can eliminate this problem and improve the understanding of the shape of the flame front.
- The maximum angle of the angular schlieren setup is given by the refractive index of the windows of the experimental setup, but for practical purposes the angle is smaller.
- There is a maximum length of a funnel shape that is uniquely determined, i.e. only one flame front along the optical axis. This length is given by the angle of the light and the width of the funnel at the point where the curvature of the flame and the angle of light equals.

References

[1] Settles G. S. (2001) Schlieren and Shadowgraph Techniques: Visualizing Phenomena in Transparent Media, Springer Verlag, New York

[2] Markstein G.H. (1964) Experimental studies of flame-front instability. In: Markstein G.H (ed) Nonsteady Flame Propagation, Pergamon Press, New York

[3] Urtiew P.A., Oppenheim A.K. (1966) Experimental observations of the transition to detonation in an explosive gas. Proc. Royal Soc. London. A295, 13-28

[4] Clanet C, Searby G (1996) On the tulip flame. Combustion and Flame 105, Issues 1-2: 225-238

[5] Dunn-Rankin D, Sawyer R.F. (1998) Tulip flames: changes in shape of premixed flames propagating in closed tubes. Experiments in Fluids 24:130-140

[6] Gonzales M, Borghi R, Saouab A (1992) Interaction of a Flame Front with Its Self Generated Flow in an Enclosure: The "Tulip Flame" Phenomenon. Combustion and Flame 88:201-220

[7] Taylor G.I. (1950) The instability of liquid surfaces when accelerated in a direction perpendicular to their planes. Proc. Royal Soc. London A201: 192-196

[8] Gaathaug A.V, Bjerketvedt D, Vaagsaether K (2009) Experiments with Flame Propagation in a channel with One Obstacle and Premixed $H_2 - Air$. Proc ICDERS 165 2009 Minsk Belarus

ISBN 978-82-7206-392-3
ISSN 1893-3068

www.hit.no
2015